Mesure de l’hétérogénéité au sein de la population bactérienne monoclonale en gouttelettes microfluidiques ancrées : le cas de la de réponse antibiotique

Léna Le Quellec

To cite this version:

Léna Le Quellec. Mesure de l’hétérogénéité au sein de la population bactérienne monoclonale en gouttelettes microfluidiques ancrées : le cas de la de réponse antibiotique. Biotechnology. Institut Polytechnique de Paris, 2023. English. NNT : 2023IPPAX075 . tel-04519742

HAL Id: tel-04519742
https://theses.hal.science/tel-04519742

Submitted on 25 Mar 2024

NNT : 2023IPPAX075

Thèse de doctorat

Measuring heterogeneity within monoclonal bacterial population in anchored microfluidic droplets : The case of antibiotic response

Thèse de doctorat de l'Institut Polytechnique de Paris
préparée à Ecole polytechnique

École doctorale n°626 Ecole doctorale IP Paris (ED IP PARIS)
Spécialité de doctorat : Biomécanique

Thèse présentée et soutenue à Paris, le 22 septembre 2023, par

LENA LE QUELLEC

Composition du Jury :

Gilles Charvin Directeur de recherche, Université de Strasbourg (IGBMC)	Président
Meriem El Karoui Professor, University of Edinburgh (Centre for Engineering biology	Rapportrice
Lydia Robert Chargée de recherche, INRAE (Institut Micalis	Rapportrice
Imane El Meouche Chargée de recherche, INSERM (IAME)	Examinatrice
Gregory Batt Directeur de recherhce, INRIA et Institut Pasteur)	Examinateur
Charles Baroud Professeur, Ecole polytechnique et INstitut Pasteur	Directeur de thèse

Measuring heterogeneity within monoclonal bacterial population in anchored microfluidic droplets : The case of antibiotic response

Lena LE QUELLEC

December 6, 2023

Pour Vincent.

Acknowledgment

First and foremost, I would like to express my gratitude to my supervisor, Charles Baroud. Despite your demanding schedule, you provided guidance throughout my Ph.D. journey while also granting me considerable freedom to pursue my research.

Gracias Salomé for warmly welcoming me into this project.

Я хотела бы особенно поблагодарить Андрея. We collaborated closely, and your help was invaluable, particularly in the areas of microscopy and image analysis.

Merci Gabriel, Danke Erik, for your valuable assistance and guidance in data analysis, as well as your help in proofreading and providing feedback on my paper, mi-thesis report, and this manuscript.

I would like to thanks all the PμB lab members. You are creating a joyfull and positive atmosphere in the lab. A special thanks to Nadia and Sebastien with whom I had the pleasure of sharing gossips and an office for three years.

I would like to thank the jury members for accepting to evaluate my work, and especially Lydia Robert and Meriem El Karoui for reviewing the manuscript.

Merci à Christophe et Tiphaine qui m'ont accueilli à Montroc où j'ai pu rédiger mon manuscrit dans le calme de la montagne, loin des distractions parisiennes.

Lastly, I would like to extend my love and gratitude to my friends and family. You have been a constant source of encouragement, patiently listening to my complaints about the challenges of being a Ph.D. student. I would also like to express my appreciation to all of you who have taken the time to read this thesis and show interest in my work.

Résumé

Ce manuscrit de thèse présente le développement d'une nouvelle plateforme microfluidique basée sur les gouttelettes ancrées et son utilisation pour étudier la réponse bactérienne aux antibiotiques au niveau unicellulaire. L'utilisation intensive des antibiotiques en agriculture, en médecine vétérinaire et en médecine humaine a conduit à l'émergence d'une résistance aux antibiotiques chez de nombreuses bactéries pathogènes, qui constitue désormais une menace majeure pour la santé publique. Dans ce contexte, il est particulièrement important de développer de nouvelles approches pour comprendre le mécanisme de réponse aux antibiotiques, telles que des techniques de dépistage rapide et fiable de la sensibilité aux antibiotiques, ainsi que des études sur des cellules individuelles. Ces dernières années, un nombre croissant de processus cellulaires ont été étudiés au niveau de la cellule unique, grâce au développement de nouveaux outils, permettant de déchiffrer la diversité parfois frappante entre les individus isogéniques. Cette thèse s'inscrit dans cette démarche et aborde à la fois le développement d'une nouvelle méthode et la caractérisation de la susceptibilité aux antibiotiques unicellulaires, qui va au-delà de la mesure classique de la concentration minimale inhibitrice (CMI) au niveau de la population.

Dans cette étude, nous proposons une nouvelle plateforme utilisant des microgouttelettes ancrées et des protocoles d'analyse d'images pour mesurer la croissance de petites communautés à partir de cellules bactériennes individuelles. En raison de l'indépendance de chaque gouttelette, ce format de culture cellulaire 3D nous permet de contrôler précisément le contenu de chaque gouttelette tout en suivant la descendance d'une cellule individuelle. Grâce à cette approche, nous pouvons suivre la croissance d'une cellule individuelle jusqu'à la formation d'une colonie en utilisant la vidéomicroscopie. De plus, en exposant les cellules des gouttelettes microfluidiques à la ciprofloxacine, un antibiotique, nous pouvons observer les changements morphologiques au niveau de chaque cellule individuelle. Grâce à notre dispositif microfluidique, nous pouvons étudier de manière quantitative la réponse aux antibiotiques des cellules individuelles au sein d'une population bactérienne monoclonale.

Cette thèse est divisée en 5 chapitres, correspondant à l'introduction, puis trois chapitres présentant la méthode et les résultats et enfin un chapitre de discussion.

L'introduction présente les caractéristiques de base de la microfluidique et sa pertinence pour les études microbiologiques. Différentes techniques microfluidiques sont décrites : les systèmes microfluidiques monophasés, les gouttelettes libres et ancrées. Les méthodes de mesure CMI classiques et les essais microfluidiques déjà développés pour les tests de sensibilité aux antibiotiques (AST) sont aussi présentées.

Le deuxième chapitre présente la méthode expérimentale, décrivant la puce microfluidique et le processus de fabrication, ainsi que l'imagerie et l'analyse d'images. Bien que la technique des gouttelettes ancrées ait déjà été utilisée en laboratoire, la configuration microfluidique et les protocoles expérimentaux sont améliorés, notamment en terme de débit et de vitesse. Une pipeline d'analyse dédié a été développé, et des expériences de contrôle ont été réalisées pour s'assurer que la croissance bactérienne ne soit pas perturbée dans les gouttelettes. Ce réglage minutieux donne

lieu à une méthode efficace et puissante.

Dans le troisième chapitre, cette méthode est utilisée pour caractériser la sensibilité à l'antibiotique ciprofloxacine. Au niveau de la population, une CMI peut être définie à partir des expériences microfluidiques qui s'avèrent similaires à la concentration bactéricide minimale (CMB) dans les cultures liquides. La croissance d'une microcolonie dans une gouttelette dépend à la fois de la concentration en antibiotiques et du nombre initial de cellules. À partir de ces données et à l'aide d'un modèle probabiliste simple, la susceptibilité à une cellule est estimée : la probabilité qu'une seule cellule forme une microcolonie. La méthode microfluidique permet ainsi de combler les échelles unicellulaires et de population, ce qui constitue un grand pas en avant.

Le quatrième chapitre étend ces résultats à quatre autres antibiotiques avec différents mécanismes d'action. Bien que les courbes de sensibilité à une seule cellule soient similaires, les antibiotiques bactéricides donnent des résultats plus reproductibles que les antibiotiques bactériostatiques. Cette observation intrigante démontre le potentiel de la méthode pour révéler des caractéristiques inattendues de la réponse antibiotique. Au niveau de la cellule unique, différents phénotypes peuvent être observés en fonction des antibiotiques, tels que la filamentation en présence de ciprofloxacine. Les différentes réponses à la lumière des différents modes d'action des antibiotiques sont comparées. Par exemple, l'implication de la réponse SOS dans la filamentation.

Dans la discussion, les forces et les limites de la méthode sont résumées. Des améliorations potentielles, telles que l'utilisation de l'intelligence artificielle dans l'analyse d'images pour analyser les phénotypes bactériens sont présentées. D'autres applications intéressantes de la méthode, par exemple pour étudier l'hétérogénéité phénotypique dans la sporulation ou la respiration sont aussi proposées.

En résumé, en utilisant ce système microfluidique et cette méthodologie d'imagerie, nous fournissons des informations à la fois qualitatives et quantitatives sur la réponse des antibiotiques. Nous avons développé une plateforme microfluidique et un pipeline d'analyse dédié pouvant aborder la susceptibilité aux antibiotiques dans la nouvelle perspective de l'individualité unicellulaire. Cette approche nous permet d'accroître notre compréhension du fonctionnement des divers antibiotiques en fournissant des informations sur leur mécanisme d'action. Cette thèse présente un travail interdisciplinaire, combinant la microfluidique de pointe avec des questions biologiques pertinentes.

Abstract

The emergence of new resistant bacterial strains is a worldwide challenge. A resistant bacterial population can emerge from a single cell that acquires resistance or persistence. Hence, new ways of tackling the mechanism of antibiotic response, such as fast and reliable antibiotic susceptibility testing screening techniques and single cell studies are required. It is necessary to see what happens at the single cell level, in order to understand what happens at the population level.

Here, we present a new platform based on anchored micro-droplets and image analysis protocols to measure the growth of small communities starting from individual bacterial cells. As each droplet is independent from one to another, this 3D cell culture format allows us to finely control the content within each droplet, while following the progeny of an individual cell.

Therefore, we can follow the growth from individual cell to a colony using time lapse imaging. Plus, by adding ciprofloxacin, the cells in the microfluidic droplets can be subjected to antibiotic stress and we are able to observe the morphological changes at the single cell level. Using our microfluidic device, we can quantitatively investigate the antibiotic response of individual cells from a monoclonal bacterial population. We demonstrate that it is possible to detect heterogeneity outcomes within a monoclonal population of E. coli from which we can deduce single-cell susceptibility to antibiotic that we call the µf·MIC (microfluidic Minimum Inhibitory Concentration). This µf·MIC gives us access not only to the population antibiotics susceptibility but also to the antibiotic susceptibility within the population.

Using this microfluidic and imaging pipeline, we offer both qualitative and quantitative insights into the response of antibiotics. This approach enables us to enhance our comprehension of how different antibiotics function by providing information about their mechanism of action.

Contents

Abbreviations

AI: Artificial Intelligence
AMR: AntiMicrobial Resistance
AST: Antibiotic Susceptibility Testing
B. subtilis: *Bacillus subtilis*
CFP: Cyan Fluorescent Protein
CFU: Colony Forming Unit
DIC: Differential Interference Contrast
DNA: DeoyriboNucleic Acid
E. coli: *Escherichia coli*
EPS: Extracellular Polymeric Substance
EU: European Union
F-gases: Fluorinated gases
FISH: Fluorescence *In Situ* Hybridization
IC50: Half maximal Inhibitory Concentration
IPTG: Isopropyl-beta-D-thiogalactopyranoside
K. pneumoniae: *Klebsiella pneumoniae*
LB: Lysogeny Broth
LIF: Laser Induced Fluorescence
LOC: Lab-On-a-Chip
MBC: Minimal Bactericidal Concentration
MIC: Minimal Inhibitory Concentration
MOPS: 3-(N-MOrpholino)PropaneSulfonic acid
OD: Optical Density
PCR: Polymerase Chain Reaction
PDMS: PolyDiMethylSiloxane
RFP: Red Fluorescent Protein
RNA: RiboNucleic Acid
USD: US Dollar
UV: Ultra Violet
V.cholerae:*Vibrio cholerae*
WHO: World Health Organisation
YFP: Yellow Fluorescent Protein
µf·MIC: microfluidic MIC

Introduction

If I were to summarize my thesis in just two words, they would be *bacteria* and *droplet*. My journey into the realm of bacteria began during my research internship in the MEK lab at the University of Edinburgh, which took place in my third year at Ecole polytechnique. Under the guidance of Meriem El Karoui, I discovered the exciting intersection of engineering and microbiology.

The world of droplets came into focus during my time working with Charles Baroud, my thesis supervisor. Through this experience, I learned that droplets possess incredible versatility, allowing for the encapsulation of various substances simply for the sheer enjoyment of exploration.

Throughout my years at Ecole polytechnique and the University of Edinburgh, I developed a particular affinity for experimental work that took me far away from the confines of a computer. This kind of work combines manual labor with creativity, presenting opportunities to overcome technical challenges along the way.

During my thesis, my work revolved around a highly experimental nature. I devised a comprehensive protocol that integrated multiple disciplines, including microfabrication, microscopy, image analysis, data analysis, and microbiology. This endeavor brought together various fields such as biology, optics, engineering, and computing, among others.

While I took the lead in spearheading the experimental aspects of the project, it was truly a collaborative effort with the invaluable assistance of Andrey Aristov, who contributed expertise in image analysis, as well as Gabriel Amselem and Erik Maikranz, who provided support in data analysis.

General Introduction

According to the World Health Organization, antimicrobial resistance, specifically antibiotic resistance, is recognized as one of the most significant threats to public health [1]. Therefore, there is a growing need to develop new tools and methods to enhance our understanding of bacterial resistance. When studying bacterial response to antibiotics, most microbiology studies typically report the minimum inhibitory concentration (MIC) at which cell growth is halted, using a specified initial inoculum size (usually 5.10^5 CFU/ml) and after a 24-hour incubation period. However, interpreting these MIC measurements is complex and can indicate various phenomena occurring within the cultures, such as high variability, inoculum effect, or mechanism of action [2]. It is important to note that individual cells' response to antibiotics, which can lead to colony formation, can display large heterogeneity [3, 4]. To complement the MIC, the minimum bactericidal concentration (MBC) is sometimes used for a more precise measurement. Determining the MBC is a laborious and time-consuming process and, similar to the MIC, it only provides information about antibiotic susceptibility at the population level. However, due to the imperfections of these methods, significant efforts have been made to measure bacterial response at a more microscopic level.

For instance, one approach to estimating single-cell minimum inhibitory concentration (MIC) involves measuring the MIC for different inoculum sizes and extrapolating the value to single cells [5]. However, traditional laboratory methods pose challenges when it comes to scaling to single-cell manipulation, both in terms of the volumes of interest and the number of experiments required for an adequate number of replicates. In contrast, the development of microfabrication methods and microfluidics has facilitated the measurement of individual cells in controlled environments [6].

In this field, two platforms have emerged to investigate antibiotic response. The first is the so-called mother machine and its variations, in which individual cells are trapped in narrow channels and observed over multiple generations [7]. These devices rely on time-lapse microscopy to track the initial "mother" cells, while removing their daughter cells as they emerge from the microchannels. Through detailed analysis of the acquired images under different antibiotic treatments, valuable insights can be gained regarding the relationship between mother and daughter cells [8], or the impact of rare mutations on single-cell fitness [9].

Concurrently, droplet microfluidics has opened up new avenues of investigation. By encapsulating one or a few bacterial cells within water-in-oil droplets, it is possible to detect the development of small colonies from individual cells [10] or observe their metabolic signatures [11] using optical readouts. The introduction of antibiotics into the droplets allows for the determination of bacterial susceptibility. Over the years, these principles have been further developed in two main directions. One direction focuses on enhancing the simplicity of use [12, 13], while the other aims to improve measurement precision [14, 15, 16]. The potential transfer of these droplet approaches to clinical studies has been reviewed in recent papers [17, 18, 19].

However, these droplet methods have two significant limitations. Firstly, they require sophisticated instrumentation to generate meaningful data. The interpretation of droplet data relies on the assumption that all droplets are nearly the same size, which necessitates high-end flow control systems (such as syringe pumps or pressure controllers) to ensure size homogeneity. Additionally, the flowing droplet systems often rely on high-speed acquisition of time-series data, which entails the use of fast electronics, lasers, and data acquisition equipment. Secondly, the connection between single-cell measurements obtained through droplet-based methods and classical biological measurements has not been thoroughly investigated. Consequently, it is challenging to establish a meaningful relationship between droplet-based measurements and data obtained from conventional experiments.

Here we introduce an open-access microfluidic platform that tackles these challenges. The platform is based on the *rails and anchors* technique, which was introduced a few years ago [20]. In this approach, droplets are generated within microfabricated wells and remain stationary throughout the experiment, allowing for the observation of biological processes within them [21, 22]. As a result, the platform requires simple microfabrication and low-precision flow control, and it can be used with a standard microscopy setup. To enhance its functionality, we have developed an original image acquisition and analysis pipeline specifically designed for this platform. This automated pipeline extracts the relevant information from the microfluidic chips. By providing the image and data analysis as open-source code, the platform can be easily integrated into most academic labs.

Furthermore, this study marks the first investigation into the interpretation of biological measurements obtained using this platform. It establishes a connection between the droplet-level approach commonly employed in droplet-based experiments and a single-cell analysis. This analysis enables unique measurements of the susceptibility of individual cells to antibiotics providing qualitative and quantitative measurments.

Structure

Over the course of the past three years, I have engaged in genuine bioengineering work, dedicating myself to the development of a comprehensive experimental pipeline. As a result, this Ph.D. thesis encompasses a significant methodological component while also seeking to tackle biological inquiries that can be effectively addressed through the utilization of this experimental pipeline.

This manuscript is split into 4 chapters:

- The first chapter provides an overview of the intersection of microfluidics and microbiology, shedding light on current advancements and the evolving nature of these fields.
- The second chapter delves into the comprehensive experimental pipeline, which encompasses significant time investment, continuous improvement, and the occasional challenge of unraveling biological mysteries that may prove challenging for physicists.
- The third chapter illustrate how we apply this pipeline specifically to Antibiotic Susceptibility Testing (AST), a critical issue in the realm of public health. Leveraging our collected data, I will also explore the incorporation of mathematical techniques in an attempt to contribute to a deeper understanding of Antibiotic Susceptibility, thereby paving the way for future advancements in this field.

- In the final chapter, a comparison of various antibiotics is carried out using the tools established in the second and third chapters. The focus is placed on the qualitative insights derived from the experimental pipeline that was developed.
- Lastly, I will conclude by discussing the ongoing and future work, as well as the potential applications that exist for the microfluidic pipeline I have developed.

Chapter 1

Microfluidics for Microbiology

A substantial part of my thesis work focused on developing methodological tools to address inquiries regarding heterogeneity in antibiotic response utilizing microfluidics. Consequently, I chose to conduct a review of various techniques and applications of microfluidics in the field of biology, with a particular emphasis on antibiotics susceptibility testing.

1.1 State of the art

Microfluidics

Microfluidics has a significant historical background that traces its roots to the 1980s when it first emerged within the microelectronics industry. Since its inception, this field has expanded its applications across diverse domains, including biomedical and chemical research. The advancement of novel materials and fabrication techniques in microfluidics has been shaped by various factors, such as government funding [23].

Microfluidics refers to an engineering domain focused on utilizing fluidic flow within channels that are smaller than one millimeter in at least one dimension. This field revolves around the precise control and manipulation of fluids at the microscale by employing channels, chambers, and pumps [24]. It offers several benefits, including decreased consumption of reagents, precise control over mixing and manipulation of particles, the ability to integrate and automate multiple assays (commonly known as lab-on-a-chip technology), and enhanced capabilities for imaging and tracking [23].

Microfluidics has diverse applications in various fields. In the realm of biomedical research, it has proven invaluable in modeling physiological processes such as the blood-brain barrier. This allows for studying disease mechanisms and developing innovative therapies. Microfluidic devices have also played a significant role in the creation of organs-on-chips, enabling drug efficacy testing and toxicity assessments [25, 26, 27]. Furthermore, they have contributed to the investigation of the microbiome and its impact on human health [19, 24, 28].

In the domain of chemical research, microfluidic devices have been essential in the synthesis and analysis of both small molecules and biomolecules [29]. They have also facilitated the exploration of fluid dynamics and the study of transport phenomena [30].

Additionally, microfluidic devices have found application in environmental monitoring. They have been utilized for the detection of pollutants and pathogens in water and air, thereby enhancing environmental monitoring capabilities. Furthermore, microfluidics has enabled investigations into the behavior of microorganisms in natural environments [31].

Microfluidic devices can be fabricated using different approaches, each offering distinct advantages and disadvantages. As shown in Figure 1.1, One commonly used method is soft lithography, which involves creating a master mold through photoresist lithography and replicating it using a material called polydimethylsiloxane (PDMS). PDMS is popular due to its optical transparency, biocompatibility, and ease of use. However, it may be susceptible to swelling and absorption of small molecules, potentially interfering with certain assays [32, 33].

Another approach is micromachining, which utilizes etching techniques to carve channels and chambers on substrates like silicon or glass. Micromachining is well-suited for producing intricate structures such as micropumps and valves. However, it can be costly and requires specialized equipment [35].

Alternatively, 3D printing can be employed, leveraging additive manufacturing techniques to construct structures layer by layer. This method allows for rapid prototyping and customization of microfluidic devices. Nonetheless, the resolution of

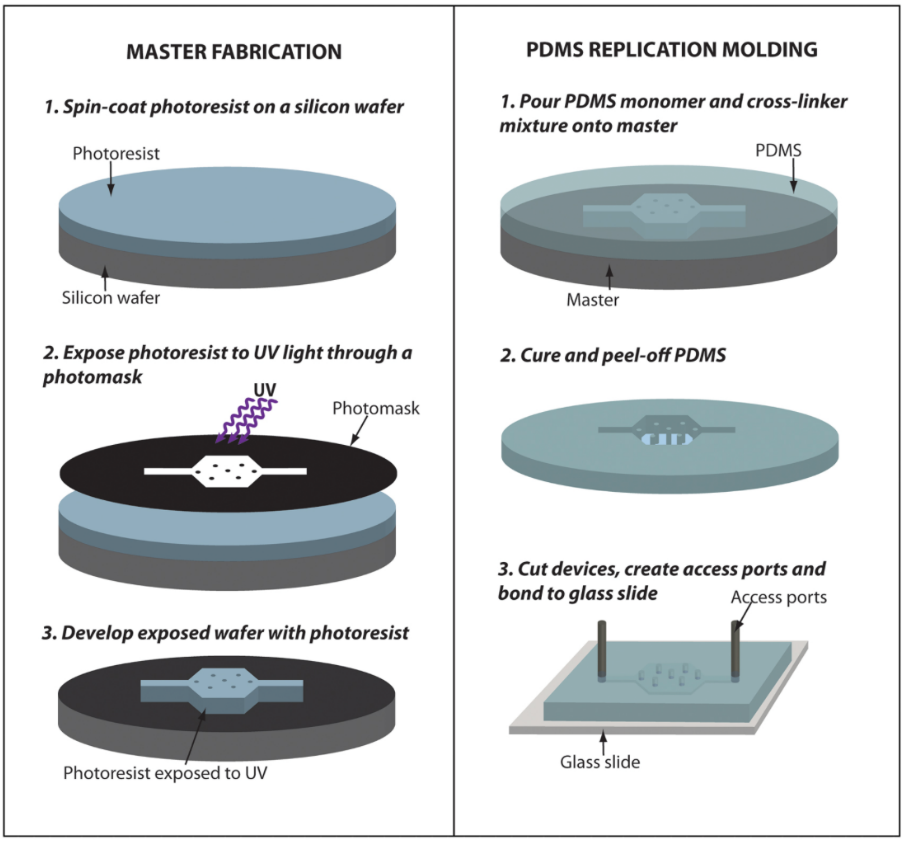

Figure 1.1: **PDMS microfabrication** Fabrication of microfluidic devices with PDMS replica molding (From [34] Copyright 2013, Adriana San-Miguel and Hang Lu).

3D printing is generally lower compared to other fabrication techniques [36, 37].

Microfluidics is a dynamic and rapidly evolving domain that encompasses numerous captivating advancements. It has revolutionized scientific research and production by introducing enhanced levels of control, precision, and sensitivity. Researchers are continuously pushing the boundaries by investigating novel manufacturing techniques, exploring innovative materials, and discovering fresh applications for microfluidic devices. Indeed, it holds the promise of surpassing conventional techniques in both biomedical and chemical research. The present applications of microfluidics encompass a wide range of areas, including the development of lab-on-a-chip devices for point-of-care diagnostics, environmental testing, droplet microfluidics, and flow chemistry [23].

Microbiology

Microbiology encompasses a wide-ranging field dedicated to the study of microorganisms, such as bacteria, fungi, and protists [38]. Several methods are employed in microbiology to investigate these microorganisms.One such method is culturing, which involves cultivating microorganisms in a controlled laboratory environment to examine their growth, metabolism, and other characteristics. Techniques such as streaking, pour-plate, spread-plate, and subculture techniques are utilized to culture microorganisms [38].

Identification methods are used to recognize microorganisms based on factors such as colony characteristics, cellular morphology, biochemical procedures, serological procedures, and molecular techniques [38].

Antimicrobial susceptibility testing examines the sensitivity of microorganisms to different antibiotics or antimicrobial agents, providing valuable information about their response to treatment [38].

Microscopy techniques play a crucial role in observing microorganisms and their structures. These techniques include fluorescence microscopy, scanning electron microscopy, transmission electron microscopy, among others [38].

The aforementioned methods, commonly employed in microbiology, suffer from significant experimental limitations. These drawbacks include time-consuming processes, as it takes a considerable amount of time for detection. The environmental control during these methods is inadequate. Moreover, they exhibit low throughput capabilities and require substantial reagent consumption.

Microfluidics demonstrates great promise as a technology with the potential for applications in the field of microbiology. Certain established methods in microbiology can be adapted and implemented within microfluidic systems. These new methods should go beyond the capabilities of existing techniques, either by offering improved functionality, increased throughput, or reduced cost. Additionally, a significant factor driving the adoption and implementation of new technologies is their ability to save experimental time [39].

Indeed, microfluidics offers several advantages that contribute to its significance. Firstly, through miniaturization, it enhances analytical sensitivity by reducing detection times and enabling the detection of single cells. Certain microfluidic devices even improve bacterial detection by allowing larger sample volumes to flow through the device, facilitating the capture or trapping of bacteria [24, 40].

Secondly, microfluidics enables improved profiling of microbiome composition and structure. It provides a more accurate analysis by accounting for the majority of microbial species that are typically unculturable. Microfluidics allows for low-cost and high-throughput taxonomic resolution at various levels, from genus to strain. Gene annotations also enable inferences about physiological functions. Additionally, successful isolation and cultivation of previously uncultured lineages have expanded the database capacity, enabling reproducible investigations, mechanism validations, and the implementation of various industrial applications [40, 41].

Lastly, microfluidics plays a vital role in creating and maintaining microenvironments necessary for studying bacteria at a microscopic level. Microfluidic microscopy facilitates the growth of bacteria in chemically and physically controlled environments, allowing for noninvasive, in situ monitoring. It generates automated, real-time data on cell behavior and morphology with single-cell resolution. Thus, microfluidics provides the essential technology for establishing and sustaining crucial microenvironments for the microscopic study of bacteria [17, 24].

In summary, microfluidics is an interdisciplinary technology that integrates principles from engineering, physics, chemistry, biology, and computing to control fluid flow within microchannels. It serves as an outstanding platform for analyzing microorganisms and their nucleic acids, undergoing transformative advancements with highly positive outcomes. This technology enables bacteria to be cultured in environments that are chemically and physically controlled, allowing noninvasive in situ monitoring while generating automated, real-time data on cell behavior and morphology at the single-cell level. Microfluidics offers numerous advantages over traditional experimental approaches, including higher throughput, precise sample stimulation, enhanced reproducibility, and increased researcher efficiency through automation of repetitive tasks. The versatility of microfluidic systems will expedite comparative biology analyses and empower researchers to select the most suitable model organism for specific biological phenomena, even if it is less commonly utilized.

1.2 Different techniques...

Single phase microfluidics systems

Single phase microfluidics refers to systems where aqueous solutions and suspensions of microorganisms are guided directly through channels without the need for carrier oil. It offers extensive integration and automation capabilities on the microchip. Typically, flow control is achieved using syringe pumps, pneumatic microvalves, or by leveraging electrokinetic effects [17].

Single phase systems find utility in situations where there is a requirement for a continuous supply of culture medium, microorganism sedimentation [42], or the creation of a spatial gradient of solutes, gases, or temperature [43]. An extensively employed single phase system in this regard is the mother machine.

The Mother Machine is a microfluidic device designed for continuous culture, where bacteria are grown in closed channels with a diameter of approximately one micron. This device was created to maintain balanced growth conditions, which are crucial for achieving consistent and reproducible outcomes [7]. The Mother Machine platform has been extensively used in researching various fields, including cell aging [7], cell cycle control [7], gene regulation [9], antibiotic resistance [44, 45], and investigating the impact of mechanical forces on cell wall growth.

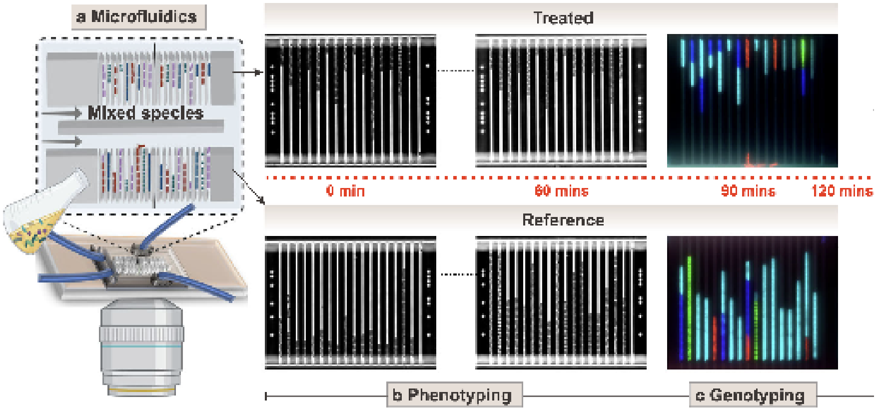

Figure 1.2: **Mother machine microfluidics setup (a)** Cartoon of the microfluidics set up with mixed species loaded on the chip. **(b)** Time-lapse phase contrast images of the cells in the traps with (top) and without (bottom) antibiotics. **(c)** Fluorescence images of the bacteria (adapted from [44]. Copyright 2022, Vinodh Kandavalli *et al.*).

In 2022, Kandavalli *et al.* utilized the mother machine to conduct rapid antibiotic susceptibility testing (depicted in Figure 1.2 a). The mother machine allowed for the swift capturing of individual bacteria and monitoring of their growth in the presence of antibiotics, with results obtained within a timeframe of two hours (as illustrated in Figure 1.2 b). Furthermore, they were able to identify the species by employing fluorescence probes on the ribosomal RNA, as demonstrated in Figure 1.2 c. This approach enabled the simultaneous testing of up to ten species in a single round.

Droplet microfluidics

Droplet-based microfluidics constitutes a subfield of microfluidic. It involves the generation and manipulation of droplets within an immiscible fluid.

The field of droplet microfluidics is experiencing rapid growth and finds applications in diverse areas including biology, chemistry, and materials science. This technique revolves around the generation and manipulation of droplets within microscale channels, creating a meticulously controlled environment for highly precise and efficient reactions. Leveraging droplets facilitates high-throughput experiments, reduces reagent consumption, and enables the study of single cells, among a multitude of other advantages [46].

Droplets formation can be achieved with different techniques. Three types of microfluidics geometries can be used (Figure 1.3): Cross-Flowing [47], Flow focusing [48] and Co-Flowing [49]. The size of the generated droplets is primarily governed by factors such as the flow rate ratio between the continuous phase and dispersed phase, the interfacial tension between the two phases, and the specific geometry of the channels employed for droplet generation.

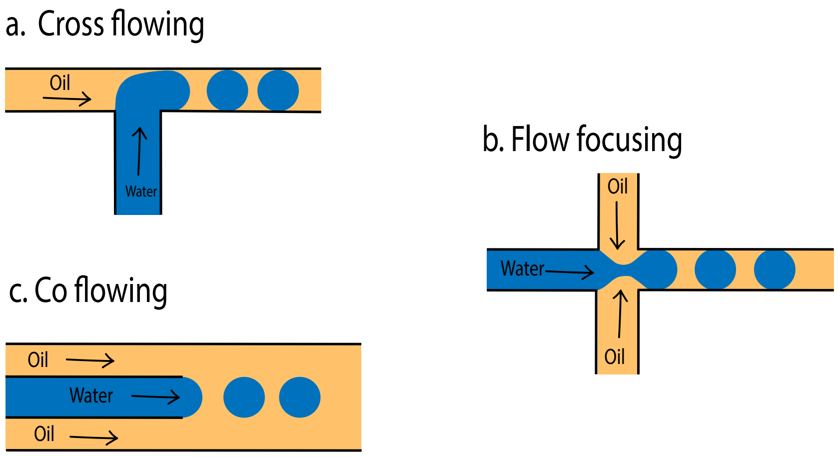

Figure 1.3: **Droplets generation strategies.** In a planar chip format (**a**) Cross-flowing schematic from a top view. The main channel facilitates flow from left to right. The continuous fluid (referred to as 'oil' in this case) is directed along the main channe. The fluid to be dispersed (referred to as 'water' in this case) is supplied through the perpendicular inlet." [47]. (**b**) Flow focusing schematic from a top view. The dispersed phase converges with the continuous phase, usually at an angled intersection, and subsequently undergoes a restriction that induces droplet formation [48].(**c**) Co flowing schematic from a top view. The dispersed phase channel is contained within the continuous phase channel. Towards the end of the dispersed phase channel, the fluid is subjected to stretching forces until it reaches a point of rupture due to shear forces, resulting in the formation of droplets [49]. Blue corresponds to the water, orange to the oil.

Anchored droplets

Anchored droplets refer to droplets that maintain a stationary position within a microfluidic chamber. This is achieved by confining the fluids everywhere except in specific regions where the channels have a greater height, utilizing a technique known as ”rails and anchors” [21, 50, 51]. These modern devices utilize three-dimensional geometries within the microfluidic channels to both contain and, in some cases, generate the droplets (Figure 1.4). By capitalizing on the precision offered by microfabrication techniques, these devices enable reliable operations even in situations where flow control may be suboptimal or absent. Consequently, the designs stemming from this approach are significantly more user-friendly for non-experts, given the availability of microfabrication tools [21].

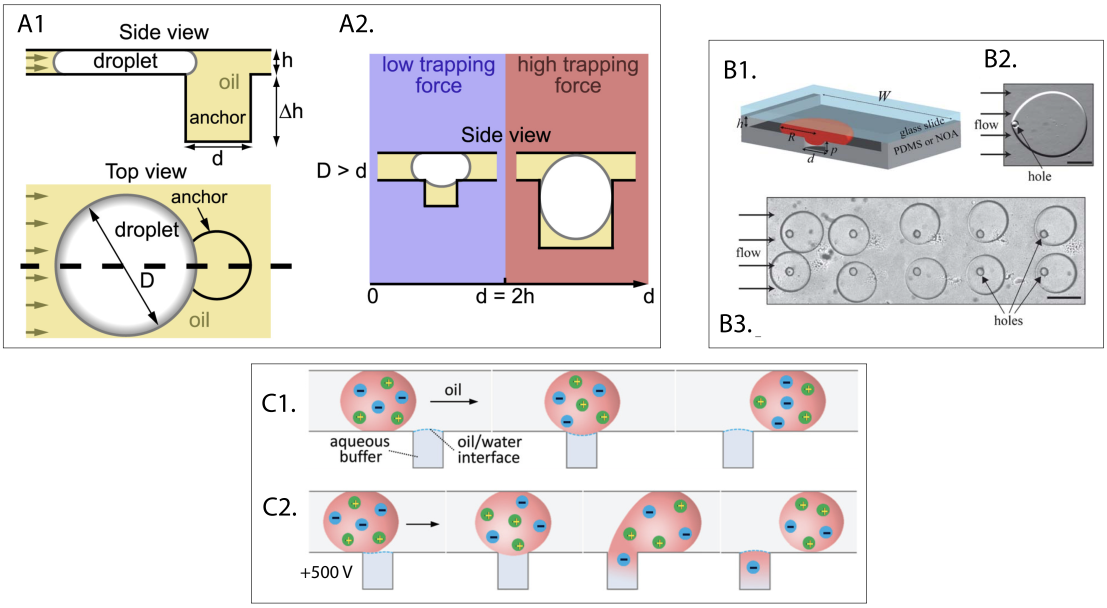

Figure 1.4: **Anchored droplets.** (**A1** Side view and top view of a confined aqueous droplet near a capillary anchor; **(A2)** Two anchoring strengths can be distinguished: for narrow anchors (blue regions), the droplet only partially enters the anchor, whereas for wide anchors (red regions), the droplet entirely enters the anchors (adapted from [52], Copyright 2020, Tomasi *et al.*. **(B1)** Sketch of the experimental device which defines the geometric parameters; **(B2)** A water drop anchored to a hole in the channel roof with oil flowing left to right; **(B3)** An array of anchored droplets. The scale bar represent 250µm in all images (from [20], Copyright 2011 The Royal Society of Chemistry). The schematic of the process in a side view highlighting the droplet flowing throughh the oil/water interface **(C1)** in the absence of voltage and **(C2)** in the presence of voltage (adapted from [53], Copyright 2011, Zeng *et al.*.

Figure 1.4 illustrates various systems for anchoring droplets. These droplets are generated using a droplet generator, specifically through flow focusing. Subsequently, the droplets move towards a chamber where they are anchored. Both Tomasi *et al.* and Abbyad *et al.* employ mechanical traps to anchor the droplets. In this setup, the droplet is confined within a flattened pancake shape in a microchannel (Figure 1.4 A1). Due to this vertical constraint, the droplet becomes sensitive to changes in the microchannel’s depth. Consequently, in a microchannel with varying heights, the flattened droplets are captured by regions of reduced confinement [20].

The trapping efficiency depends on the size of the trap: if the anchor diameter is approximately twice the height of the droplet, it will penetrate the anchor, resulting in high trapping efficiency. Conversely, if the anchor diameter is insufficient, the droplet only partially enters the anchor, leading to a lower trapping force (Figure 1.4 A2 and B1) [52].

Zeng *et al.*, on the other hand, utilize an electric field-based method. This approach not only facilitates the breaking of the droplet but also enables its coalescence with an aqueous buffer. The electric field aids in draining the oil film between the droplet and aqueous buffer, thereby enabling the breaking and subsequent coalescence [53].

Nonetheless, the process of generating droplets through flow focusing or other techniques depicted in Figure 1.3 can pose certain challenges. Primarily, these methods demand sophisticated instrumentation for droplet generation. In fact, the accurate interpretation of droplet data relies on the assumption that all droplets are almost uniform in size, which necessitates the use of advanced flow control systems (such as syringe pumps or pressure controllers) to ensure consistent size homogeneity.

Another approach, which does not involve the use of a droplet generator, is the breaking method illustrated in Figure 1.5. This method bears resemblance to the technique employed in Figure 1.4c, but it does not require an electric field. Amselem *et al.* have developed a microfluidic device that simultaneously forms and traps the droplet.

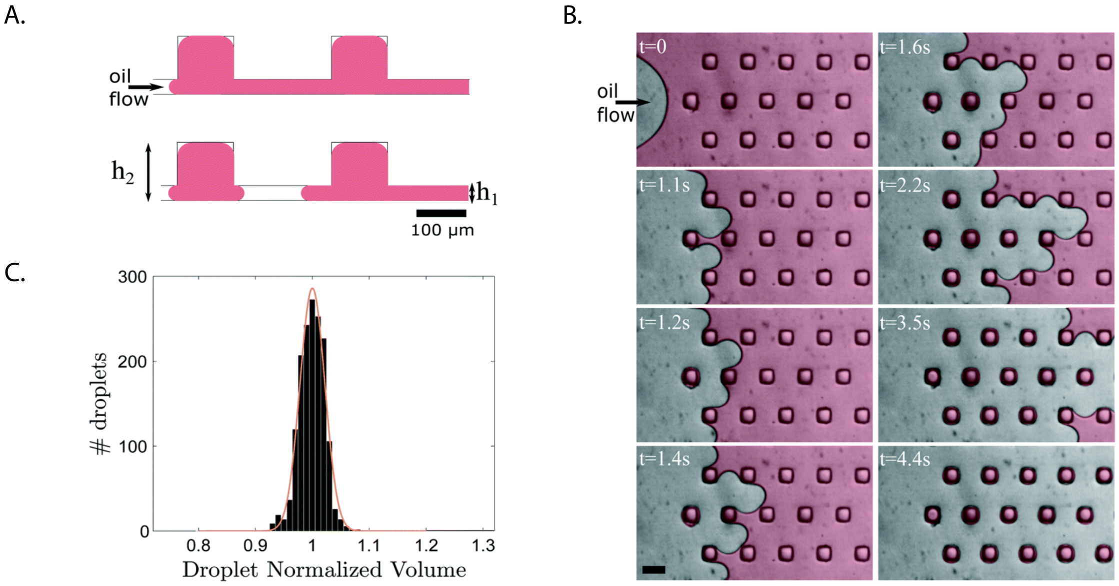

Figure 1.5: **Breaking anchored droplet.** **(A)** Cross-sectional schematic of the breaking process on anchors. The aqueous sample initially fills large regions and then gets divided into isolated droplets that fill each of the anchors.; **(B)**Time-lapse of the drop formation process. Scale bar: 200 m. ; **(C)** Experimental histogram of the normalized droplet volumes on one chip. (adapted from [22], Copyright 2016, Amselem *et al.*

In this configuration, the droplets exhibit precise size control, with a standard deviation ranging from 2% to 5%. The variation in droplet size remains relatively minor across different chips, and it depends on the accuracy of microfabrication and the quality of the hydrophobic surface treatment [22].

Anchored droplets offer numerous promising applications, such as facilitating the observation of behavioral heterogeneity within a population and enabling bioassays [22].

Droplets within microfluidic systems can undergo various manipulations, such as splitting, titration with additional reagents, incubation, and subsequent analysis [17, 52]. These manipulations enable the production of droplets with exceptional uniformity, a crucial factor in encapsulating individual cells within each droplet [54].

Microscopy

Microscopy techniques have a vital role in microfluidics as they enable the observation and extraction of valuable information from biological or chemical samples [55]. A range of microscopy techniques has been employed in microfluidics, encompassing bright-field and fluorescence microscopy, phase contrast microscopy, differential interference contrast (DIC) microscopy, and laser scanning confocal microscopy [55]. Table 1.1 provides an overview of the advantages and limitations of these different techniques. Confocal microscopy is a highly suitable technique to employ in droplet microfluidics. It enables comprehensive scanning of the entire droplet, offering excellent vertical and horizontal resolution [56].

Technique	Light Source	Advantages	Limitations	References
Bright Field	White light	Cheap, no change of the color	Low contrast, low resolution, low magnification	[57]
Phase Contrast	White light	High contrast	Shade off on the edges, Halo effect, not for thick specimen	[57], [58]
Differential Interference Contrast	White light	No halo effects, thick specimen	Not for 3D images	[58], [59]
Wide Field Fluorescence	High energy light high power LEDs, lasers	Quantitative images, labelling, tracking, sensitivity	Photobleaching, phototoxicity, chromatic and spherical aberration	[60]
Confocal Fluorescence	High energy light high power LEDs, lasers	3D images, high resolution, no background resolution	Harmfull, expensive	[61], [56]

Table 1.1: **Microscopy techniques.** Advantages and limitations of microscopy techniques for biology

The majority of research in microbiology pertaining to droplet microfluidics has predominantly utilized fluorescent labeling techniques. This is primarily due to the accessibility and well-established nature of this technology in conventional microbiological experiments [17]. However, fluorescent labeling does have its limitations. While it is convenient and widely adopted to employ fluorescent protein-expressing bacteria [3, 9, 62], this approach is restricted to genetically engineered strains and cannot be readily extended to other microorganisms.

Marker dyes, which indicate microbial metabolism or enzymatic activity, offer broader applicability across various species and strains [15]. However, a common challenge associated with their utilization is the potential leakage of fluorescent signal molecules from droplets into the carrier oil and neighboring droplets. Additionally, the utilization of marker dyes necessitates a sufficient quantity of bacteria to attain detectable levels, thereby impeding the feasibility of single-cell analysis [40].

1.3 ...For different applications

1.3.1 Microbial biotechnology

Microfluidics demonstrates a broad spectrum of applications in the field of molecular biology. It has facilitated the development of platforms for conducting quantitative biology studies [63], analytics and screening (PCR) [24, 64], sequencing [65], and fluorescence in situ hybridization (FISH) techniques [66].

A lab-on-a-chip (LOC) refers to a compact device that combines one or more laboratory functions onto a single integrated circuit, typically known as a ”chip,” which spans from millimeters to a few square centimeters in size. The purpose of an LOC is to enable automation and facilitate high-throughput screening processes [67].

LOCs find utility in a wide range of laboratory operations, encompassing DNA sequencing, biochemical detection, chemical synthesis, clinical diagnostics, and biomarker validation. LOC technology has the capacity to execute nearly any laboratory procedure on a scaled-down level.

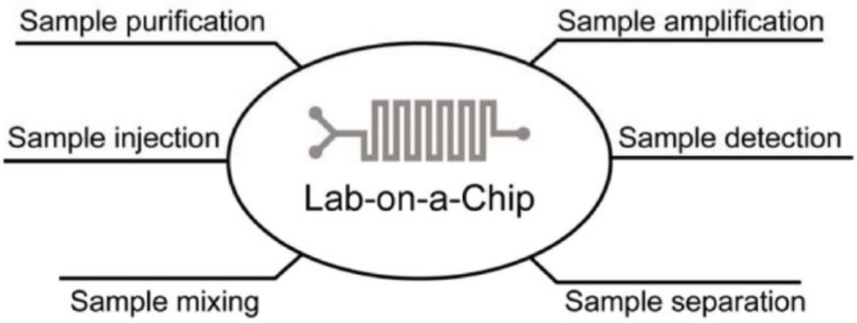

Figure 1.6: **Lab-on-a-chip system.** Unit components making up the lab-on-a-chip system. (From [68] Copyright 2013, Korean Continence Society).

LOC systems offer several advantages. They allow for precise control of small test volumes, reducing the amount of required reagents [68]. Additionally, the smaller length scales involved in microfluidics enable faster analysis and higher reaction efficiencies, leading to reduced reaction times [68]. Microfluidics also facilitates the direct integration of multiple components or functionalities on a single device, such as test preparation, detection, and data processing [40, 69, 68] (Figure 1.6). Furthermore, microfluidic systems can be fully automated and designed to be user-friendly, making them accessible even to individuals without specialized expertise [17, 70].

Therfore, microfluidics plays a critical role in advancing microbial biotechnologies, particularly in sectors such as the food industry, agriculture, and pharmaceuticals. Its application enables various advancements and innovations in these fields [71, 72].

1.3.2 Microbial culture

Biofilm research

A biofilm refers to a intricate community of microorganisms that attach to a surface and are enveloped by a matrix of extracellular polymeric substance (EPS) produced by themselves [73]. Once biofilms are formed, the microbial resistance to antibiotics increases significantly, reaching up to 1000 times higher than that of free-floating bacteria [73]. This becomes particularly concerning considering that more than 80% of microbial infections in the human body are attributed to biofilms [74]. Consequently, it is evident that the presence of biofilms should be minimized in health-related matters such as infections, wound healing, and medical implants.

Microfluidics offers a promising approach to investigate biofilms due to its ability to precisely control relevant parameters and enable real-time monitoring of biofilm development [75].

By employing 3D culture, cell confinement, and co-culture systems, microfluidics has the ability to replicate the biological environment. The microfluidic devices can create models that closely resemble the in vivo conditions within 3D culture platforms. This enables the assessment of individual factors influencing biofilm growth as well as the investigation of compounded effects. The microfluidic approach holds the potential to unravel the mechanisms underlying biofilm formation and address various challenges associated with biofilms [76, 77].

Yazdi *et al.*, conducted a study on biofilm and bacterial aggregation utilizing a microfluidic device (depicted in Figure 1.7) that generates a vortical flow mimicking certain microbial conditions. Their findings demonstrate that the accumulation of bacteria within these vortices leads to the formation of biofilm streamers within a few minutes.

Microbial interactions

Microbial community dynamics and functions are primarily influenced by microbial interactions, which play a vital role [78]. These interactions involve the recognition of environmental cues and the subsequent transfer of molecular and genetic information. However, detecting and studying the diverse types of interactions in microbial ecosystems pose significant challenges due to the complex, highly diverse, and dynamically changing nature of these communities [40]. Investigating microbial interactions holds significant importance in the fields of synthetic and natural microbial consortia engineering and control. Microfluidic cultivation and analysis devices serve as versatile tools for studying microbial interactions at the single-cell level, enabling deeper insights into these complex systems [79, 80].

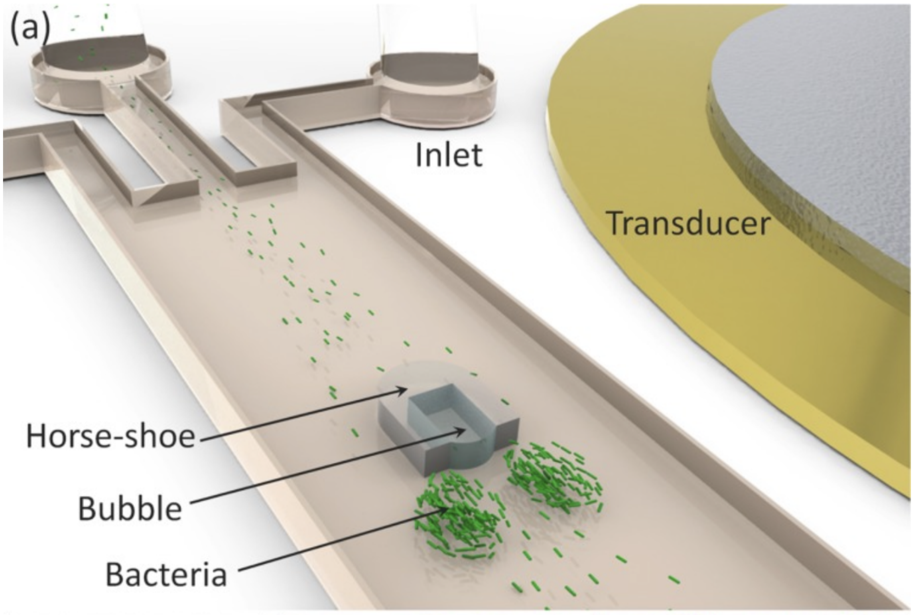

Figure 1.7: **Biofilm research.** Schematic of a microfluidics device with a built in horseshoe structure. Bacterial suspension is injected from the inlets and collect in a pair of vortices induced by oscillating microbubble trapped in the horseshoe. (Adapted from [73] Copyright 2012, American Institute of Physics).

Microfluidics devices offer the ability to examine single-cell dynamics with complete spatio-temporal resolution and provide controlled environmental conditions (including physical, biological, and chemical stimuli) in a high-throughput manner. Moreover, microfluidic fabrication methods enable the creation of diverse geometries that can mimic natural habitats or provide insights into biofilm formation [81].

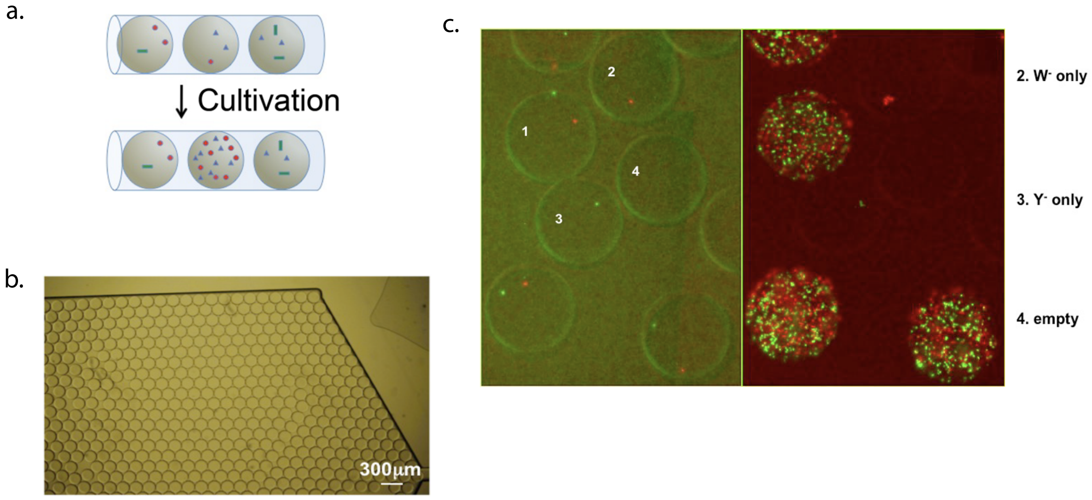

Figure 1.8: **Microfluidics device for microbial co-cultivation. (a)** Compartmentalized co-cultures enable detection of symbiotic relations among community members. **(b)** Droplets filling a large chamber in the microfluidics device. **(c)** A scetion of the cultivation chamber illustrating a number of droplets carrying combinations of the two-strain system. *E.coli* strain Y- is labeled with yellow fluorescence protein (EYFP) and W- with red fluorescence (mCherry). Left, before cultivation and right after 18 hours cultivation. (Adapted from [80] Copyright 2011, Park *et al.*.

In their study, Park *et al*, conducted a study where they developed a straightforward microfluidic device designed for the parallel co-cultivation of symbiotic microbial communities (as shown in Figure 1.8). This device enabled the generation of approximately 500 droplets per second, with a maximum capacity of up to 1400 droplets within a cultivation chamber. Within these droplets, they utilized cross-feeding mutants of *E.coli* to simulate various compositions found in natural microbial communities (Figure 1.8 c. The study demonstrated that through the use of microfluidics, it becomes feasible to predict the distribution of encapsulated subsets within a microbial community. Additionally, they successfully demonstrated the ability to co-cultivate and detect symbiotic relationships using this microfluidic system.

By utilizing these methods collectively, a deeper understanding of growth dynamics, heterogeneity, culture stability, spatial organization, and other relevant factors in mixed cultures can be achieved. This acquired knowledge can then be harnessed to effectively control and engineer both natural and synthetic consortia [17, 81].

1.4 Antibiotics susceptibility testing

Antibiotic susceptibility testing (AST) is a laboratory technique employed to evaluate how susceptible bacteria are to various antibiotics. The primary objective is to ascertain the most suitable antimicrobial treatment for individual patients, by determining the effectiveness of specific antibiotics against the bacteria and detecting any resistance the bacteria may have developed towards particular antibiotics [82].

AST encompasses various methodologies (Table 1.2), including agar dilution, broth dilution, and disc diffusion assays [83]. These tests evaluate the susceptibility of microbes to antimicrobial drugs by subjecting standardized concentrations of the organism to specific concentrations of the drugs. Qualitative, semiquantitative, or nucleic acid-based techniques can be employed for testing. Additionally, AST can assess the impact of combining different antimicrobials through synergy testing [82].

AST utilizes agar dilution, disk diffusion and broth dilution methods as common approaches to determine the minimum inhibitory concentration (MIC). The MIC represents the lowest concentration of an antibiotic that effectively inhibits bacterial growth. In the disk diffusion technique, the MIC is estimated based on the size of the zone of inhibition, while the microbroth dilution technique measures it using optical density [2, 84]. AST reports typically provide a quantitative outcome expressed in µg/mL and a qualitative interpretation. This interpretation usually categorizes the results as susceptible (S), intermediate (I), resistant (R), sensitive-dose dependent (SD), or without interpretation (NI) [83, 85].

The disk diffusion process offers several advantages, including its simplicity, cost-effectiveness, and ease of interpretation. However, its main drawback is that it requires manual processing and lacks automation [82].

AST utilizing agar and broth dilution methods represents one of the oldest approaches to determine the MIC. The agar dilution method allows testing of only one antibiotic at a time, whereas the broth dilution method enables testing of multiple antibiotics simultaneously. Dilution processes are known for their reproducibility and cost-effectiveness. However, they are labor-intensive and costly [82].

Additionally, these methods provide qualitative rather than quantitative results. Table 1.2 provides an overview of the advantages and limitations of these methods.

Classical AST			
Technique	Disk diffusion	Broth dillution	Agar dilution
Advantages	Simple and direct interpretation, accessible, versatile, low-cost.	Multiplexing, quantitative and qualitative results.	Low cost, simple and direct interpretation, versatile.
Limitations	Lack of consistency in the determination of the MIC, low-throughput, requiring a significant amount of manual labor, qualitative results.	High volume of reagents is necessary, requiring a significant amount of manual labor.	Requiring a significantamount of manual labor, qualitative results, low-throughput.
References	[85], [86]	[87]	[87], [86]

Table 1.2: **Classical AST techniques.** Advantages and limitations of classical techniques for AST

To address certain limitations associated with the conventional AST, Alexander *et al.* devised a seeding experiment (depicted in Figure 1.9) that employed a 96-well plate to investigate how antibiotics affect the initial development of resistant strains. They employed highly diluted strains, which they introduced into the 96-well plate containing antibiotics. Each antibiotic concentration corresponded to one 96-well plate, and the average inoculum size per well was 0.5, 1, or 2 cells. In order to determine the probability of establishment for a single cell, they employed likelihood-based methods to fit a stochastic model of population growth [84]. However, despite having an adequate number of replicates to accommodate very low cell counts and utilizing a mathematical model to infer information at the single-cell level, they still lacked direct access to individual cell data, which necessitated a considerable amount of manual effort. Furthermore, the duration of the incubation period for this experiment spans between three to five days, which is actually longer than the typical timeframe for classical MIC experiments.

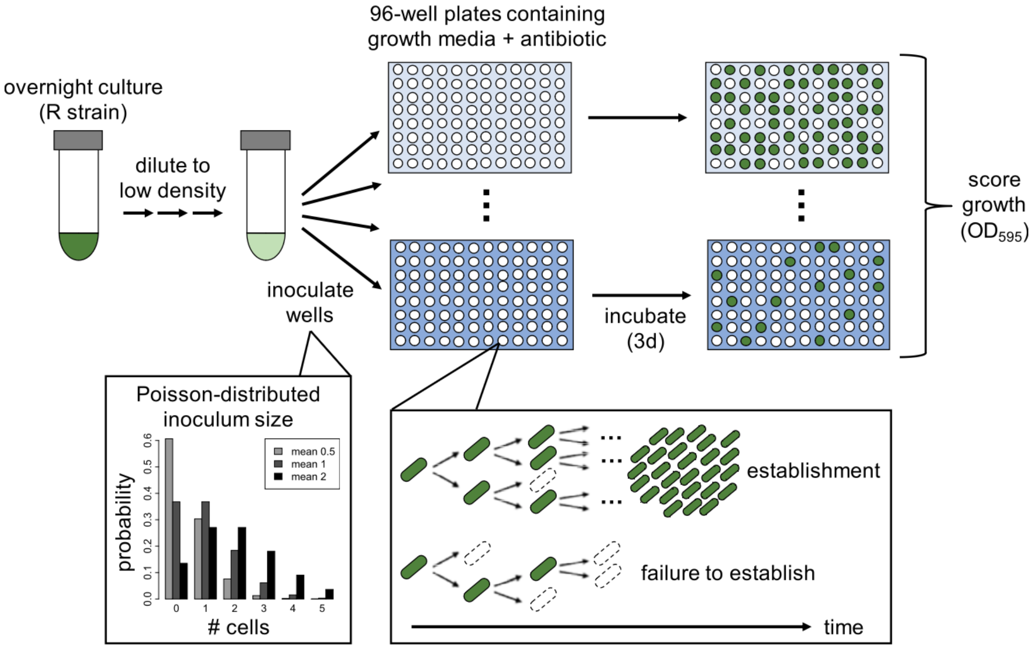

Figure 1.9: **Design of seeding experiments.** An overnight culture of the resistant strain is highly diluted and used to inoculate 96-well plates containing growth media with antibiotic at various concentration (shades of blue) (from [84], Copyright 2020, Alexander *et al.*).

Microfluidics has emerged as a potential solution for expediting AST procedures. Microfluidic platforms have the capability to swiftly assess the effectiveness of antimicrobial drugs in AST. Various microfluidic-based platforms have been developed for AST (Table 1.3), such as the mother machine ([7, 45]) , gradient microfluidics [3], and droplet microfluidics [40, 82]. These platforms utilize microfluidic techniques to enhance the efficiency and accuracy of AST processes.

Microfluidics AST			
Technique	Mother machine	Gradient	Droplets
Advantages	Single-cell, long-term observation.	High-throughput, small volumes, multiplexing.	Rapid, automated, single-cell, high-throughput, small volumes quantitative and qualitative results.
Limitations	Low-throughput, non continuous exposure to antimicrobials.	Low-precision in the determination of the MIC.	Difficulty to handle.
References	[7], [45]	[3], [88]	[40], [24]

Table 1.3: **Microfluidics AST techniques.** Advantages and limitations of microfluidics techniques for AST

Droplet microfluidics presents a promising technology for high-throughput, rapid, precise conduction of AST. This approach allows for studies at the single-cell level, enabling the detection of heteroresistance and the identification of persister cells and small colony variants within the bacterial population [40, 82].

The majority of current techniques involve generating droplets that encapsulate bacteria along with antibiotics.These droplets are subsequently incubated and subjected to fluorescence or marker dyes for detection and analysis [16, 89, 28]. Table 1.3 provides an overview of the advantages and limitations associated with microfluidics methods.

For instance, Zhang *et al.* introduced a platform called SCAle-AST (Single Cell Assembly Line AST) that offers full integration capabilities [89]. The platform, illustrated in Figure 1.10, involves the passage of specific picodroplet clusters containing bacteria, antibiotics, and resazurin through a dedicated 37°C incubation channel. If the encapsulated bacterium is susceptible to the applied antibiotic, it ceases to grow, resulting in the reduction of resazurin and a weak fluorescent signal. On the other hand, if the bacterium is resistant to the antibiotic, it continues to proliferate, causing resazurin to become fluorescent, resulting in a strong signal detected by a laser-induced fluorescence (LIF) detector. By comparing the fluorescence intensity of picodroplets exposed to different antibiotics, the researchers can generate an antibiogram, which provides information on bacterial susceptibility to multiple antibiotics [89].

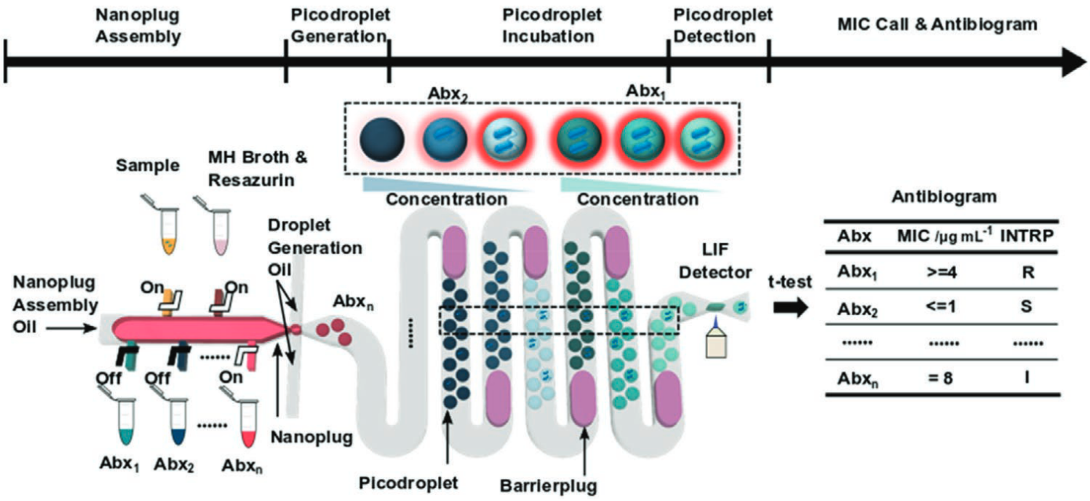

Figure 1.10: **Overview of SCALe-ASt (Single Cell Assembly Line AST.** Integrated device with programmable microvalves assambles bacteria samples, growth media, resazurin and antibiotics into groups of picodroplets encaspuling single bacteria. (from [89], Copyright 2021 Wiley-VCH GmbH).

A significant advantage of this device is the utilization of the marker dye resazurin. This obviates the need for genetically modifying cells to produce fluorescence, allowing direct use on clinical strains. However, a limitation of employing resazurin is its requirement for a certain cell count to achieve fluorescence [40]. Consequently, it is not possible to differentiate between an empty droplet (lacking any bacteria) and a droplet containing a susceptible bacterium. Although the LIF detector does not offer access to single-cell resolution, the platform can produce up to 10,000 droplets, enabling testing with numerous concentrations of different antibiotics.

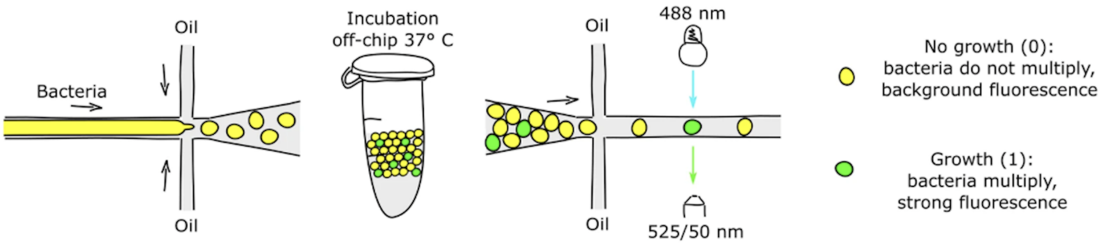

Figure 1.11: **Microfluidics workflow for the single cell droplet assay.** The aqueous phase, consisting of bacteria, growth media and antibiotics, are encapsulated in surfactant-stabilized water-in-oil droplets (adapted from [16], Copyright 2020, Scheler *et al.*).

Scheler et al. have also designed a microfluidic workflow for single-cell assays, employing a high-throughput system [16]. In this approach, they generate 10,000 nanodroplets with identical antibiotic concentrations, out of which 1,500 droplets contain bacteria. On average, each droplet accommodates approximately 0.18 bacteria. To ensure an adequate number of droplets with encapsulated bacteria, a substantial quantity must be produced. Following encapsulation, as illustrated in Figure 1.11, the droplets are incubated off the chip, allowing the bacteria within them to proliferate and synthesize YFP, unless their growth is inhibited by the antibiotic. Subsequently, the fluorescence of each droplet is measured using confocal microscopy as a readout.

Similar to the device designed by Zhang et al. (Figure 1.10), there is no initial readout available after encapsulation, making it challenging to precisely determine the exact number of cells within each droplet. Furthermore, since the droplets are incubated off the chip, it is not possible to monitor their progression over time. However, the use of confocal microscopy following incubation enables a more accurate assessment of each droplet, allowing the researchers to determine whether the bacteria are clumping or not [16].

1.5 Conclusion

This chapter introduces the concept of microfluidics and its potential applications in microbiology. Microfluidics offers numerous advantages compared to traditional methods, including improved analytical sensitivity, faster detection times, and the capability to detect single cells.

Commonly used techniques such as disk diffusion, broth dilution, and agar dilution for antibiotics susceptibility testing have advantages but require manual processing and lack automation [82, 83, 85]. Several microfluidic platforms have been developed to study microbiology questions. These platforms include the mother machine, droplet microfluidics, and other approaches. Microfluidics presents an alternative approach that can automate the process and enable high-throughput screening of antibiotics.

Microfluidics can be applied to various techniques and applications in biology, and in particular on antibiotics susceptibility testing. It has the potential to offer enhanced functionality, increased throughput, and reduced cost compared to current techniques [40, 89, 28]. Furthermore, microfluidics can improve analytical sensitivity through miniaturization and enable the detection of single cells

Still, there are challenges associated with implementing microfluidic devices in microbiology research, including device fabrication, integration with existing laboratory equipment, and data analysis [24]. Nonetheless, ongoing research and development in this field could lead to significant advancements in microbiology research.

Microfluidic devices have already shown promise beyond biomedical and chemical research. With advancements in device fabrication, integration with existing laboratory equipment, and data analysis techniques, microfluidics could revolutionize the approach to microbiology research. Compared with non-microfluidic techniques, the above microfluidic approaches produce large amounts of data that can be related to the behavior of individual cells. As such they enable investigations into the heterogeneity of outcomes from individual cells. The mother machine provides a way to observe a several thousand individual cells, for many division cycles, while controlling and even modulating their environment [7]. However this technique requires very precise microfabrication, which is dictated by the size of an individual bacterial cell. Moreover, it cannot address interactions between cells nor inheritability of specific traits.

Moreover, droplet microfluidics offers numerous possibilities for AST. However, beyond its application in susceptibility testing, the utilization of anchored microfluidic droplets in conjunction with advanced microscopy techniques allows for direct access to single-cell data by tracking the content of each droplet over time within a single device. This approach has the potential to provide both quantitative and qualitative information, going beyond traditional AST methods. Droplet methods can also yield large statistics, e.g. of the response to an antibiotic, while being based on simpler micro-fabrication. The standard droplet methods however have mainly been used to yield digital (positive vs. negative droplet) data at the end-point of an experiment [16, 89, 19]. They cannot access time-dependent phenomena, such as colony growth rates, nor do they provide access to morphological information about the cells.

In the following chapters I will describe the development of an experimental platform and analytical pipeline that use stationary droplets to obtain similar statistical power as other droplet methods, combined with access to dynamics and morphological information on the progeny of individual cells.

Key takeaway

Context: Microbiology's classical techniques, while effective, are time-consuming and operate at the population level.
Microfluidics, on the other hand, is revolutionizing biology by introducing innovative tools.
Droplet microfluidics, specifically, prove to be valuable instruments for conducting antibiotic susceptibility testing.
Problematic: How can we perform antibiotic susceptibility testing while simultaneously assessing the variability between individual cells? Can we have access to more information than just the MIC ?

Chapter 2

Developing an automated platform for high-throughput and high quality imaging of single cells

In this chapter, I will provide a global overview of the technical tools devised during my thesis to observe and analyze bacteria at various levels, ranging from single-cell analysis to population-level studies within anchored droplets. I will focus on the experimental protocol, which was developed and optimized over the initial two years of my thesis. The summarized representation of this pipeline can be found in Figure 2.1.

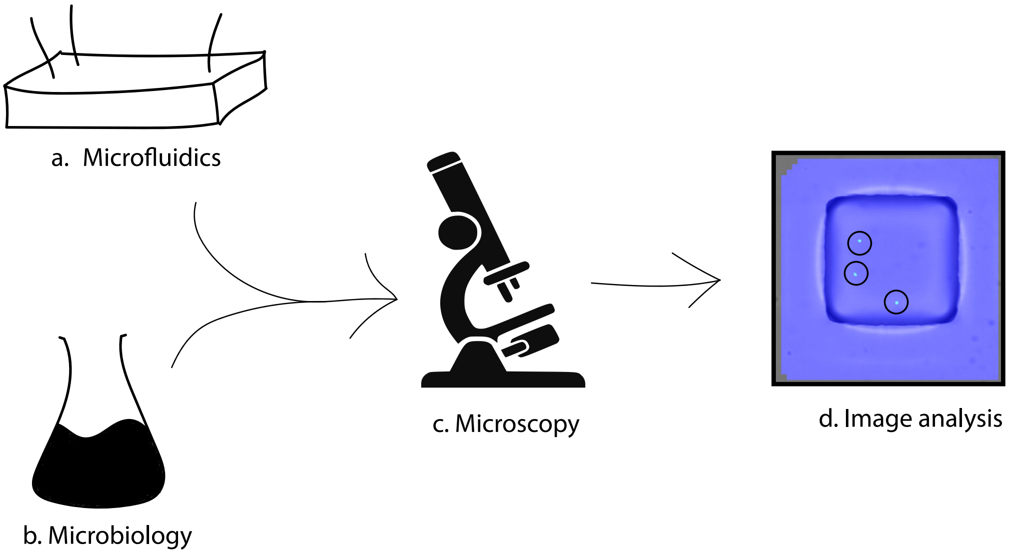

Figure 2.1: **Experimental pipeline.** Summary of the experimental pipeline, combining **(a)** microfluidics and **(b)** microbiology with **(c)** microscopy and **(d)** image analysis.

I will begin with the microfluidics aspect by describing the chip's design and the fabrication process involved in creating the mold through photoresist lithography.

Following that, I will address the aspects related to microbiology, covering topics such as bacterial strains, media selection, and antibiotics. I will also explain the procedures involved in combining microbiology and microfluidics, particularly the encapsulation of bacteria in droplets.

The third section will shed light on the chosen microscopy techniques employed to observe bacteria.

Next, I will describe the image analysis pipeline that was developed alongside the experimental protocol. This pipeline includes the registration of images and cell counting.

Lastly, I will delve into the assessment of biological compatibility concerning the microfluidic device. Additionally, I will discuss specific limitations encountered during the pipeline's development in greater detail.

2.1 Microfabrication

2.1.1 Design

Various techniques exist for fabricating microfluidic chips, utilizing different materials [90].

In our particular case, while developing the experimental protocol and the image analysis pipeline simultaneously, we designed the chip in a way that it complements the image analysis algorithm, and conversely. The chip's design and functionality were optimized to support the requirements of the image analysis process, creating a synergistic relationship between the two components.

Initially, we began by designing the microfluidic chip, building upon a previous design utilized in our laboratory [22]. The structure of the chip consisted of two layers, as illustrated in Figure 2.3. The bottom layer comprised channels featuring two inputs and one output. On the other hand, the upper layer consisted of inverted microwells, each measuring 120x120 micrometers and spaced 240 micrometers apart. These microwells were arranged in a grid formation, with 13 rows containing 39 wells for odd rows and 38 wells for even rows. The height of the channels was set to 30 micrometers, while the microwells were designed to be 130 micrometers in height.

For our modified version of the chip, we introduced several alterations. As shown in Figure 2.2, this included incorporating a total of 500 microwells, with the microwell positioned at the center of the chip rotated by 45°C. Additionally, we removed the top left microwell. These modifications were implemented to facilitate the automated alignment of the chip using the algorithm for image analysis purpose (Figure 2.10).

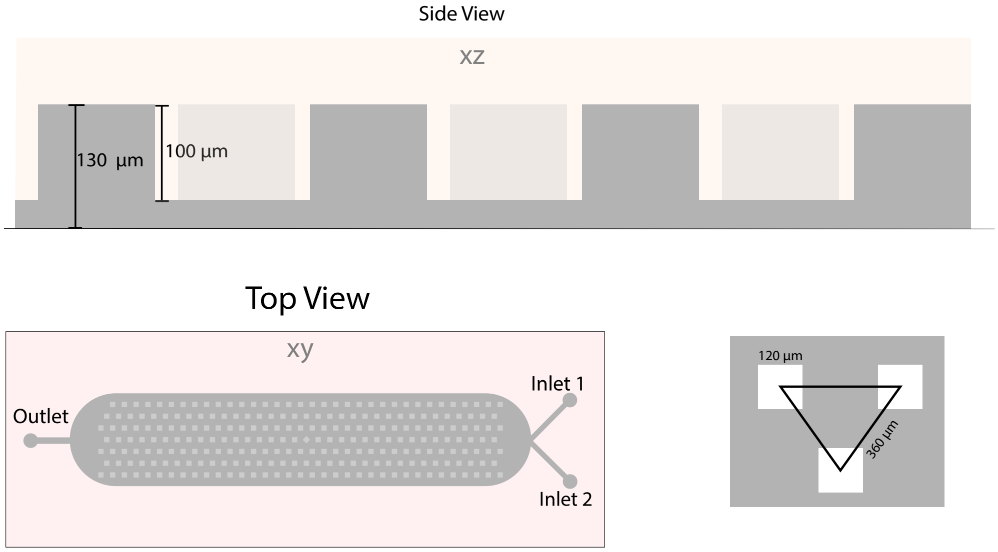

Figure 2.2: **Microfluidic chip design.** Side and top view of the chip. Each square represent an anchor, of depth 130 µm, of size 100 µm by 120 µm and at distance 360 µm. The top view includes the chip with 500 wells, 2 input channels on the right and 1 output channel on the left.

Subsequently, the two layers of the chip design were printed onto a transparency sheet, as depicted in Figure 2.3. This transparency sheet, known as the mask, was created specifically for the purpose of photoresist lithography in the fabrication process.

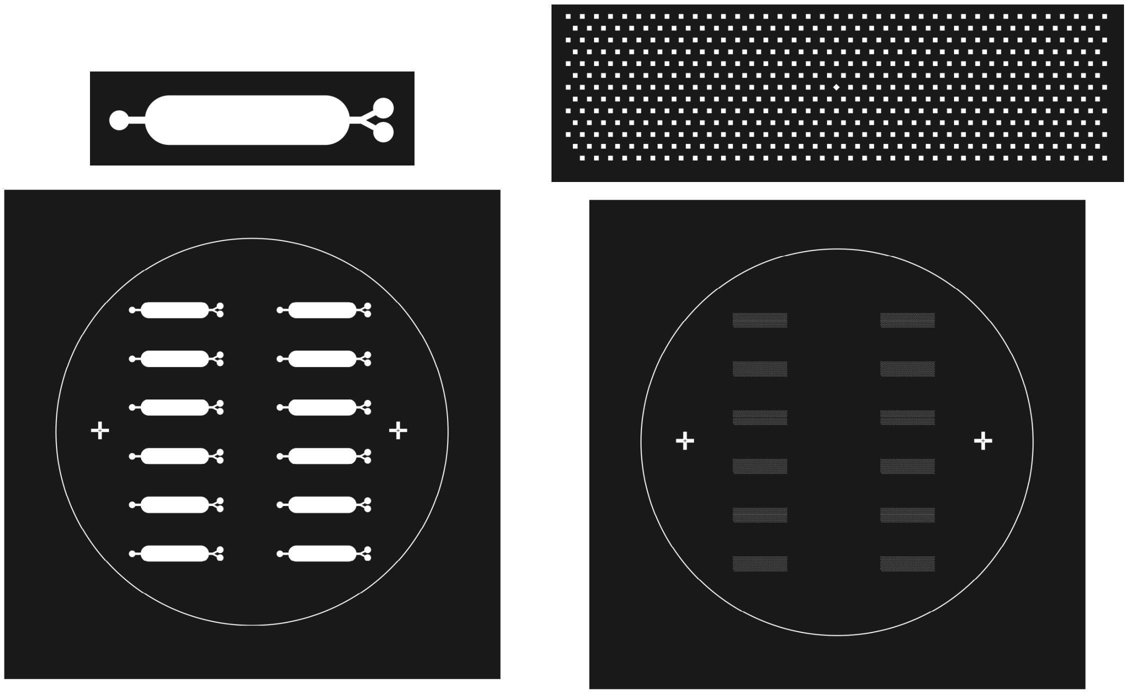

Figure 2.3: **Mask** Print of the mask used for the lithography. On the left, the first layer corresponding to the main channel, inlets and outlet of the chip (30 µm high). The top left correspond to a close up of the first layer. On the right, the second layer corresponding to the wells (100 µm high). The top right corresponds to a close up of the scond layer.

2.1.2 PDMS soft lithography

We employed a custom mold created through a two-layer SU-8 photoresist lithography process, in order to fabricate microfluidic chips for our experiments,. Lithography is a highly precise procedure that necessitates careful execution in a series of controlled steps.

The various stages of the mold fabrication process are outlined in Figure 2.4. First, the glass wafer, serving as our substrate surface, was thoroughly cleaned using isopropanol and subjected to heating at 180°C for 15 minutes to eliminate any moisture.

Next, the SU-8 resin was spin-coated onto the wafer. The choice of resin viscosity was predetermined based on the desired height (see Table 2.1 for the information). In our case, the first layer, which corresponds to the height of the microfluidic channels (Figure 2.2), was 30 micrometers thick and we used the resin SU-8 2025. The second layer, corresponding to the depth of the microwells (Figure 2.2), measured 100 micrometers and we used the resin SU-8 2100. The rotation speed and acceleration during the spin-coating step were also considered to achieve the desired resin layer thickness (Table 2.1).

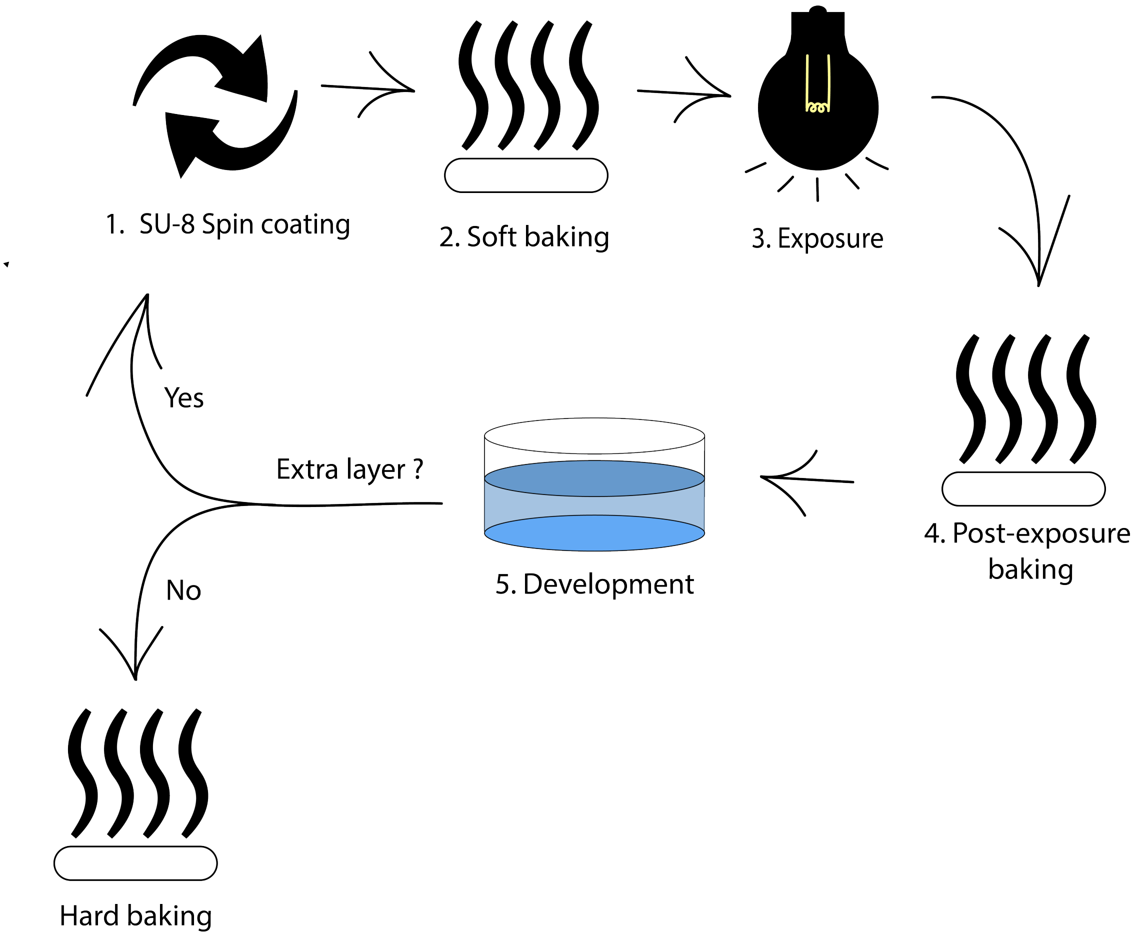

Figure 2.4: **SU-8 mold fabrication process**. The required steps for lithography: spin coating, soft baking, post exposure baking, development and hard baking

Prior to exposing the SU-8 resin to light, a soft bake was performed to evaporate the solvent. Subsequently, the exposure step was carried out to induce cross-linkage. The photoresist can be either positive or negative, and in our case, the SU-8 resin acted as a negative photoresist: the areas exposed to UV light through the mask became cross-linked and hardened. After the post-exposure baking, the unexposed areas were dissolved by Propylene glycol methyl ether acetate during the development process. The post-exposure baking step is essential as it continues the resin hardening process and enhances its adhesion to the wafer.

Following this, the process was repeated for the second layer of resin to shape the microwells. Finally, a hard baking step was performed to complete the resin hardening process.

	First layer	Second layer
Height	30 µm	100 µm
Type of resin	SU-8 2025	SU-8 2100
Spin coating speed	3000 rpm	3000 rpm
Soft Bake	1min30 at 65°C + 5min30 at 95°C	5min at 65°C + 20min at 95°C
Exposure time	15 seconds	24 seconds
Post exposure baking	1min 65°C + 5min30 at 95C°	5min at 65°C + 10min at 95°C
Development time	4min30	10min

Table 2.1: **Lithography information** Specific speed, times and resins for the fabrication of the mold of our micrfluidic chip

The detailed procedure is available in the appendix 6.1.1.

2.1.3 Microfluidic Chip Production

Polydimethylsiloxane (PDMS) was employed for the microfabrication process. PDMS is an elastomer that offers several advantages for use in microfluidic devices. It can be molded with high resolution, reaching scales as small as a few nanometers, and it possesses optical transparency [91].

From a biological perspective, PDMS is particularly interesting due to its biocompatibility [92]. First, it exhibits sufficient porosity to facilitate gas exchange necessary for cell culture within the chip [17]. Second, it demonstrates deformability. This property enables the establishment of leakproof fluidic connections between microchannels [90].

A mixture of PDMS and its curing agent, PDMS SYLGARD 184 from Dow Corning, is prepared by combining them in a 1:10 ratio of curing agent. This mixture is then poured into the mold created through lithography. To remove any air bubbles, the mold is placed in a vacuum chamber for 30 minutes. Subsequently, the PDMS is cured at a temperature of 70°C for 3 hours. Once the PDMS is fully cured, the chip is carefully separated from the mold. To create a sealed microfluidic device, the chip is plasma bonded to a coverslip using the CUTE Plasma system from Femto Science (refer to Figure 2.5). The detailed procedure is available in the appendix 6.1.2.

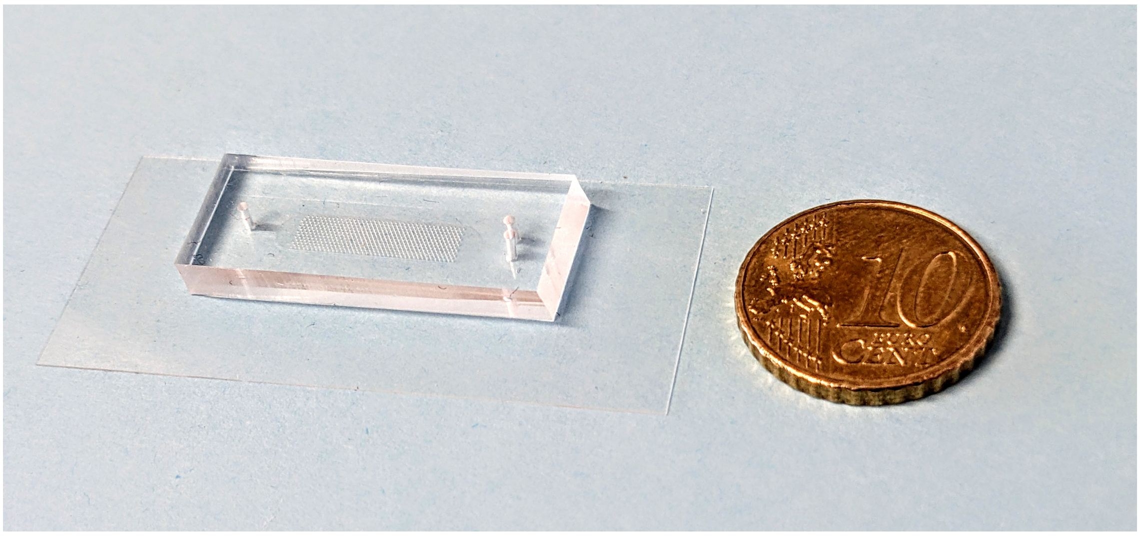

Figure 2.5: **Microfluidic chip** Size comparaison of the microfluidic chip.

While PDMS offers excellent biocompatibility, there are certain limitations that can restrict its use in certain biological applications. One drawback is its permeability, which allows for gas exchange but can also result in water evaporation through diffusion across the PDMS material [93]. This evaporation can lead to complete drying of the chip or alterations in the osmolarity of the medium. However, this issue can be mitigated by carefully managing and maintaining humidity levels in the surrounding environment. One approach, for instance, involves immersing the chip in water during the incubation period or utilizing a humidity chamber.

2.1.4 Hydrophobic treatment, surfactant and oil

PDMS has the tendency to absorb small molecules present in the solution through diffusion due to its porous nature [90]. To mitigate this issue, it is important to avoid direct contact between the aqueous phase of the droplets and PDMS. In our approach, we utilize fluorinated oil (FC40) and a biocompatible fluorinated surfactant (008-FluoroSurfactant provided by RAN Biotechnologies) to form the droplets.

Fluorinated oils possess hydrophobic and lipophobic properties, minimizing or eliminating the solubility of biochemical compounds and their diffusion between neighboring droplets. This significantly reduces the risk of cross-contamination among droplets [94]. Moreover, due to the biologically inert surface within the water droplets, these oils are biocompatible [95]. They also allow for gas exchange, which is essential for long-term aerobic growth and proliferation within the droplets [17]. They are also compatible with most materials, including PDMS, unlike mineral or silicone oils that cause swelling and leaking of microchannels [95].

In addition to the oil, a biocompatible surfactant (008-FluoroSurfactant) is employed to stabilize the droplets.

To prevent wetting and achieve highly fluorophilic microfluidic chips, all the chips undergo treatment with a hydrophobic solution (NOVEC 1720 surface modifier/electronic grade coating, 3M).

However, it is important to consider the environmental impact of fluorinated compounds. Due to their contribution to greenhouse gas emissions, particularly fluorinated greenhouse gases (F-gases), the EU green deal has set ambitious goals to reduce such emissions significantly [96]. Consequently, the production of fluorinated compounds has ceased, necessitating the exploration of alternative biocompatible options.

2.2 Microbiology

2.2.1 Cell culture, media and antibiotic

Strain

The strain used in this study is *E. coli* W3110 with a fluorescent reporter in the ptac site (ptac::RFP) inducible by IPTG. The Red Fluorescent Protein (RFP) is used as a reporter for cellular growth and division.

Media

In our study, we employed two distinct types of media: MOPS and LB. MOPS Minimal Media is specifically formulated for the cultivation of enterobacteria, such as *E. coli*, under minimal conditions. It supplies only the essential nutrients and energy sources necessary for bacterial growth, including potassium phosphate (K_2HPO_4), glucose, and magnesium sulfate ($MgSO_4$). This medium proves valuable for investigating bacterial growth, protein synthesis, and other metabolic processes under simplified conditions, as it lacks many of the intricate components present in richer media like LB medium [97].

LB medium, known as Lysogeny broth or Luria-Bertani medium, is a nutrient-rich medium widely utilized for bacterial cultivation, particularly *E. coli.* The primary constituents of LB medium typically encompass sodium ions for transport and osmotic balance, tryptone for providing crucial amino acids, and yeast extract for supplying various organic compounds that support bacterial growth [98].

Antibiotic Solution

Ciprofloxacin (Sigma-Aldrich) was solubilized in MilliQ 0.1 N HCl (Sigma-Aldrich) at 25 mg/mL. The stock was then diluted with MilliQ water to 1 µg/ml.
Tetracyclin (Sigma-Alrich) was solubilized in MilliQ water at 50mg/mL. The stock was then diluted to 1mg/mL.
Chloramphenicol (Sigma-Aldrich) was solubilized in ethanol at 10mg/mL. The stock was then diluted with MilliQ water to 5mg/mL.
Gentamicin (Sigma-Aldrich) was solubilized in MilliQ water at 50mg/mL. The stock was then diluted with MilliQ water to 5mg/mL.

Cell culture

In each experiment we want to work with a population of cells that is monoclonal, i.e. of a single clone. To do so, starting from the -80°C stock, the cells were streaked onto an LB agar plate and left to incubate overnight at 37°C. The following day, a single isolated colony was selected and inoculated into the culture medium. IPTG was added at a concentration of 0.05 mM to induce the expression of the RFP. The bacterial suspension was then incubated overnight at 37°C with shaking. Then the bacterial suspension was diluted into fresh media with IPTG and incubated at 37°C with shaking until exponential phase was reached.

For the experiments, supplemented minimal media (MOPS) with a final glucose concentration of 0.4% and Lysogeny Broth (LB) were used.

Cell dilution

To be able to observe bacteria at the individual cell level, it is necessary to isolate only one or a small number of cells within each droplet. Prior to the loading process, we can adjust the concentration of cells in the bacterial solution based on the measurement of optical density. In order to determine the appropriate optical density, which corresponds to the correct dilution and consequently the desired number of cells per droplet, a calibration process is conducted.

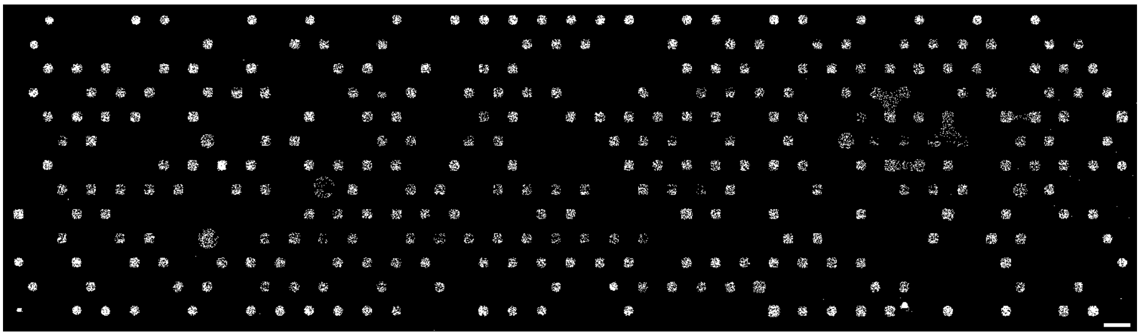

Figure 2.6: **Microfluidic chip in fluorescence channel** Fluorescent image of a chip after an overnight incubation used for cell calibration (scale bar 300 µm) showing empty and non empty droplets.

To achieve a targeted range of one to five cells per droplet, the optical density of the solution was calibrated by measuring it at 600nm. The calibration process involved the following steps: The known calibration was obtained through digital counting. The chip was loaded with a diluted bacterial suspension without antibiotics, incubated overnight at 37°C, and subsequently imaged (Figure 2.6). The empty wells were counted, and based on the assumption that a well can only be empty if no cells were loaded, the initial loading parameter λ was calculated. λ represents the Poisson parameter, which corresponds to the average number of cells per droplet. It can be estimated by computing the fraction $\frac{N_{(-)}}{N_{total}}$ of empty to total droplets and using the relation :

$$\lambda = \ln\left(\frac{N_{(-)}}{N_{total}}\right). \tag{2.1}$$

where $N_{(-)}$ is the number of negative droplets and N_{total} is the total number of droplets. λ is monitored by the concentration of the bacterial suspension and directly linked to the optical density. The Poisson distribution implies that λ also corresponds to the mean number of cells per droplet. Hence, a higher value of λ means that initially the droplets contain more cells on average.

Using this calibration, an adjusted optical density of 1.10^{-3} corresponds to a $\lambda = 2.28 \pm 1.28$ cells/droplet.

2.3 Loading

The chip was specifically designed to generate anchored droplets using the "breaking method." The loading procedure was optimized to ensure it was both quick and straightforward.

As illustrated in Figure 2.7, the chip is initially filled through the first input with a continuous oil phase consisting of 3M Fluorinert FC40 mixed with a non-ionic surfactant (RAN fluoSurf) at a final concentration of 1%. During this process, air bubbles are carefully purged using syringe pumps (NEMESYS). Subsequently, the bacterial suspension is introduced through the second input, replacing the continuous oil phase. Finally, the continuous oil phase is reintroduced at a very low flow rate (5 µl/min) to break the droplets apart and secure them within the wells. The entire chip loading process typically takes a few minutes. It is crucial to ensure that no air bubbles are present in the chip, as even a small trapped bubble can expand and disrupt the integrity of the droplets. The complete procedure is available in the appendix 6.1.2.

The loading procedure is resilient to variations in flow rate, making it robust. Therefore, in laboratories with stricter biosafety requirements or limited equipment setup, the loading process can be performed without the use of syringe pumps.

2.4 Microscopy

2.4.1 Optics

During the image acquisition process, we capture images from the bottom of the chip, where the droplet is in contact with the glass coverslip (refer to Figure 2.8). We use a spinning disk confocal microscopy coupled with a positioning system that employs piezoelectric actuators (NIDAQ piezo Z) to control Z-axis movement to image the droplet. This enables us to achieve both speed and precision in acquisition. Indeed, imaging the entire droplet volume comes with specific requirements. First, three-dimensional imaging is necessary, which requires precise acquisition with the focal plane traversing through the entire volume (Figure 2.8). Second, since the bacteria within the droplet are in a live state and exhibit movement, bacteria swim at 50 µm/sec, rapid imaging in the Z-axis is essential.

Compared to widefield or confocal microscopy, spinning disk confocal microscopy, as illustrated in Figure 2.8, allows for simultaneous illumination of the sample while eliminating out-of-focus signal interference [61]. By combining this technique with the piezo Z device, we can swiftly move the focal plane through the Z-axis within a few seconds, effectively scanning the entire droplet.

All microscopy images were captured using a spinning disk confocal microscope (Nikon Ti2 + Yokogawa). A 20x 0.7 NA air objective lens from Nikon Inc. was employed, and a 2x2 pixel binning was applied directly through the camera properties (Hamamatsu Orca 4). To obtain images of the entire chip, images were stitched together with a 5% overlap.

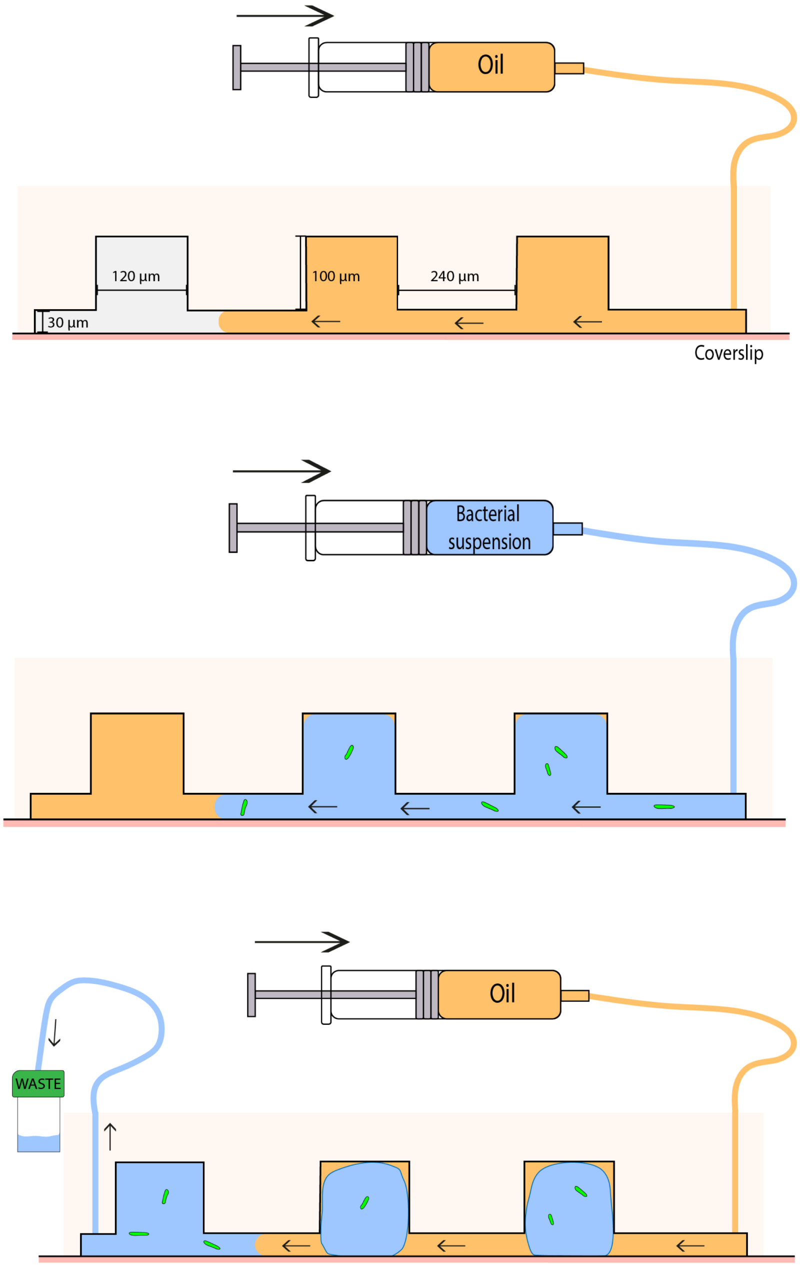

Figure 2.7: **Chip loading.** **(a)** Side view of the chip (not to scale), showing the channel height c=30 µm and anchor depth d = 100 µm. The loading protocol begins by filling the chamber with oil, then **(b)** replacing the oil with bacterial suspension, and **(c)** breaking the bacterial suspension into individual droplets anchored to the wells in PDMS.

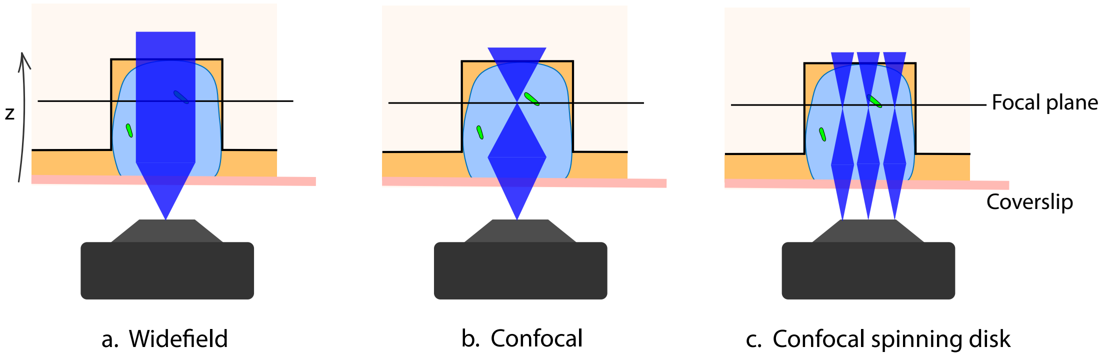

Figure 2.8: **Different microscopy techniques (a)** Widefield microscopy. **(b)** Confocal microscopy. **(c)** Spinning disk confocal microscopy. In blue, the laser excitation. In green, the bacteria.

2.4.2 Image acquisition

The imaging process involves acquiring a two-dimensional bright-field image of the complete chip. Subsequently, a three-dimensional fluorescence channel image is obtained. Z-plane images are captured with a step size of 5 µm with a total penetration of 120 µm, resulting of 25 images for each XY position. The piezo Z device facilitated precise control of microscope focus in all three dimensions. With the assistance of a fast Z drive, the entire droplet could be scanned, ensuring that no moving cells were missed. All the microscopy settings can be found in the appendix 6.1.5.
The device's total area measures approximately 1.4 by 0.4 mm, resulting in a dataset length of 4 million pixels with a pixel size of 350 nm. However, some chips may exhibit tilting due to manual bonding, which increases the required scanning area, resulting in larger images.

Initially, the acquisition protocol involved imaging one chip at a time, which took approximately an hour for capturing bright-field and fluorescence channel images. To enhance throughput, a 3D-printed chip holder capable of accommodating up to 6 chips (Figure 2.9) was introduced. Bright-field and fluorescence imaging are performed independently. Bright-field imaging is done first only in the XY plane. Then fluorescence imaging is done with priority given to acquiring the Z-stack using the NIDAQ Piezo Z device, followed by XY positioning. With this approach, imaging six chips now takes around 10 minutes for bright-field acquisition and about an hour for fluorescence acquisition. By employing two holders and factoring in loading time, we can now image up to 12 chips within approximately 3 hours. This significant reduction in loading and acquisition time has decreased the overall process from 10 hours to 3 hours.

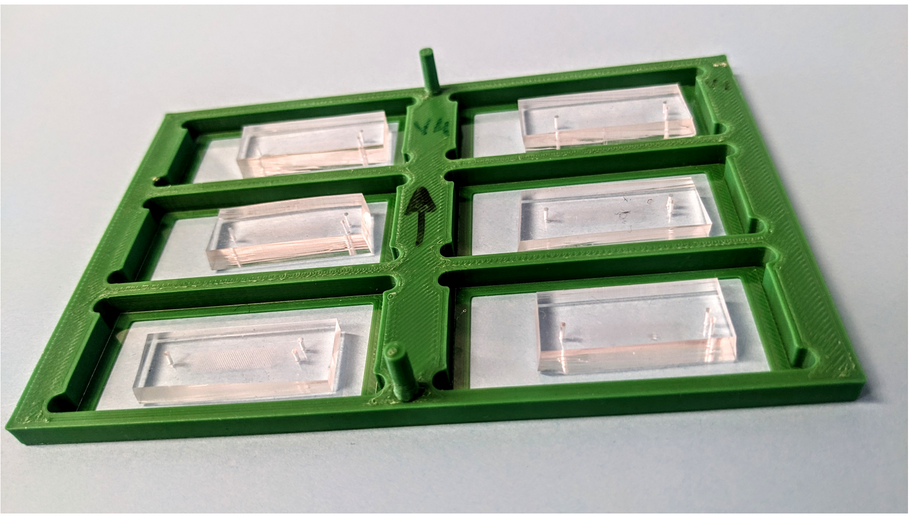

Figure 2.9: **Chip holder** 3D printed chip holder that can hold up to 6 chips

2.5 Image analysis

2.5.1 Image registration

After image acquisition, two separate files are generated for each condition: one for the bright-field channel (2D) and one for the fluorescence channel (3D). The 3D file of the fluorescence channel is converted into a 2D fluorescent image by applying max projection along the Z-direction (Figure 2.10 b.).

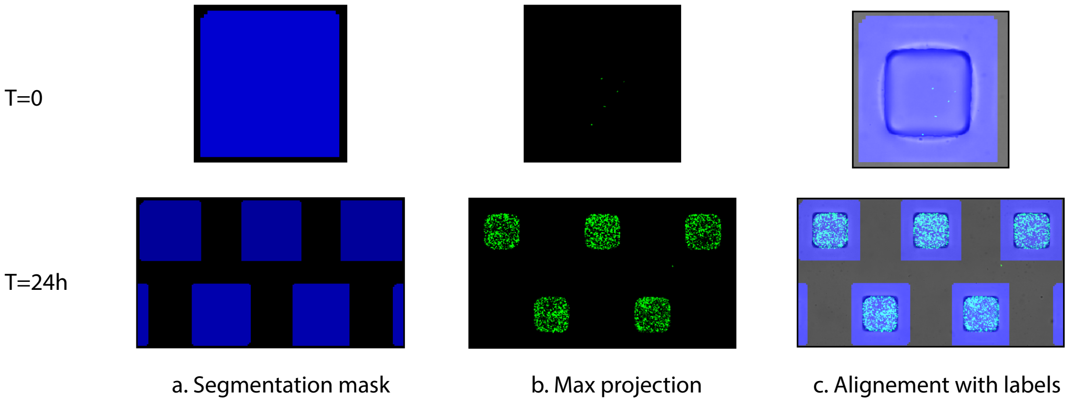

a. Segmentation mask

b. Max projection

c. Alignement with labels

Figure 2.10: **Image registration.** Immediately after the loading (T=0) and after an overnight incubation (T=24h) each chip is imaged in bright-field and using a stack of confocal images. **(a)** The bright-field image is used to identify the alignment for the microscope stage and to create a unique mask (in blue) around the positions of individual anchors.**(b)** The fluorescent image is converted in a 2D image using max projection and **(c)** align with the template image and segmentation mask

Simultaneously, a ”template image” is created from the 2D bright-field image using a homemade python script (Appendix 6.2.1). It consists in taking the 2D bright-field image and labelling each well with a number corresponding to the XY coordinates of the well’s center.

Additionally, a ”segmentation mask image” is generated. Using the 2D bright-field image, each region corresponding to the labeled wells is partitioned and registered as a segmentation mask (Figure 2.10 a). The mask area is defined by a 300 µm square centered at the middle of the well.

The template and segmentation mask are then aligned with the 2D fluorescent image (Figure 2.10 c.), merged together, and saved as a tif stack. The alignment process is performed by the algorithm utilizing the chip's geometry and orientation.

For visualization purposes, Napari, a Python-based multi-dimensional image viewer, is employed (Figure 2.11). Napari offers features for browsing, analyzing, and annotating large multi-dimensional images.

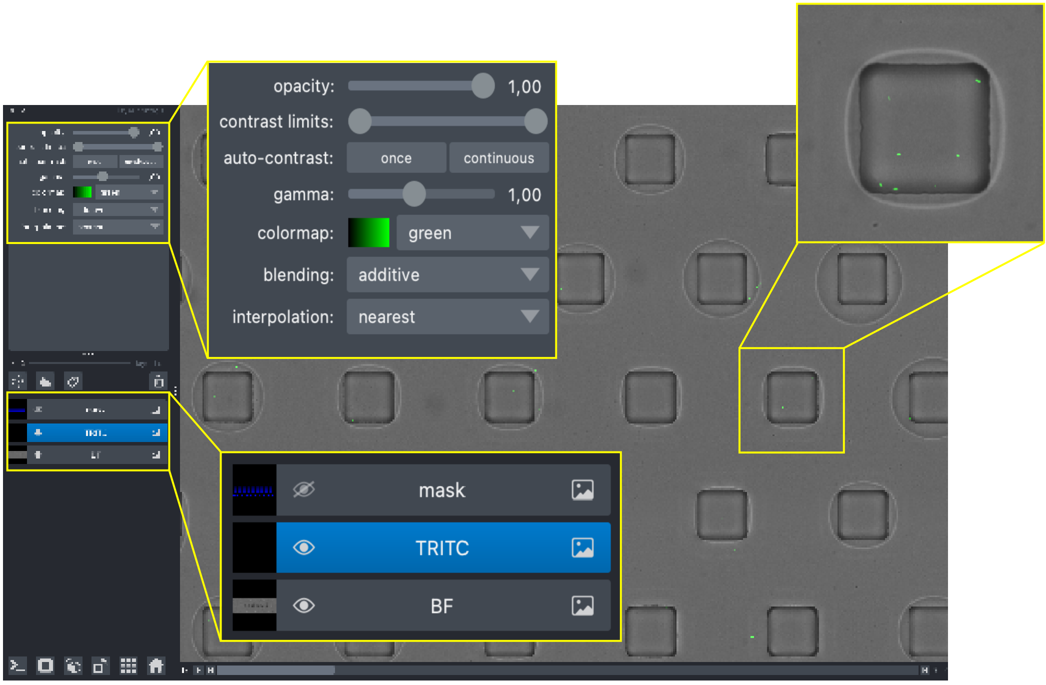

opacity: 1,00
contrast limits:
auto-contrast: once continuous
gamma: 1,00
colormap: green
blending: additive
interpolation: nearest

mask
TRITC
BF

Figure 2.11: **Napari viewer** Visualisation of the chip in Napari. Bright-field and fluorescence channel are aligned. In each channel the contrast and color can be modified.

The aforementioned registration steps are specifically designed for time point experiments, where image acquisition is conducted after loading and overnight incubation. However, they can be adapted for different scenarios. For instance, time-lapse microscopy can be employed to capture time-resolved measurements on the chips. Similarly, confocal imaging can be utilized at later time points to obtain more precise cell counts, fluorescent intensity measurements, or to examine cell morphology in specific cases. While these situations may require minor modifications to the pipeline, the core elements of the analysis can still be used in a modular manner.

2.5.2 Counting the cells in the droplets

Following image registration, each droplet is associated with the corresponding labeled area defined by the segmentation mask. We use a gaussian filter followed by peak detection to detect individual the fluorescent bacteria. The Gaussian filter is applied to mitigate false detections caused by noise. Peak detection is done using the Scipy function peak_local_max. The number of peaks per label is then recorded in a table for further analysis.

The ability to acquire and analyze large volumes of imaging data is necessary for obtaining antibiotic response curves that are resolved at the single-cell level. While the microfluidic format facilitates measuring droplet contents at different time points, the necessity of detecting single cells at early stages necessitates high-resolution imaging. Consequently, managing a large number of experiments poses challenges in terms of data handling. To address these constraints, we developed an automated imaging and analysis pipeline that played a important role in achieving the results presented here. These pipelines encompass both confocal and epi-fluorescence imaging techniques, along with algorithms for identifying droplet contents and establishing the relationship between initial and final states of individual droplets. The image and data analysis pipelines are openly available as open-source packages in the GitHub repository: `https://github.com/BaroudLab/anchor-droplet-chip`.

The objective of the pipeline is to generate a table that contains information about each droplet, including a unique label, the antibiotic concentration, the initial cell count, and the final state of the droplet. The process of generating this table begins immediately after loading the chip to capture the initial state of each droplet. Although the droplets are organized in a regular matrix corresponding to the positions of the anchors, each chip may experience arbitrary rotation and linear shift during the cutting and bonding of the PDMS chips. To align the fluorescence image with a template that indicates the labeled positions of the droplets, an initial correction for shift and tilt is applied, leveraging the known anchor arrangement (refer to Figure 2.10 c).

a. Napari visualisation

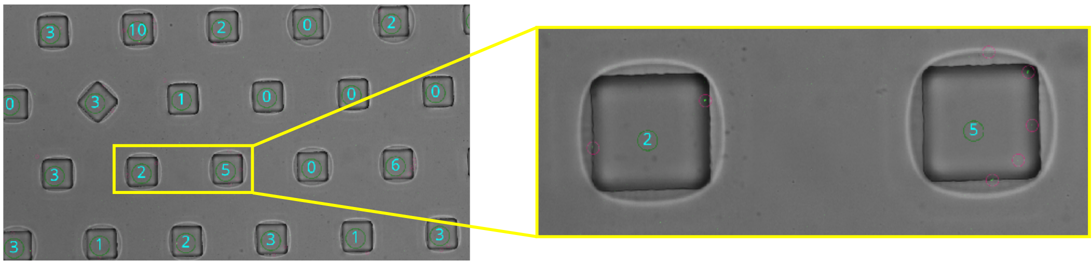

b. Final table

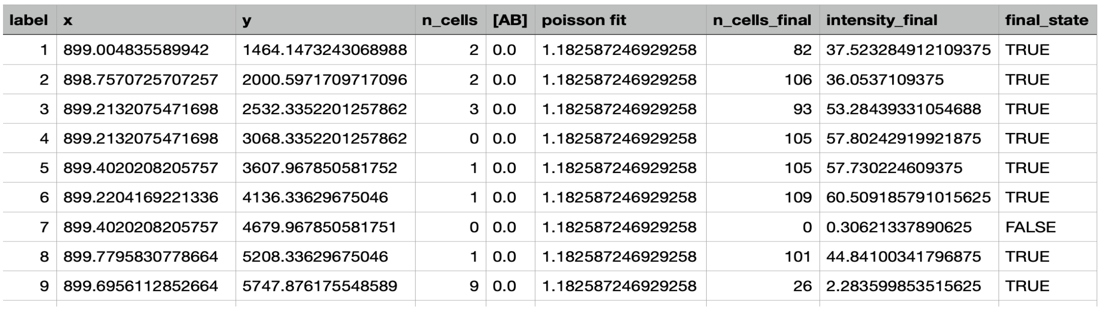

label	x	y	n_cells	[AB]	poisson fit	n_cells_final	intensity_final	final_state
1	899.004835589942	1464.1473243068988	2	0.0	1.182587246929258	82	37.523284912109375	TRUE
2	898.7570725707257	2000.5971709717096	2	0.0	1.182587246929258	106	36.0537109375	TRUE
3	899.2132075471698	2532.3352201257862	3	0.0	1.182587246929258	93	53.28439331054688	TRUE
4	899.2132075471698	3068.3352201257862	0	0.0	1.182587246929258	105	57.80242919921875	TRUE
5	899.4020208205757	3607.967850581752	1	0.0	1.182587246929258	105	57.730224609375	TRUE
6	899.2204169221336	4136.33629675046	1	0.0	1.182587246929258	109	60.509185791015625	TRUE
7	899.4020208205757	4679.967850581751	0	0.0	1.182587246929258	0	0.30621337890625	FALSE
8	899.7795830778664	5208.33629675046	1	0.0	1.182587246929258	101	44.84100341796875	TRUE
9	899.6956112852664	5747.876175548589	9	0.0	1.182587246929258	26	2.283599853515625	TRUE

Figure 2.12: **Final output** The output of the pipepline provides **(a)** a Napari file with the number of cells in each droplet and **(b)** a table with information on each droplet before and after incubation.

The output obtained (Figure 2.12) provides a Napari file with the number of cells in each droplet and a table with the label of each well, the XY coordinates of the center of each well, the antibiotic concentration, the average number of cell per droplet λ , the cell count within each droplet at the beginning of the experiment, the cell count at the end of the experiment, the intensity in each droplet at the end of the experiment, the final state of each droplet.

The algorithm employed in the pipeline, called 'Anchor'(6.2.1), has proven to be robust enough to perform unsupervised automated analysis of the data from the chips. Various quantities can be derived from the final image as indicators of the cells' ability to grow within the droplet. This includes the fluorescence intensity of the droplet in the final image, the mean fluorescence intensity, or the number of cells per droplet. The main requirement is that these measurements enable a reliable distinction between positive and negative droplets.

2.6 Validity of the microfluidic device

2.6.1 Biology compatibility

Prior to utilizing the microfluidic device for various biological applications, we conducted a benchmarking process to assess the bacterial fitness within the device compared to a standard multiwell plate experiment. This benchmarking procedure involved monitoring the fluorescent intensity within the droplets using time-lapse epifluorescence microscopy. Simultaneously, we performed a standard growth curve measurement on a fluorescence plate reader using the same batch culture. By comparing the results obtained from both approaches, we were able to evaluate the performance and reliability of the microfluidic device for our intended applications.

We loaded cells at various dilutions ranging from 500 to 500,000 cells per well of volume 200 µl to characterize the growth of cells in 96-well plate,. Subsequently, the plate was placed in a Thermo Scientific Varioskan LUX plate reader and incubated at 37°C with shaking for a period of 24 hours. Measurements of optical density at 600 nm and RFP fluorescence signal (excitation at 488 nm and emission at 520 nm) were taken at 10-minute intervals throughout the incubation period.

Concurrently, cells were loaded into the microfluidic chip with an average λ value of one, indicating an average of one cell per droplet of volume 2 nl. The chip was then positioned under a microscope, and the RFP signal was measured every 30 minutes. This allowed for the monitoring of fluorescence changes within the individual droplets over time.

Figure 5.3 a illustrates the growth curves for the two scenarios. In the case of the microfluidic device, the curves exhibit significant variability among individual cells, which can be attributed to variations in the initial number of cells and inherent cell-to-cell variability [99]. Conversely, the growth curves obtained from the multiwell plate experiments display a reproducible and regular growth pattern, as they are less influenced by these stochastic factors. Despite these differences, fitting the individual growth curves using a Gompertz function ($f(t) = ae^{-be^{-ct}}$, commonly employed for growth kinetics analysis [100]), reveals that the extracted growth rates (set by c) are statistically indistinguishable between the microfluidics and multiwell plates, as depicted in Figure 5.3b. This consistency in doubling times provides an initial benchmark indicating that the results obtained from the microfluidic device can be compared to standard microbiology techniques.

It is important to note that while the growth rate remains the same, the carrying capacity may differ. Indeed, the microfluidic device and a 96-well plate differ

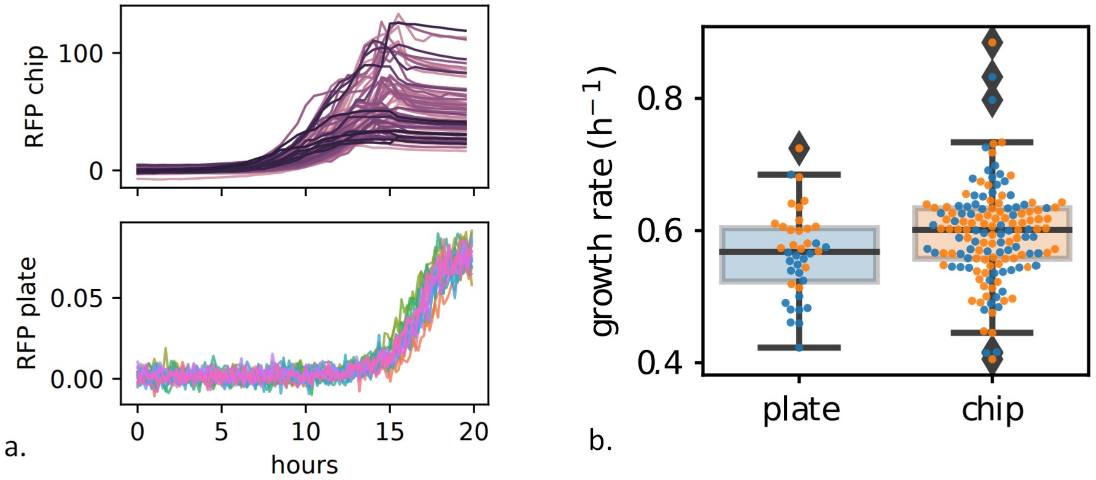

Figure 2.13: **Comparing growth conditions (a)** Growth curves in the individual droplets on the chip and in a 96-well plate. **(b)** Measured growth rates for the microfluidic chip and the 96-well plate (2 replicates each), obtained by fitting a Gompertz function to the growth curves.

significantly in terms of volume. While a droplet in the microfluidic device contains only 2 nl, each well in the 96-well plate can hold up to 200 µl. This disparity in volume can lead to variations in the availability of nutrients and space.

2.6.2 Microscopy and algorithm limitations

Comparing the process data from the image analysis directly to the images, we noticed that some wells with no bacteria detected at T=0 were positive after 24 hours incubation. That led us to think of two explanations. First, the algorithm might make a mistake in the counting of the cells. Second, this error come from the image acquisition.

Looking a bit closer at the images, we noticed that some cells were located on the edge of the wells and that the mask around the anchor was too small. We corrected that by adding a few pixels to each mask so no cells were missed in the counting. Despite this, droplets that are thought to be negative sometimes still produce a signal, i.e. we do not observe every cell present and there is a detection error.

To overcome this detection error we introduce new quantities :

- p_n as the probability of having n initial cells.
- $\tilde{p}_n$ as the probability of observing n initial cells.
- $\tilde{p}_{n|m}$ as the probability of observing n cells when there are m cells.

If we assume that every cell is independently detected with probability ρ we have a Binomial distribution for the number of observed cells, under the condition that a given number of cells are present. This means :

$$\tilde{p}_{n|m} = \begin{cases} \binom{m}{n}\rho^n(1-\rho)^{m-n} & , n \leq m \\ 0 & , n \geq m \end{cases} \tag{2.2}$$

Hence, in this model, we can not observe more cells than those that are present. For the number of observed cells we obtain if p_n is indeed Poissonian i.e. $p_n = e^{-\lambda}\frac{\lambda^n}{n!}$:

$$\begin{aligned}\tilde{p}_n = \sum_{m=0}^{\infty} \tilde{p}_{n|m} p_m &= \sum_{m=0}^{\infty} \binom{m}{n} \rho^n (1-\rho)^{m-n} e^{-\lambda} \frac{\lambda^m}{m!} \\ &= e^{-\lambda} \frac{\rho^n \lambda^n}{n!} \sum_{m=0}^{\infty} (1-\rho)^{m-n} \frac{\lambda^{m-n}}{(m-n)!} \\ &= e^{-\lambda} \frac{\rho^n \lambda^n}{n!} e^{\lambda(1-\rho)} = e^{\lambda\rho} \frac{(\lambda\rho)^n}{n!}\end{aligned} \tag{2.3}$$

Thus, the number of initially observed cells is Poissonian distributed with parameter $\lambda\rho$. If we estimate λ from the number of observed cells, we actually estimate $\lambda\rho$ and as a consequence, it is not as direct to assume cells behave independently in the droplets.

2.6.3 Initial cell distribution

We assumed that the initial number of cells in the droplets was following a Poisson distribution [22]. Hence, we assume the probability of having n initial cells per droplet, p_n :

$$p_n = e^{-\lambda} \frac{\lambda^n}{n!} \tag{2.4}$$

The mean value and the variance of this distribution is λ.

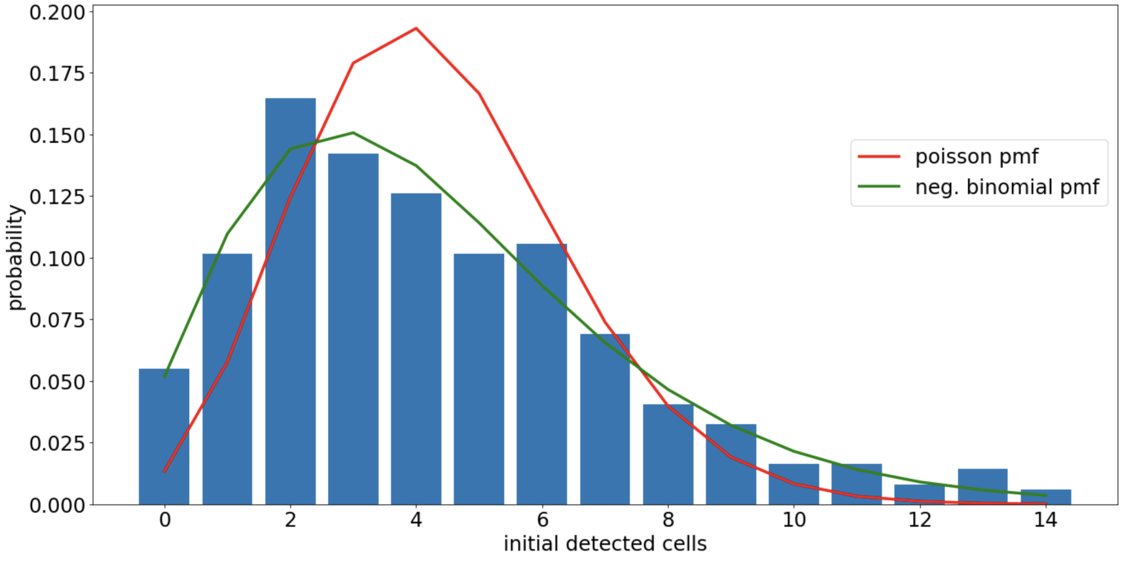

Figure 2.14: **Initial cells distribution** Example of a distribution for initial cells per droplet with a Poisson distribution fit in red and a Negative-Binomial distribution fit in green.

At first sight, the Poisson distribution seemed to be a good fit, but we noticed that it most of the time was deviating from the observed distribution of the cells (Figure 2.14).

But if we consider that λ is not fixed but is itself a random variable, the initial number of cells per droplet follows a Negative-Binomial distribution 2.14. This implies that λ is distributed as a Gamma distribution with mean λ and variance ν,

$$p_n = \frac{\Gamma(r+n)}{n!\Gamma(r)} \left(\frac{\lambda}{\lambda+\nu}\right)^r \left(\frac{\nu}{\lambda+\nu}\right)^n \tag{2.5}$$

With $r = \frac{\lambda^2}{\nu}$. The mean value is now λ and the variance is $\lambda + \nu$. The variance can also be written as $\lambda(1 + \frac{\lambda}{r})$ from which we see that in the limit of large $r = \frac{1}{\frac{\nu}{\lambda^2}}$, the distribution becomes Poissonian. This variability in λ needs to be further investigated but it could be due to the volume variability of the droplets, the fluctuation in the concentration of cells (clumping happening before the loading), or to the detection of the cells.

2.7 Conclusion: the anchored droplet microfluidic pipeline

This chapter presents a comprehensive experimental and analytical pipeline designed to explore dynamic and statistical characteristics of individual cell progeny within stationary microfluidic droplets. The experimental components encompass an enhancement of previous microfluidic designs and protocols. Additionally, confocal microscopy is employed to capture high-resolution, single-cell images of *E. coli* within the droplets. The analysis involves identifying each droplet within the acquired images and extracting cell count and fluorescence intensity measurements at the beginning of the experiment and at subsequent time points. The use of anchored droplets facilitates the correlation of different time points for each individual droplet. To ensure the reliability of the setup, it was benchmarked against standard microbiology protocols, demonstrating that it does not introduce any artifacts that could affect colony growth.

In the upcoming chapters, I will demonstrate how this setup can be utilized to assess the susceptibility of individual cells within a monoclonal population to antibiotics at the single-cell level.

Key takeaway

Context: Numerous microfluidics tools have been developed to explore the individual cellular response to antibiotics or to facilitate rapid antibiogram testing. However, there is currently no device available that enables high-throughput screening of antibiotics at an actual single-cell resolution.
Results: I have developed a microfluidic device that allows bacterial colonies to grow. This device can accommodate up to six different conditions simultaneously, with each condition having 500 replicates. The experimental process includes automated image analysis and can be customized for time-based experiments or time-lapse studies.

Chapter 3

Measuring Antibiotics Susceptibility

In this chapter, we will explore a specific application of our microfluidic device: antibiotic susceptibility testing. The initial section will provide an introduction to the significance of studying antibiotic susceptibility and, more importantly, why it is crucial to examine it at the single-cell level.

The subsequent section will begin by presenting the concept of a digital antibiogram and how we can utilize it to define the minimum inhibitory concentration (µf·MIC). We will then compare this novel measurement with existing conventional methods employed in antibiotic susceptibility testing.

The following section will focus on investigating single-cell susceptibility, which is made possible through the utilization of our anchored droplet system. This approach allows us to obtain measurements at the individual cell level, providing valuable insights into the heterogeneous nature of antibiotic response.

Lastly, we will delve into the qualitative aspects of our findings. Through the implementation of time-lapse microscopy, we will demonstrate how our approach not only provides quantitative results but also allows for the acquisition of qualitative information regarding antibiotic susceptibility.

3.1 Introduction

Antibiotic resistance is a pressing global health crisis that has garnered recognition from organizations such as the World Health Organization (WHO) and the Review on Antimicrobial Resistance (AMR) [1]. This phenomenon pertains to the capacity of bacteria, viruses, fungi, and parasites to withstand the effects of antibiotics, rendering the treatment of infections caused by these microorganisms difficult or even impossible [101].

Antibiotic resistance poses a significant peril to public health on a global scale, affecting both developed and developing nations. Its ramifications extend beyond health concerns and quickly escalate into economic predicaments. It is projected that within the next 35 years, approximately 300 million individuals will experience premature deaths as a result of drug resistance. Failing to address the issue of antimicrobial drug resistance may result in a loss of economic output worth an estimated 60 to 100 trillion USD by 2050 [1]. Moreover, countries already burdened with higher rates of malaria, HIV, or tuberculosis will face even graver consequences [101].

Antibiotic resistance has become a significant challenge in the field of healthcare. To avert a regression to the "dark age of medicine," it is crucial to gain a deeper understanding of antibiotic susceptibility [1]. The rise in antibiotic resistance can be attributed to a decline in the discovery of new drugs combined with an increase in the usage of antibiotics.

Antibiotic resistance occurs naturally; however, its progression is accelerated by the improper use of antibiotics in humans and animals [101]. This resistance can manifest through mutations that are exacerbated by antibiotic usage [102]. Unraveling the workings of resistance within populations can be intricate due to factors such as phenotypic heterogeneity [15], bistability [103], dormancy, and the presence of persister cells [104, 15].

Several metrics have been proposed to assess resistance, each offering unique insights. One such metric is the minimal inhibitory concentration (MIC), which indicates the lowest concentration of an antibiotic that prevents detectable growth in a standardized experimental procedure [102]. MIC values vary significantly among different bacteria and antibiotics. Another widely used measure is the IC50, representing the drug concentration at which the growth rate decreases by 50% during the exponential growth phase [102].

For a more comprehensive understanding of the response to an antibiotic, measuring the growth rate at various drug concentrations provides good information. These growth rate profiles, known as "kill curves," are specific to the antibiotic, bacterial strain, and growth conditions, making them non-universal [102, 2]. These diverse methods effectively contribute to evaluating the level of resistance within a population. Additionally, experimental protocols utilizing these approaches have been developed to enable single-cell measurements, such as single-cell MIC determination and analyses of stochastic dynamics [5, 84].

In order to gain a better understanding of the single-cell level, several techniques utilizing droplet microfluidics have been developed. These recent methods typically involve a droplet generator system for encapsulating individual cells and a fluorescence detection system for assessing bacterial activity. In studies conducted by Lyu et al., Zhang et al., and Hsieh et al., the dye resazurin is introduced into the droplets (Figure 3.1) [15, 19, 89]. Resazurin serves as a fluorescent blue indicator dye. Once inside the cells, resazurin undergoes reduction to resorufin, emitting bright red fluorescence. The fluorescence intensity is proportional to the number of viable cells and corresponds to their metabolic activity [105]. However, this fluorescence detection requires an incubation period, limiting observations to small populations rather than individual cells [15]. In another study by Scholer et al., a fluorescent protein-producing bacterial strain is utilized, enabling the detection of bacteria at an early stage [16].

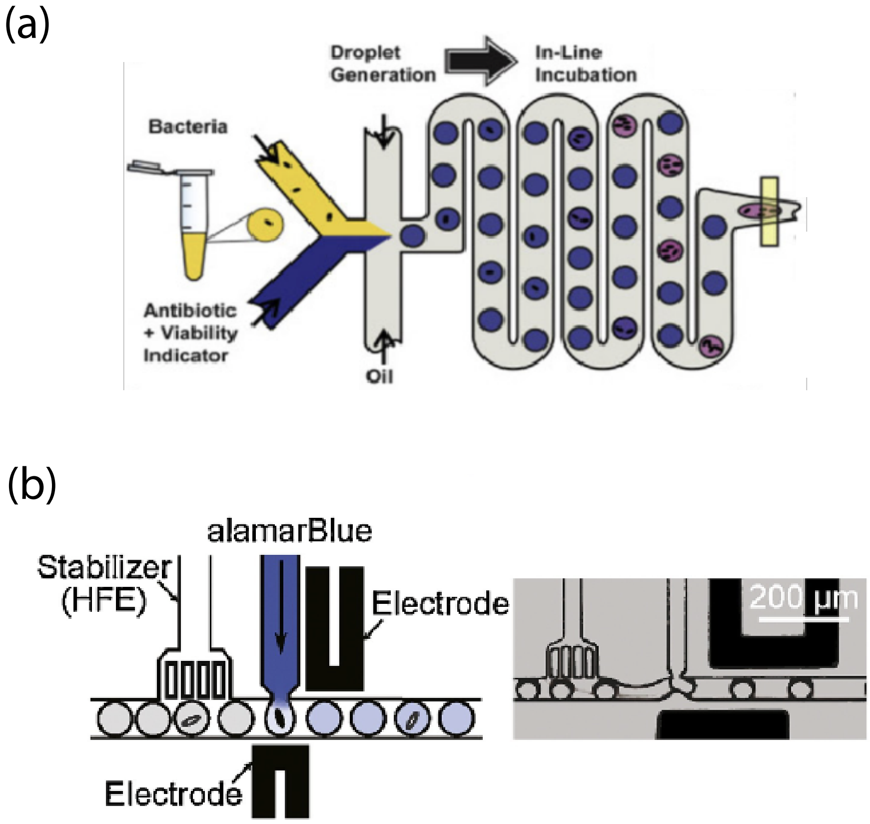

Figure 3.1: **Resazurin (a)** Encapsulation of single bacteria, antibiotics and a fluorescent growth indicator dye into picoliter droplets (adapted from [19], copyright 2017 Elsevier). **(b)** Pico-injection of alamarBlue into droplets (adapted from [15], copyright 2018 Elsevier B.V.

Although these methods offer high throughput platforms for antibiotic susceptibility testing, there is a some drawbacks associated with droplet generator systems. Once encapsulated, the droplets are incubated together, preventing the tracking of individual droplet contents over time.

In our previously described microfluidics system, we employ anchored droplets. This approach enables us to quantify the number of bacteria within the droplets following encapsulation. During the incubation process, the droplets are securely immobilized within the microfluidic chip. This feature enables us to establish a direct correlation between the initial state of each droplet and its final state, thereby facilitating the tracking and analysis of individual droplets throughout the experiment.

3.2 Digital Antibiogram

3.2.1 The microfluidic MIC, µf·MIC

By utilizing our technique for assessing antibiotic susceptibility, we are able to determine the Microfluidic Minimum Inhibitory Concentration, which we denote µf·MIC . This value corresponds to the minimum inhibitory concentration in our microfluidic device. For this purpose, we prepared 12 chips containing varying concentrations of ciprofloxacin, following the procedure outlined in Chapter 2. Each chip contains 500 droplets, with an average of one cell per droplet. Following an overnight incubation, we captured images of the chips and measured the intensity of each droplet.

Figure 3.2 displays a representative set of images obtained at the experimental endpoint (after an overnight incubation). In these images, bright spots indicate droplets where bacteria have grown, while dark spots within the regular matrix represent droplets that lack a sufficient population of cells. These dark positions correspond to either droplets initially devoid of cells or droplets where cells failed to form colonies due to antibiotic stress. For each image, the density distribution of the final intensity of each droplet is plotted. In the absence of antibiotics, the first peak in the distribution around zero corresponds to empty droplets (no initial cells), and the second peak corresponds to droplets where the initial cells developed into colonies. With increasing antibiotic concentration, fewer droplets grow into colonies, causing the distribution to shift to a single peak distribution around zero (no fluorescence).

As expected, the number of positive droplets decreases as the antibiotic concentration rises. This decline is quantified in Figure 3.3 a, which demonstrates that the fraction of positive droplets approaches zero as the antibiotic concentration increases. This trend holds irrespective of the value of the average number of cell per droplet λ. Determining the concentration of ciprofloxacin at which fewer than five positive droplets appear provides a measure of the bacteria's antibiotic susceptibility, referred to as the microfluidic minimum inhibitory concentration (µf·MIC). Less than 5 positive droplets correspond to 99% of cells not producing a colony.

3.2.2 Analogy with classic AB susceptibility measurements

The interpretation of the digital measurement obtained and its correlation with classical microbiology measurements is not immediately apparent. To comprehend its significance, we compared the measurements obtained in the microfluidic format with measurements in a standard multiwell plate.

To characterize antibiotic susceptibility at the population level, we determined the minimum inhibitory concentration (MIC) and minimum bactericidal concentration (MBC). We employed the broth dilution method in a 96-well plate for this purpose. Cells were loaded into the wells at various dilutions (ranging from 500 to 500,000 cells per well), along with different concentrations of ciprofloxacin (ranging from 2 to 36 ng/mL). After 24 hours of incubation, the MIC was determined as the antibiotic concentration of the first negative well, which refers to the well where the optical density matches that of an empty well. Subsequently, the contents of the negative wells were plated on LB agar plates. Following another 24 hours of incubation, the number of colonies was counted, and the MBC was determined as

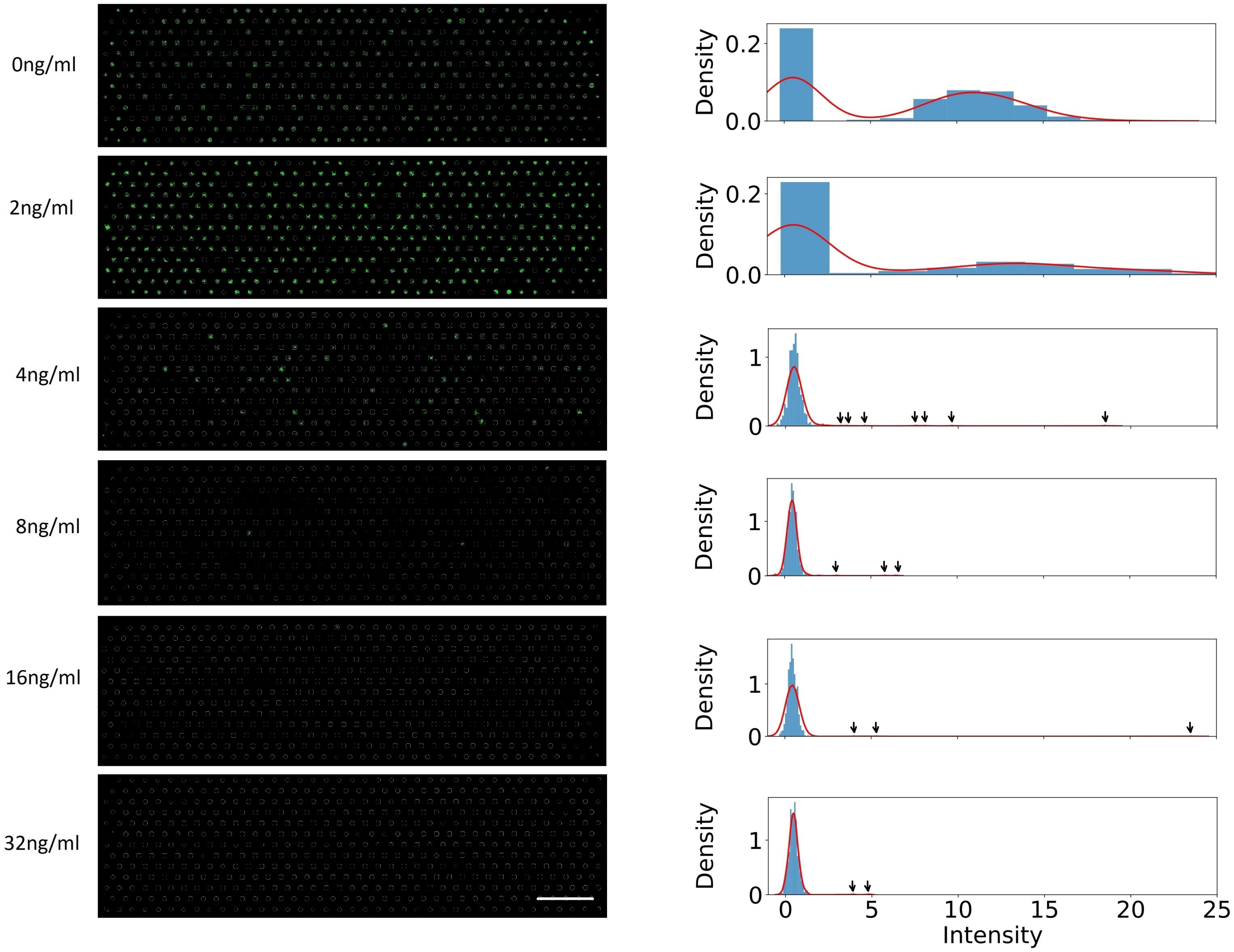

Figure 3.2: **Digital antibiogram** On the left, Z-projection of the confocal stack of the chip after 24 hours incubation with MOPS media and different concentrations of ciprofloxacin (scale bar 500μm). On the right, is the corresponding final intensity of each droplet. The arrows correspond to no visible counts and the red line to a Gaussian fit.

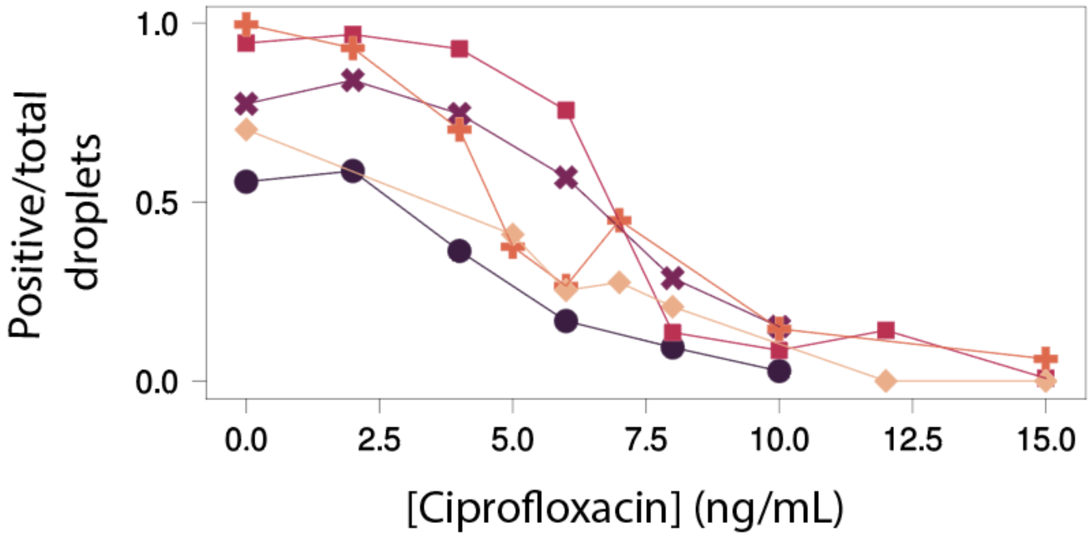

Figure 3.3: **Droplet antibiotic susceptibility** Number of positive droplets normalized by the total number of droplet per chip as a function of ciprofloxacin concentration for 5 replicates.

the concentration at which the number of colonies sharply decreases from over a hundred cells to less than a dozen cells.

The MBC provides a more precise measurement of the antibiotic concentration that is lethal to the bacteria. This counting process was performed for different inoculum sizes, ranging from 500 to 500,000 initial cells per well. It is observed that below a critical ciprofloxacin concentration, which does not depend on the initial number of cells, the number of colonies is significantly high. Beyond this concentration, the number of colonies dramatically drops to below approximately 100 colonies and then levels off at zero.

A comparison of the measurements obtained from the three techniques (µf·MIC, MIC, and MBC) is presented in Figure 3.4. The classical MIC measurement at 24 hours is shown to be the least influenced by the inoculum size among the three measurements. Conversely, the values of the MBC and µf·MIC fall within a similar range.

The strong agreement observed between the MBC and µf·MIC, obtained by pooling all the cells from the 500 droplets on the chip, suggests that the results obtained in the microfluidic chip can be considered as a measurement at the population level. Consequently, the bacteria in the droplet experiments can be viewed as a small population whose survival at a particular antibiotic concentration is dependent on its initial size. This finding reflects a form of ”superposition principle”, indicating that the cells are behaving independently.

3.3 Computing the single cell susceptibility

In addition to population-level measurements, the aim is to gain insights into the antibiotic susceptibility of individual cells within a population. To accomplish this, a probabilistic approach is adopted to assess the ability of a single cell to generate a colony at a specific antibiotic concentration. In the experimental setup, the number of bacteria in each droplet is counted at the beginning, and the droplet fluorescence

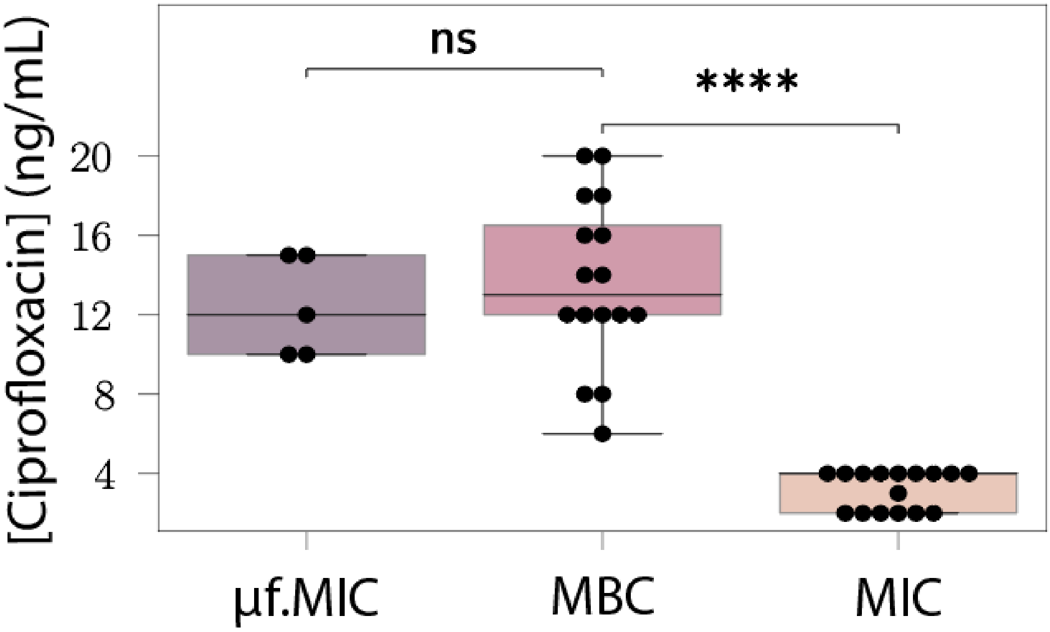

Figure 3.4: **µf·MIC, MBC, and MIC** Values of MBC (Petri dishes), MIC (96-well plates), and on the chip.

is measured at the end of the experiment for six antibiotic concentrations. Figure 3.5 depicts the relationship between ciprofloxacin concentration and the number of detected cells following an overnight incubation. Each color corresponds to an intial number of cells. Each data point corresponds to the number of cells in each droplet at a specific concentration. As the concentration of ciprofloxacin increases, the number of detected cells decreases significantly, approaching zero cell.

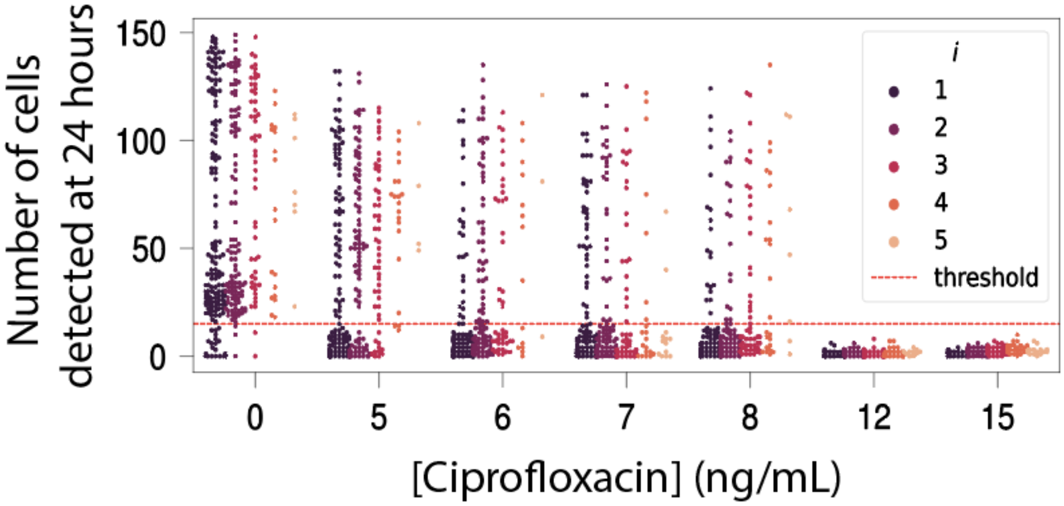

Figure 3.5: **Droplet antibiotic susceptibility** Final number of cells for each droplet as a function of ciprofloxacin concentration for each initial cell number in the droplet (i)

A threshold value for droplet fluorescence is selected to distinguish between positive and negative droplets. This threshold enables the counting of positive and negative droplets for each condition and initial number of cells. Consequently, the probability of a droplet containing a colony at the end-point can be plotted as a function of the initial number of bacteria n_0 and the antibiotic concentration. Figure 3.6 illustrates such a heat map displaying this probability distribution.

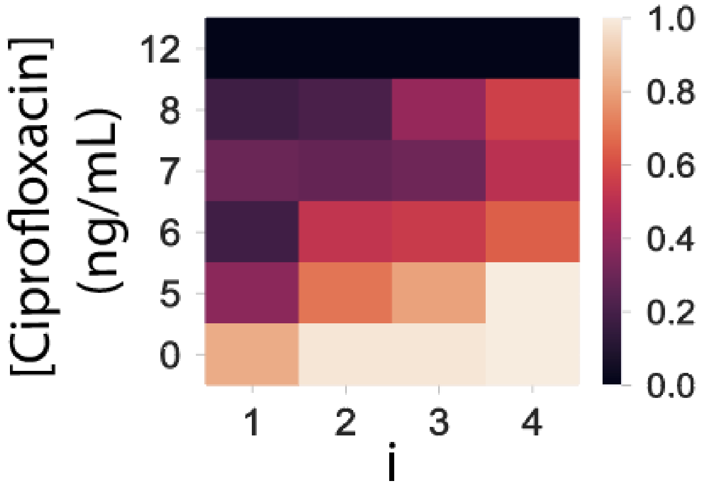

Figure 3.6: **Droplet antibiotic susceptibility** Survival probability from 0 (dark purple) to 1 (white) as a function of initial cell number and antibiotic concentration.

Counting the number of positive and negative droplets enables us to infer the susceptibility of a single cell to a concentration of antibiotic C_{AB}. The susceptibility is defined as the probability for a single cell not to form a detectable colony at concentration C_{AB} up to measurement time. Let us first introduce $p(1, C_{\mathrm{AB}})$ the probability for one individual cell to produce a colony after 24 hours, at antibiotic concentration C_{AB}. This probability can be estimated by identifying the $\mathcal{N}_1$ droplets containing a single cell at the beginning of the experiment, and then counting how many of these droplets are positive after 24 hours of incubation. Calling $N^+(1, C_{\mathrm{AB}})$ the number of positive droplets that started with a single cell, we then have:

$$p(1, C_{\mathrm{AB}}) = \frac{N^+(1, C_{\mathrm{AB}})}{\mathcal{N}_1}. \tag{3.1}$$

Likewise, calling $p(i, C_{\mathrm{AB}})$ the probability for i cells to produce a colony after 24 hours, at a given antibiotic concentration C_{AB}, we obtain:

$$p(i, C_{\mathrm{AB}}) = \frac{N^+(i, C_{\mathrm{AB}})}{\mathcal{N}_i}, \tag{3.2}$$

where $\mathcal{N}_i$ is the number of droplets containing exactly i cells at the beginning of the experiment, among which $N^+(i, C_{\mathrm{AB}})$ droplets are positive at the end of the experiment.

Both the drug concentration C_{AB} and the initial number of cells i play crucial roles in determining the probability of colony formation. Specifically, the probability $p(i, C_{\mathrm{AB}})$ of i cells forming a colony increases with an increasing initial number of cells i and decreases with an increasing drug concentration C_{AB}, as demonstrated in Figure 3.6 .

The probability of not forming a colony starting from a single cell, which we refer to as single-cell susceptibility, is denoted as $q(C_{\mathrm{AB}})$. This probability is directly linked to the probability of a single cell forming a colony: $q(C_{\mathrm{AB}}) \equiv 1-p(1, C_{\mathrm{AB}})$. If all bacteria exhibit independent behavior, the probability of i cells dying is $q(C_{\mathrm{AB}})^i$. Conversely, the probability of i cells forming a colony is the complementary probability that none of the i cells fail to form a colony. This enables to relate $q(C_{\mathrm{AB}})$ and $p(i, C_{\mathrm{AB}})$ through:

$$p(i, C_{\mathrm{AB}}) = 1 - q(C_{\mathrm{AB}})^i. \tag{3.3}$$

For each concentration of antibiotics, the probability $p(i, C_{\mathrm{AB}})$ was plotted as a function of i, and fitted to the functional form of equation (3.3) with $q(C_{\mathrm{AB}})$ as a single fit parameter. As shown in Figure **??** and in Figure 3.7, it is reasonable to consider that bacteria are independent of each other. The best fit value of $q(C_{\mathrm{AB}})$ is called $q^\star(C_{\mathrm{AB}})$. It is the best estimation of the single-cell susceptibility to drug concentration C_{AB}, using all experimental data at hand and assuming that all cells are independent.

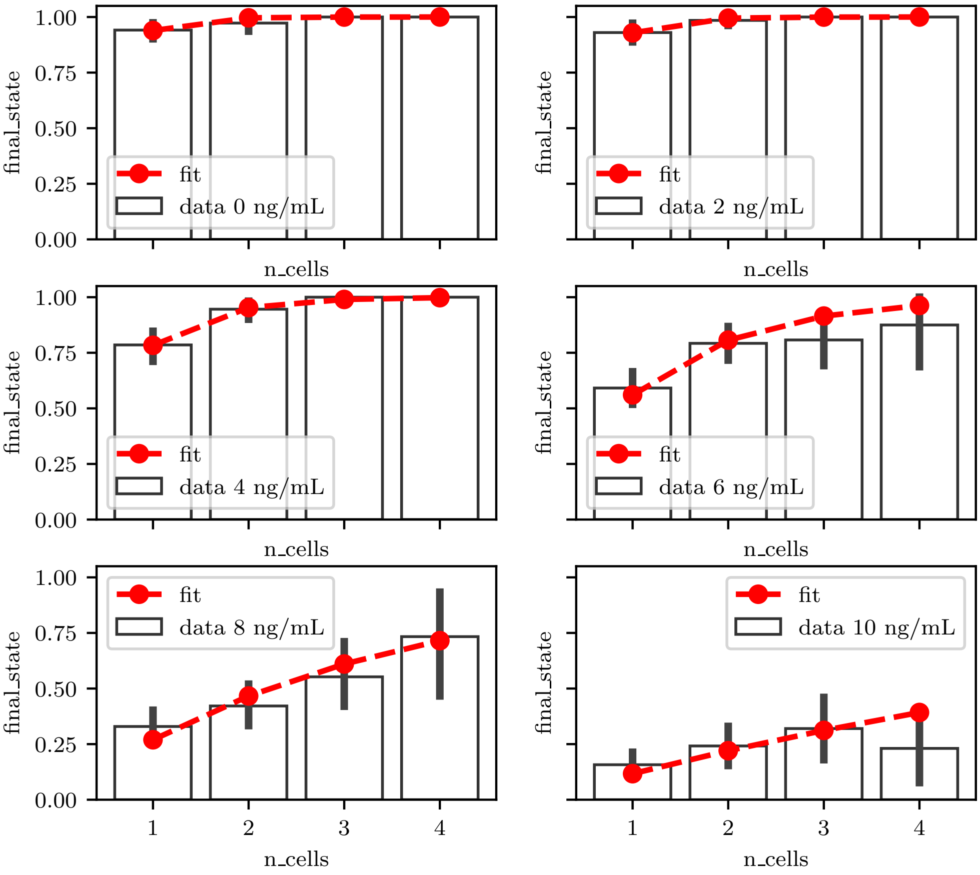

Figure 3.7: **Survival probability** A unique value for $p(i, C_{\mathrm{AB}}) = 1 - q(i, C_{\mathrm{AB}})^i$ is obtained by assuming independent outcomes for each cell and fitting for q. Here for different concentrations of ciprofloxacin.

In the absence of drugs, the single-cell susceptibility $q^\star(C_{\mathrm{AB}})$ is nearly zero, indicating that almost all bacteria are capable of forming colonies. However, as the drug concentration (C_{AB}) increases, the single-cell susceptibility rises non-linearly until it reaches a plateau at $q^{\star}(C_{\mathrm{AB}}) = 1$, meaning no colonies are formed. This behavior is depicted in Figure 3.8. The relationship between $q^{\star}(C_{\mathrm{AB}})$ and the antibiotic concentration exhibits a sigmoidal shape. To aid visualization, the antibiotic profile is fitted to a Hill function: $h(C_{\mathrm{AB}}) = C_{\mathrm{AB}}^{n}/(K + C_{\mathrm{AB}}^{n})$, K and n are two fitting parameters. By optimizing the fit, we determine that $n = 3.9$ and $K = 4.4$ provide the best match to the data.

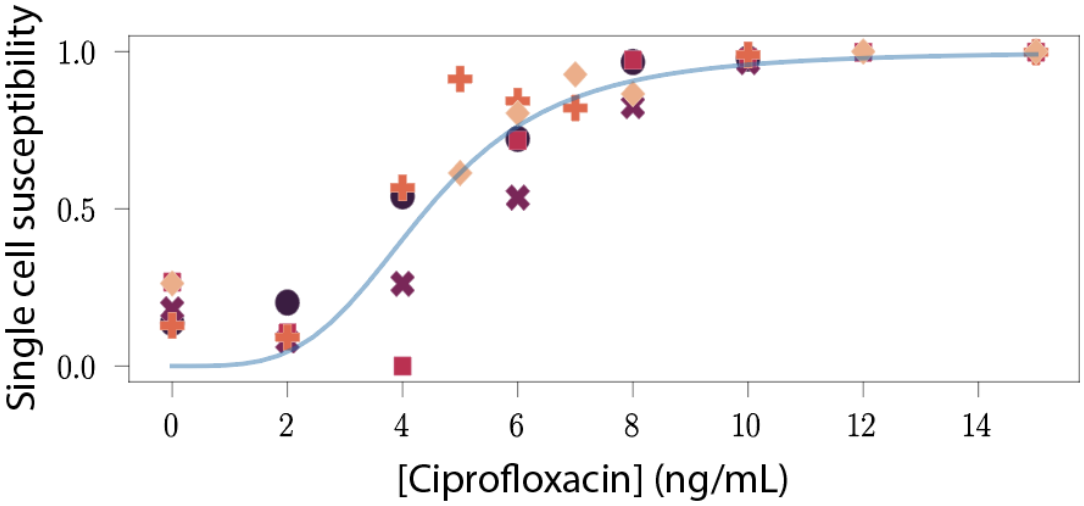

Figure 3.8: **Single cell antibiotic susceptibility** The single-cell antibiotic susceptibility q plotted as a function of antibiotic concentration for all experimental replicates. Blue line corresponds to a Hill function fit: $h(C_{\mathrm{AB}}) = C_{\mathrm{AB}}^{n}/(K + C_{\mathrm{AB}}^{n})$, where $n = 3.9$ and $K = 4.4$.

3.4 Identifying morphology changes under antibiotic stress

The combination of this microfluidic device and image analysis pipeline presents a highly effective tool for acquiring quantitative information at the single-cell level, as demonstrated in Figure 3.8. However, beyond quantitative data, the anchored droplet format offers a distinctive capability to access qualitative information and track the progression of bacterial colonies within each droplet over time.

The tracking of droplet contents can be achieved through time-lapse microscopy on the chips, leveraging the fixed position of the droplets throughout the experiment. This enables the identification of progeny originating from individual cells. Examples of droplet contents can be observed in Figure 3.9 and the accompanying movies, illustrating both the absence of antibiotics (Figure 3.9a) and a sub-MIC concentration of ciprofloxacin (Figure 3.9b).

In the absence of antibiotics, the majority of droplets exhibit bacteria in their planktonic state, swimming within the droplets, and displaying the characteristic size and shape of *E. coli* in culture. As the populations begin to grow, cells within certain droplets begin to adhere to one another, forming clumps. These clumps may

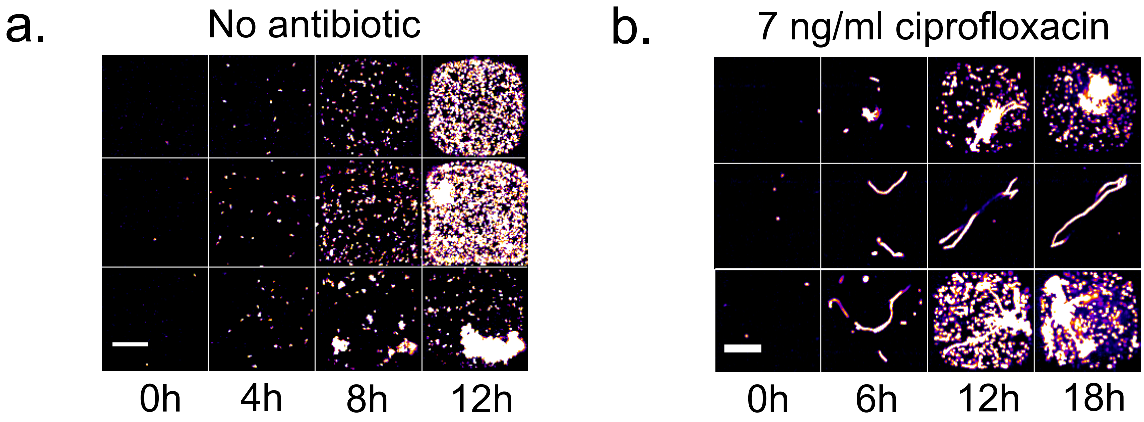

Figure 3.9: **Bacterial growth** Example of bacterial growth in three independant droplets inb MOPS **(a)** without antibiotic, and **(b)** at sub-MIC concentrations of ciprofloxacin. Scale bar: 50 μm. Even at sub-MIC concentrations, the presence of ciprofloxacin leads to a filamentous bacterial morphology.

be attributed to the presence of adhesion proteins, such as fimbrial adhesins, which potentially contribute to the formation of *E. coli* biofilms [106].

The presence of antibiotics often leads to morphological changes in bacteria, typically starting with cell elongation into long filaments. In experiments with sub-MIC antibiotic concentration (7 ng/mL), filamentation occurs in approximately 83% of cases. Filamentation is a result of the SOS response triggered by ciprofloxacin, where cell division halts, but cellular metabolism continues, leading to an increase in cell volume. After several hours, the elongated cells may either give rise to offspring in 50% of cases or arrest their growth and remain in the filamentous form in 33% of cases. These observations align with findings from agar plate experiments [3].

In certain instances, no elongation is observed. These droplets may correspond to cells in a dormant state (expected in approximately 10% of cases) [104] or cells that have experienced significant damage and perished due to the effects of antibiotics (7% of cases), indicated by the absence of fluorescence. Consequently, the vast majority of droplets containing colonies consist of filamentous cells. Nonetheless, the ability to image the contents of the droplets provides precise insights into the cellular state within them, offering valuable information regarding the cells' ability to withstand antibiotic stress.

3.5 Conclusion: AST and single cell susceptibility

With the increasing emergence of antibiotic resistance, understanding the variability of antibiotic response at the single-cell level has become crucial. Previous studies have employed dilution methods on petri dishes [4] or in liquid media [5], as well as precision microscopy on agar [3], to determine the MIC and explore antibiotic susceptibility. Microfluidic methods have also been employed to offer better control and statistics over a large number of individual cells [6, 7]. In recent years, droplet-based approaches have emerged, revealing heteroresistance within bacterial populations [15], digital antibiotic susceptibility [16, 89], and even pathogen identification [19]. These droplet-based methods have allowed for the investigation of individual cell progeny under antibiotic stress. However, previous methods relying on snapshots of moving droplets were unable to establish the connection between initial and final states of each droplet or identify the biological mechanisms enabling cells to overcome antibiotic stress at sub-MIC concentrations.

In this chapter, various methodologies are presented to explore different facets of bacterial response to antibiotics using the current platform. One approach involves quantifying the number of ”positive” and ”negative” droplets within a microfluidic chip, which can generate a digital antibiogram. By maintaining an average of approximately one cell per droplet, using 500 droplets produces statistical power comparable to that of 10000 droplets in the flowing droplet format [16, 89].

The microfluidic MIC µf·MICtechnique is compared to standard microbiology protocols and demonstrates correspondence with the minimum bactericidal concentration (MBC), indicating that the current measurements are more sensitive than conventional minimum inhibitory concentration (MIC) measurements. Additionally, the detection of individual cells and the ability to perform a large number of single-cell assays in parallel allow for the development of a probabilistic approach to describe the outcome within each droplet forming a colony after 24 hours. The probability of an individual cell producing a colony at a specific antibiotic concentration describes the heterogeneity of responses within the population. By establishing a connection between the initial and final states of each droplet, it becomes possible to measure single-cell susceptibility, which represents the probabilistic sensitivity of cells to the antibiotic. This measurement is obtained by estimating the probability of an individual cell not forming a colony at a given antibiotic concentration. The value of single-cell susceptibility exhibits a sigmoidal shape in relation to the concentration of ciprofloxacin. Furthermore, the high-resolution confocal imaging enables the characterization of cell phenotypes within a growing colony under different conditions.

This platform can now be utilized to investigate the single-cell response to antibiotics while screening different bacteria and antibiotics with diverse mechanisms of action. It is expected that this screening will yield both quantitative (shaping the single-cell susceptibility curve) and qualitative (observing cell morphology) differences among the conditions tested. The controlled encapsulation of tens or hundreds of cells within droplets enables the exploration of collective behaviors and non-monotonic time-evolution in response to antibiotics [107]. More complex experiments, such as recovering the contents of individual drops for -omics measurements or varying the antibiotic concentration over time, can be envisioned [22]. Collectively, the various operations achievable with this platform represent a significant advancement in the study of antibiotic response, benefiting both scientific inquiries and medical applications.

The subsequent chapter will compare the aforementioned measurements across a range of different antibiotics.

Key takeaway

Context: I have developed an automated pipeline for studying and observing bacterial growth. The microfluidic device features chips with 500 anchored droplets. Up to six distinct conditions can be accommodated simultaneously.
Results: With the utilization of this microfluidic device, I successfully obtained information pertaining to both population-level characteristics (digital antibiogram) and individual cell-level responses (single cell susceptibility). This microfluidic chip enables access to dynamic changes and phenotypes within each individual droplet.

Chapter 4

Comparing different antibiotics

In this chapter, we will utilize our microfluidic device and experimental pipeline to compare the effects of various antibiotics. The antibiotics selected for comparison are ciprofloxacin, gentamicin, tetracycline, chloramphenicol, and ampicillin. These antibiotics were chosen due to the diversity in their mechanisms of action. Some exhibit bactericidal properties (ciprofloxacin, gentamicin, and ampicillin), while others are bacteriostatic (tetracycline and gentamicin). Additionally, the selected antibiotics target different components, such as DNA (ciprofloxacin), ribosomes (gentamicin, tetracycline, and chloramphenicol), or proteins involved in cell wall synthesis (ampicillin).

The first section will involve the direct application of our experimental pipeline, providing an overview of the action of different antibiotics through digital antibiograms and single cell susceptibility analyses.

Subsequently, we will delve into the mechanisms of action for each antibiotic, focusing on images obtained from time point experiments. Special attention will be given to ciprofloxacin, where we will employ time-lapse experiments to observe and analyze the various phenotypes associated with its action.

4.1 Antibiotic susceptibility

4.1.1 Digital Antibiogram

This microfluidic and image analysis pipeline is a very powerfull tool to obtain quantitative information at the single level. It can be easily use with different antibiotic to access quantitative and qualitative information at the single level. Here, in addition to ciprofloxacin we tried three more different antibiotics: gentamicin, tertacyclin, chloramphenicol and ampicillin. The following results present a the data obtained with these antibiotics at different concentration with *E. coli* in LB. The use of LB media enables us to shorten the time of the experiments as the bacteria grow faster in LB than in MOPS media.

As presented in the previous chapter (3.2), we can plot the density distribution of the final intensity of each droplet for different antibiotics to obtain the digital antibiogram (Figures 4.1, 4.2, 4.3, 4.4, 4.5, 4.6, 4.7, 4.8, 4.9, 4.10).

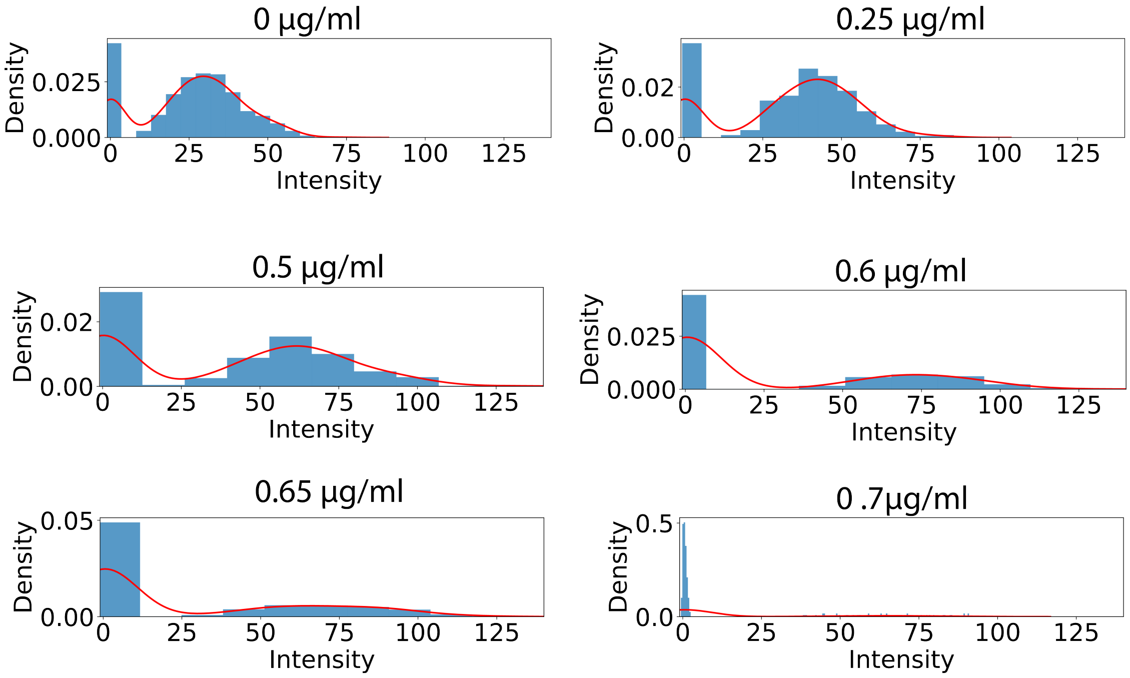

Figure 4.1: **Gentamicin antibiogram.** Final fluorescence intensity (A.U.)of each droplet with different concentrations of gentamicin. The red line corresponds to a Gaussian fit. Data from 10.01.2023-1 experiment.

For all the antibiotics, we observe the same trend. In the absence of antibiotics, the first peak in the distribution around zero corresponds to empty droplets (no initial cells), and the second peak corresponds to droplets where the initial cells developed into colonies. With increasing antibiotic concentration, fewer droplets grow into colonies, causing the distribution to shift to a single peak distribution around zero (no fluorescence). These antibiograms can help us determine visually the µf·MIC: between 0.65 and 0.7 µg/ml for gentamicin (Figure 4.1), between 3.5 and 4 ng/ml for ciprofloxacin (Figure 4.3), between 40 and 50 µg/ml for tetracyclin (Figure 4.5), between 2 and 4 µg/ml for chloramphenicol (Figure 4.7) and between 8 and 16 µg/ml for ampicillin (Figure 4.9).

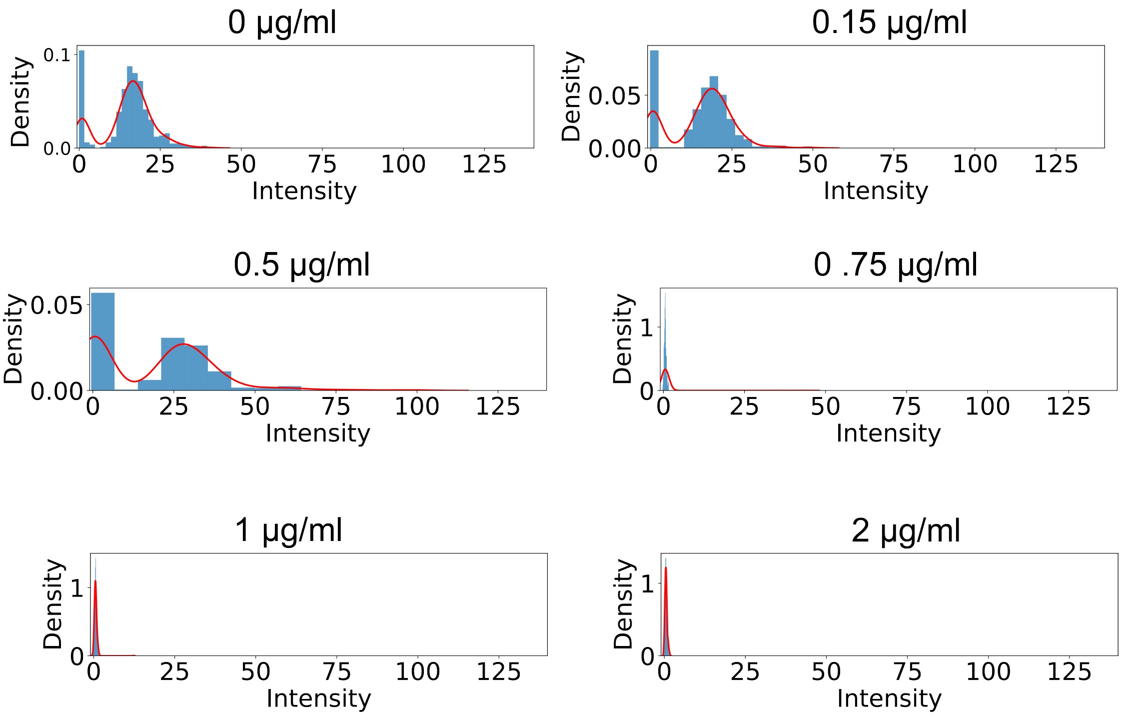

Figure 4.2: **Gentamicin antibiogram** Final intensity of each droplet with different concentrations of gentamicin. The red line corresponds to a Gaussian fit. Data from 01.11.2022-1 experiment.

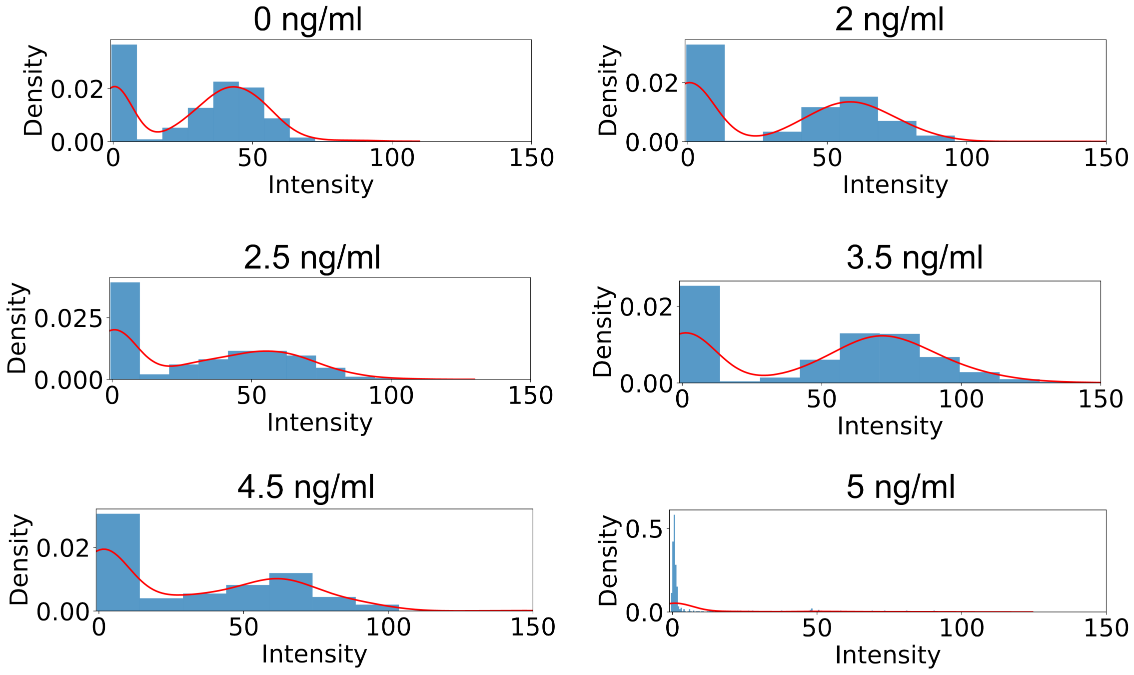

Figure 4.3: **Ciprofloxacin antibiogram.** Final fluorescence intensity (A.U.) of each droplet with different concentrations of ciprofloxacin. The red line corresponds to a Gaussian fit. Data from 31.01.2023-1 and 31.01.2023-2 experiment.

For gentamicin, ciprofloxacin and ampicillin the µf·MIC is consistent between experiments, as you can see in the antibiograms in Figure 4.2, 4.4, 4.10.

On the other hand, for tetracyclin and chloramphenicol, the µf·MIC varies from one experiment to an other. In Figure 4.6 the µf·MIC is between 60 and 80 µg/ml for tetracyclin, when it is bellow 50µg/ml in Figure 4.5. For chloramphenicol, we

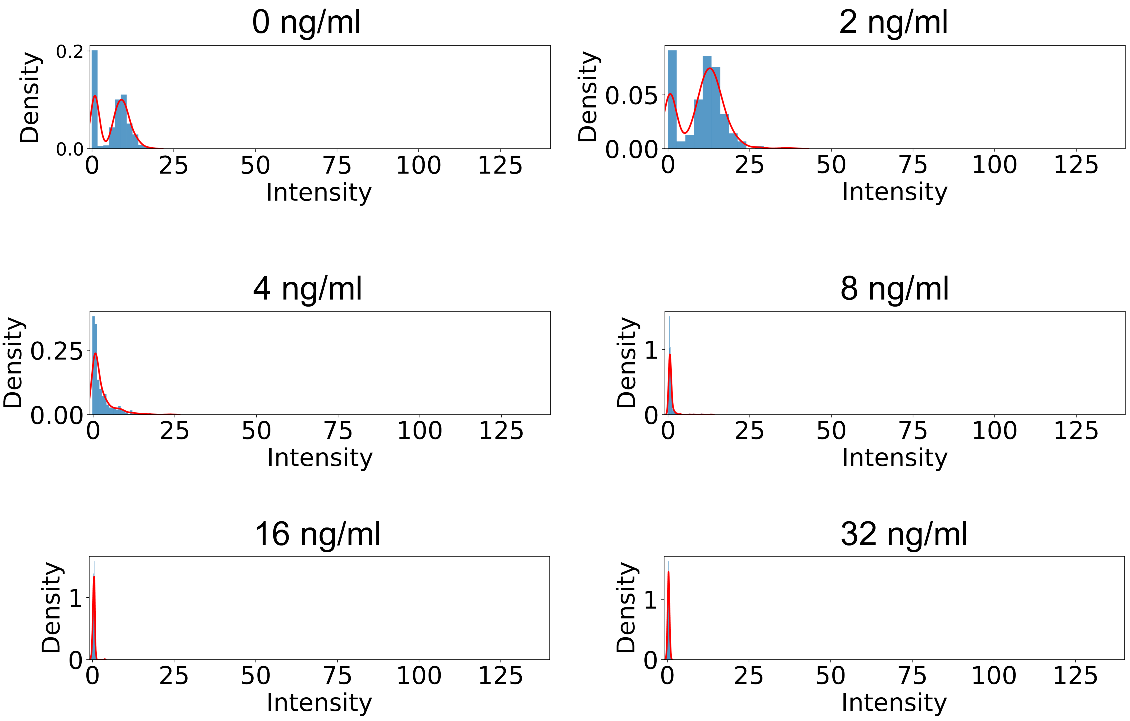

Figure 4.4: **Ciprofloxacin antibiogram** Final intensity of each droplet with different concentrations of ciprofloxacin. The red line corresponds to a Gaussian fit. Data from 31.05.2022-1 experiment.

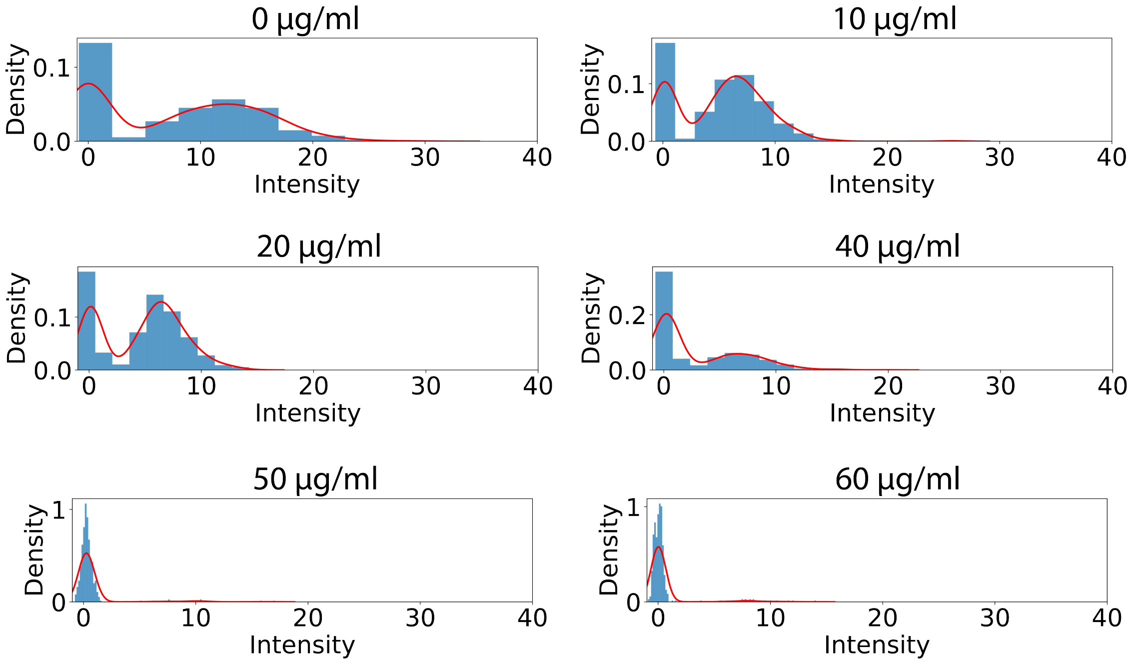

Figure 4.5: **Tetracylin antibiogram** Final fluorescence intensity (A.U.) of each droplet with different concentrations of tetracyclin. The red line corresponds to a Gaussian fit. Data from 04.04.2023-1 experiment.

found a different µf·MIC for almost all experiments.

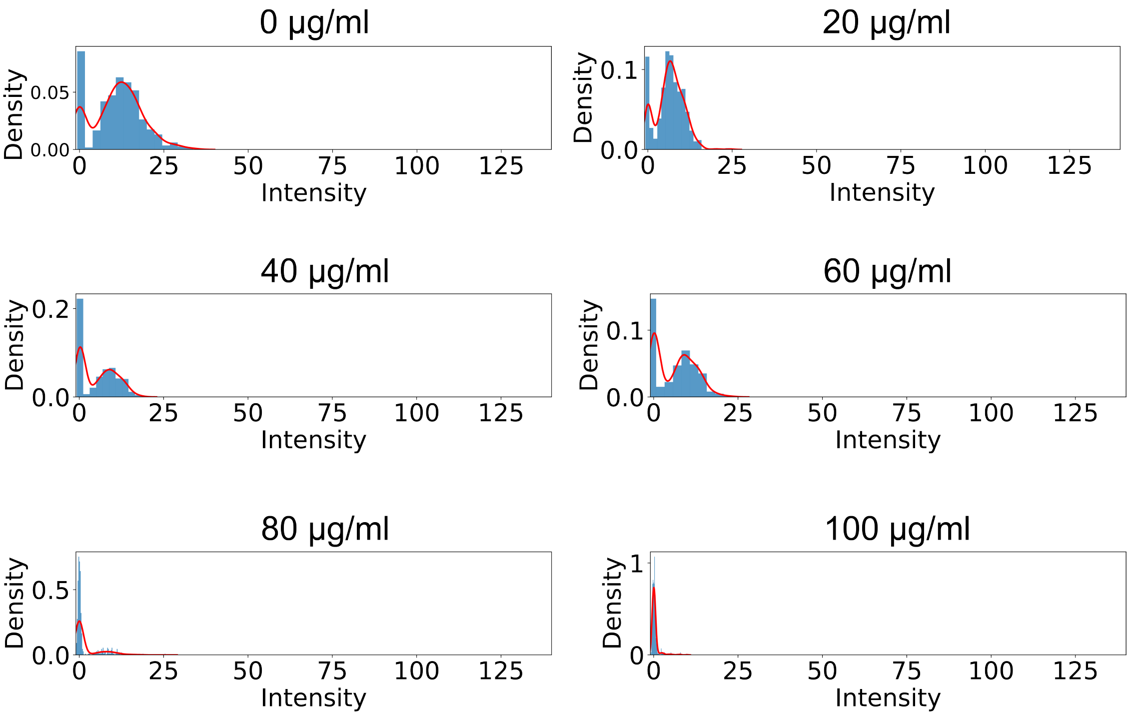

Figure 4.6: **Tetracyclin antibiogram** Final intensity of each droplet with different concentrations of tetracyclin. The red line corresponds to a Gaussian fit. Data from 15.03.2023-1 experiment.

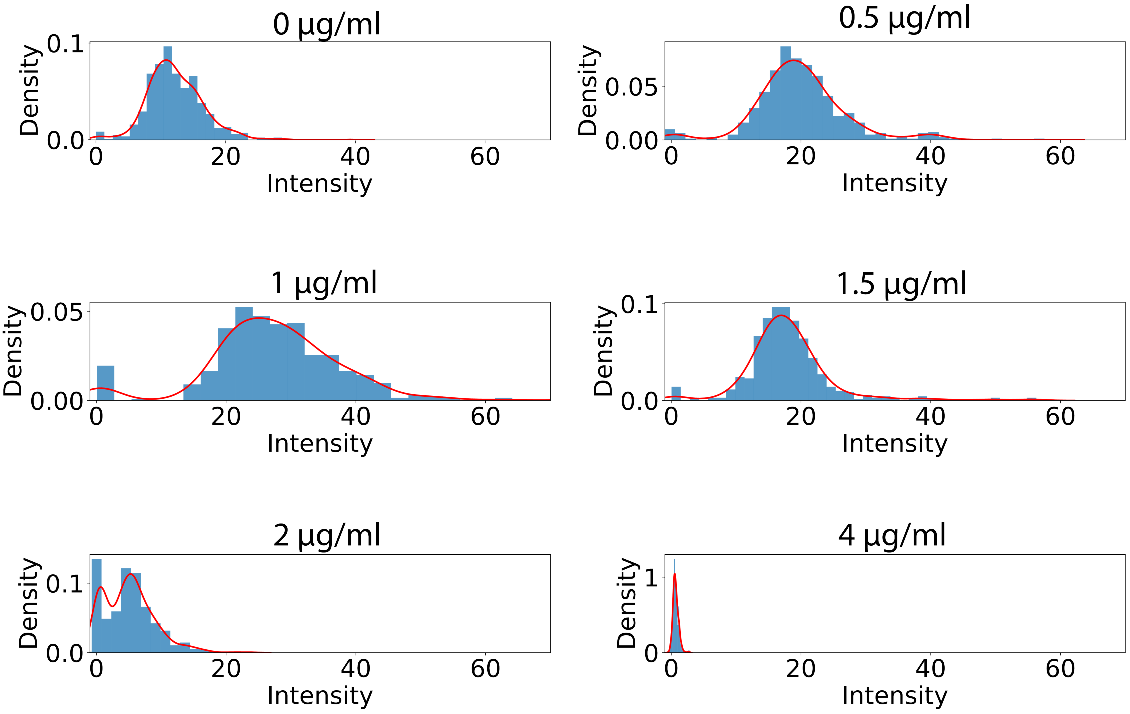

Figure 4.7: **Chloramphenicol antibiogram.** Final fluorescence intensity (A.U.) of each droplet with different concentrations of chloramphenicol. The red line corresponds to a Gaussian fit. Data from 02.11.2022-1 experiment.

4.1.2 Single cell susceptibility

As shown in Figure 4.11, the single cell susceptibility can be obtained with different antibiotics: gentamicin, ciprofloxacin, tetracyclin, chloramphenicol. The curves in

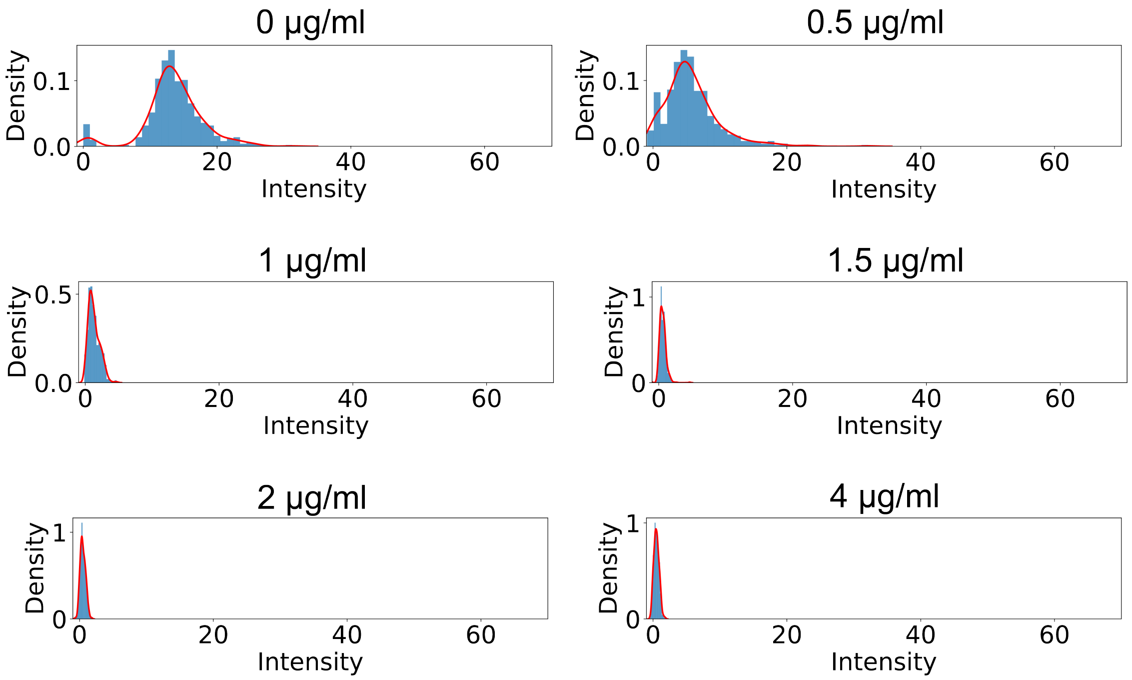

Figure 4.8: **Chloramphenicol antibiogram** Final intensity of each droplet with different concentrations of chloramphenicol. The red line corresponds to a Gaussian fit. Data from 02.11.2022-1 experiment.

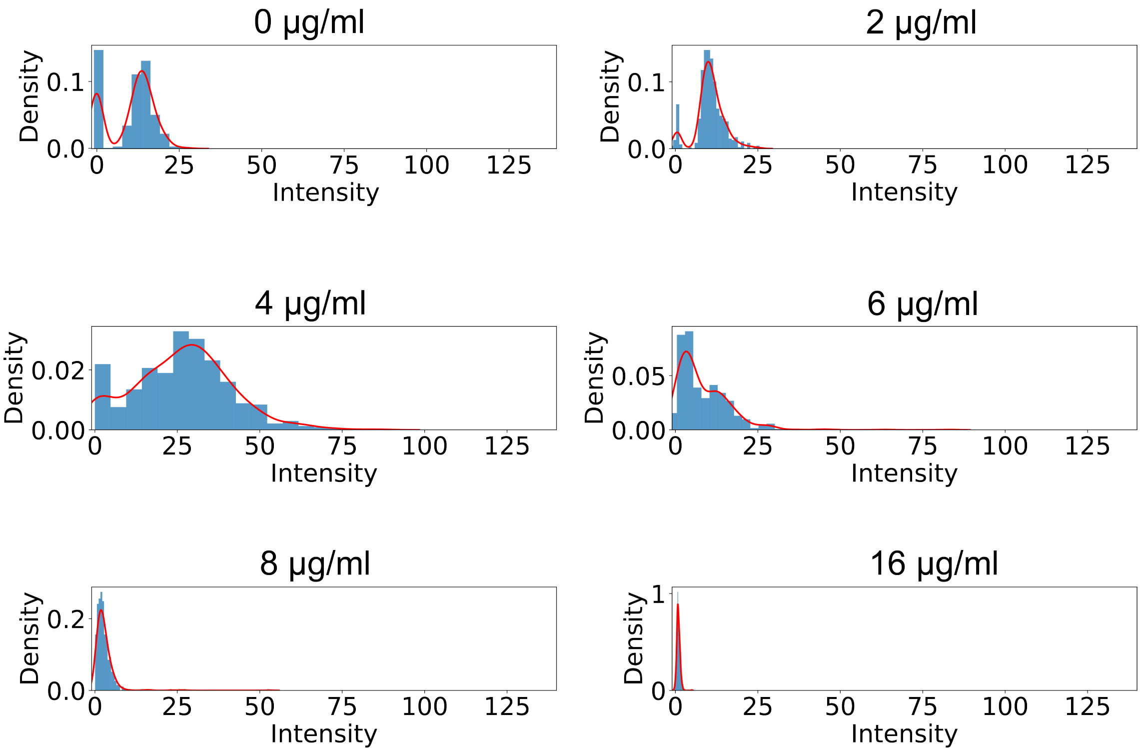

Figure 4.9: **Ampicillin antibiogram.** Final fluorescence intensity (A.U.) of each droplet with different concentrations of ampicillin. The red line corresponds to a Gaussian fit. Data from 02.06.2022 experiment.

Figure 4.11 were obtained by loading two sets of 6 chips for each day, resulting of 12 different antibiotic concentrations. For gentamicin, ciprofloxacin and tetracylcin we have two replicates in two different days. For chloramphenicol we have four replicates in four different days.

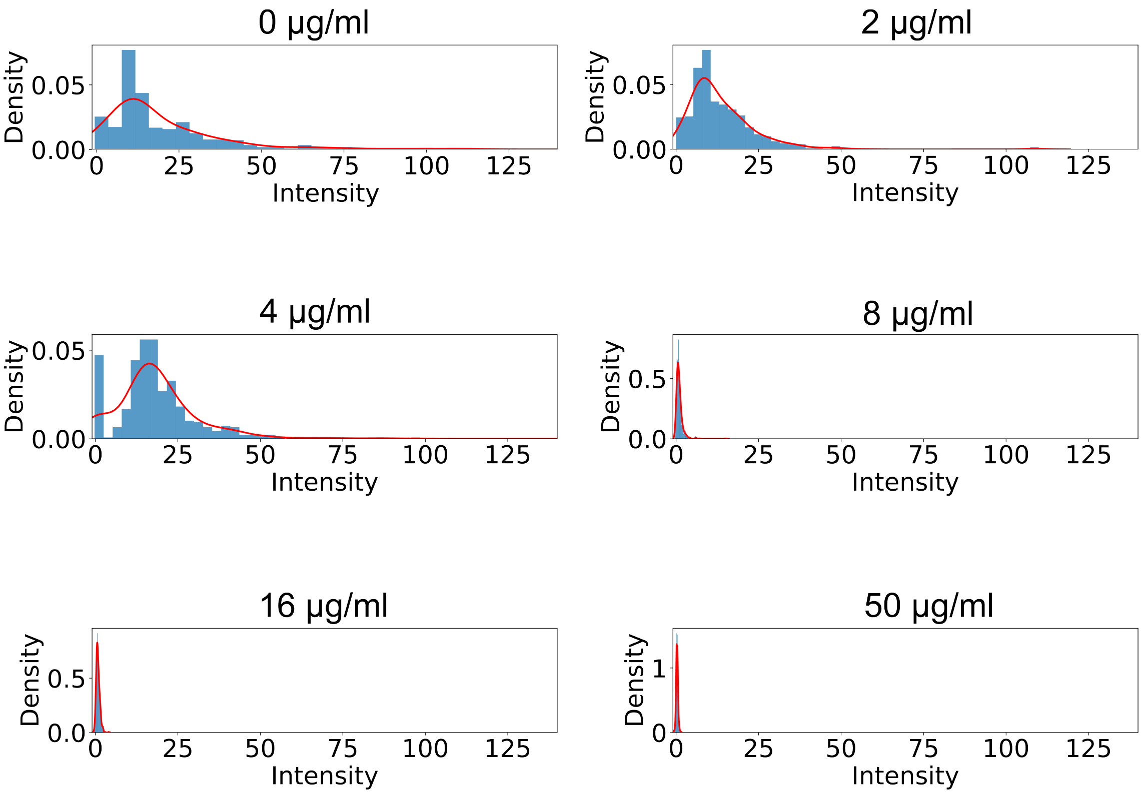

Figure 4.10: **Ampicillin antibiogram** Final intensity of each droplet with different concentrations of ampicillin. The red line corresponds to a Gaussian fit. Data from 18.05.2022 experiment.

For all four antibiotics, we have a similar offset. Without antibiotic, the probability of a cell forming a colony is aorund the same value: 0.8 for gentamicin and tetracyclin and 0.7 for ciprofloxacin and chloramphenicol. This probability is close but not equal to one, it represents the basic stochasticity in a population, where not all cells are going to grow and form a colony.

We can see that some antibiotics like gemtamicin and ciprofloxacin presents more reproducible results than with tetracycline and chloramphenicol where we can see more variability from one experiment to an other. This is in agreement with the different range of the µf·MIC found with the digital antibiograms.

Gentamicin and ciprofloxacin are bactericidal antibiotics meanings antibiotics that kill bacteria. On the other hand, tetracyclin and chloramphenical are bacteriostatics antibiotics, that will slow the growth or reproduction of the bacteria [108, 109]. These differences in the mechanism of action might explain the differences in the reproducibility in the experiments.

4.2 Mechanism of action and phenotypes

Not only does the anchored droplet provide quantitative information, but it also offers a unique ability to access qualitative data. Indeed, as shown in figure 4.12, it is possible to observe the different effects of antibiotics on the phenotype of the bacteria. In the absence of antibiotics, almost all droplets display bacteria in their

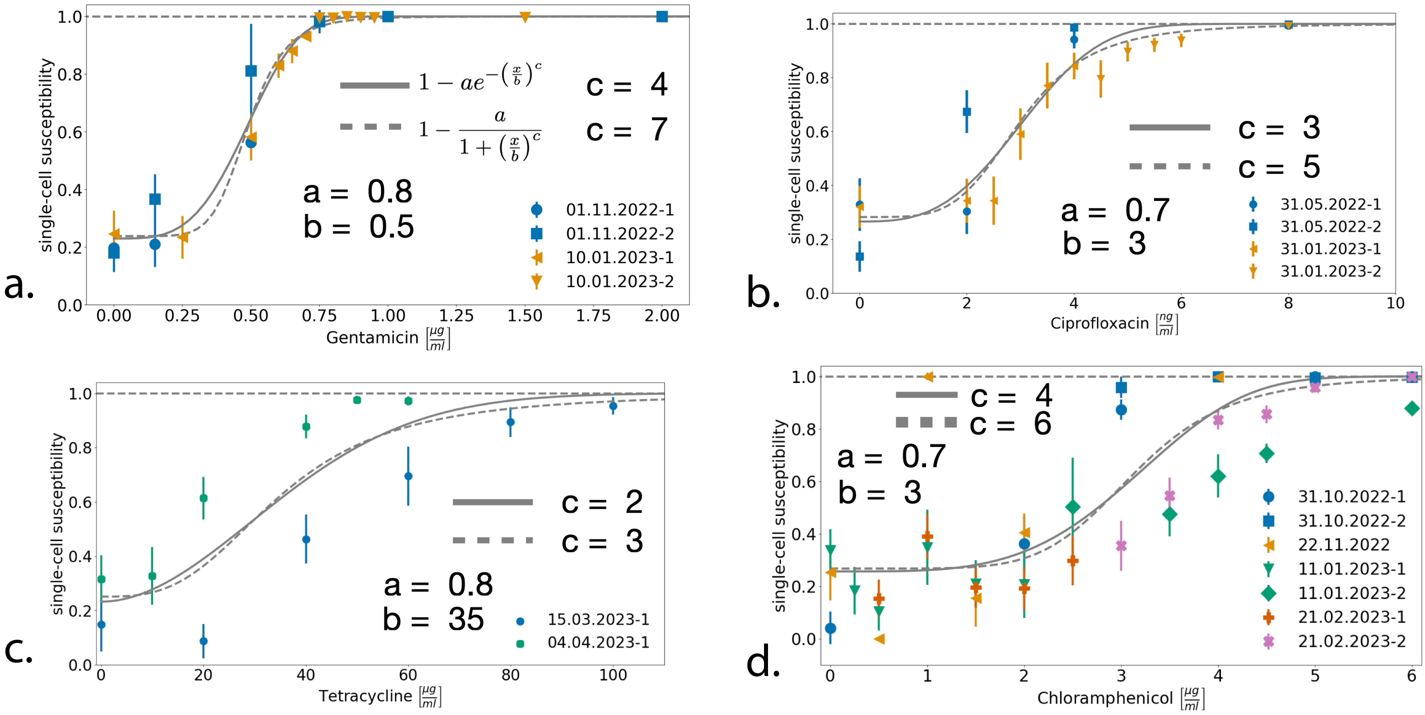

Figure 4.11: **Single cell response for different antibiotics** Single cell susceptibility for **(a)** gentamicin, **(b)** ciprofloxacin, **(c)** tetracyclin and **(d)** chloramphenicol. The bold and dash grey line are two different fit, where $1 - a$ is the offset and represents the basic stochasticity in a population. b is a scale factor. c the tail, dictates the behaviour for many bacteria. b and c, quantify the varibility within the population.

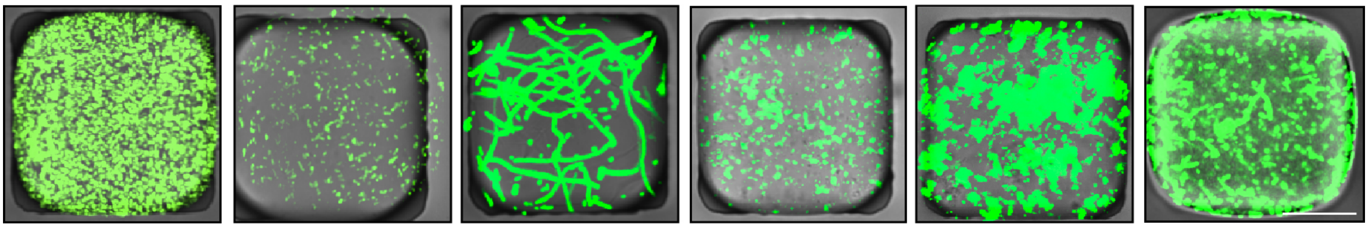
No Antibiotic

Chloramphenicol
1.5 µg/ml

Ciprofloxacin
4 ng/ml

Tetracyclin
20 µg/ml

Gentamicin
0.5 µg/ml

Ampicillin
4 µg/ml

Figure 4.12: **Phenotypic response to antibiotics.** Effect of different antibiotics on *E. coli* after an overnight incubation. (scale bar 50 μm)

planktonic state or clumping, showing the typical size and shape for *E. coli* in culture. The cells are seen to swim around in the droplets without the presence of any mean flow. Droplets with clumping display adhesion between cells. The presence of these clumps could be attributed to the presence of adhesion molecules, such as Ag43 or other factors that may contribute to biofilm formation of *E. coli* [106].

At sub-µf·MIC antibiotic concentration, different phenotypes can be observed with different antibiotics 4.12. These phenotypes can directly be linked to the antibiotic mechanism of action.

4.2.1 Ciprofloxacin

When in the presence of ciprofloxacin, the cell stops dividing and starts to elongate. This particular antibiotic of the fluoroquinolones family, targets replication by causing double stranded breaks which trigger the SOS response [110]. Since it stops the division but doesn't stop the metabolism, one observes elongated cells.

Low concentration of ciprofloxacin

In Figure 4.3, the graph depicts a noticeable increase in intensity at lower concentration. Without any antibiotics, the intensity level remains around 35. However, for droplets containing 2 ng/ml and 2.5 ng/ml of the antibiotic, the intensity becomes stronger, with a distribution around 60. Figure 4.13 provides a visual representation showing that cells appear brighter.

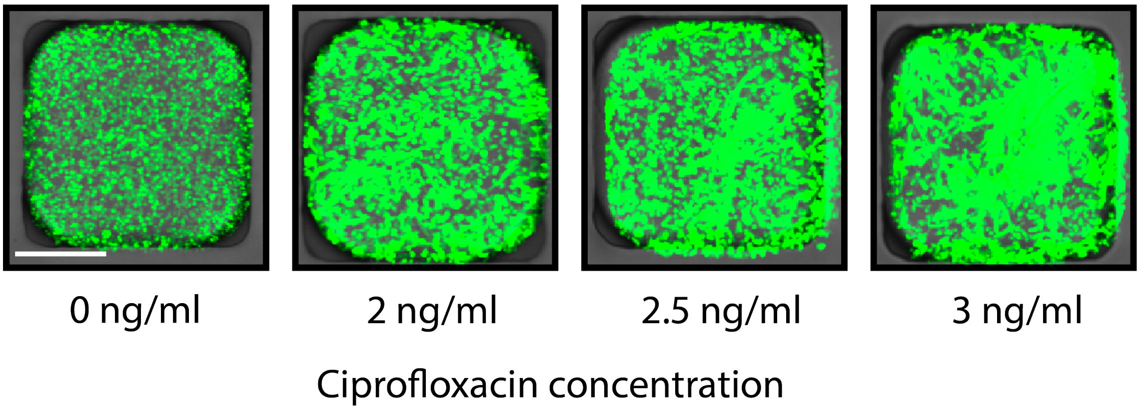

Figure 4.13: **Droplets final state with low concentration of ciprofloxacin.** Example of droplets' final state at low concentration of ciprofloxacin (scale bar 50 μm). Data from the 31.01.2023-1 experiment.

When ciprofloxacin is present at lower concentrations, it triggers a milder SOS response, resulting in cell cycle arrest and DNA repair through the activation of specific genes [111]. This heightened gene expression, combined with the elongation of cells, may explain the observed increase in the fluorescence intensity when using non-lethal doses of ciprofloxacin (Figure 4.13).

High concentration of ciprofloxacin

On the other hand, at higher concentrations of ciprofloxacin, the droplets exhibit distinct phenotypes, such as empty droplets, a small number of freely floating cells, filamentation, and clumping. These phenotypes are further described in Figure 4.14.

Following the overnight incubation, we classify the droplets into two groups: positive droplets that exhibit growth and negative droplets that show no growth. Among the negative droplets, we observe distinct types: "empty droplets" where no cells are present despite having at least one cell at T=0, droplets with one or a few planktonic cells, and droplets with one or a few cells displaying filamentation. Within the positive droplets, there are two subcategories: droplets densely filled

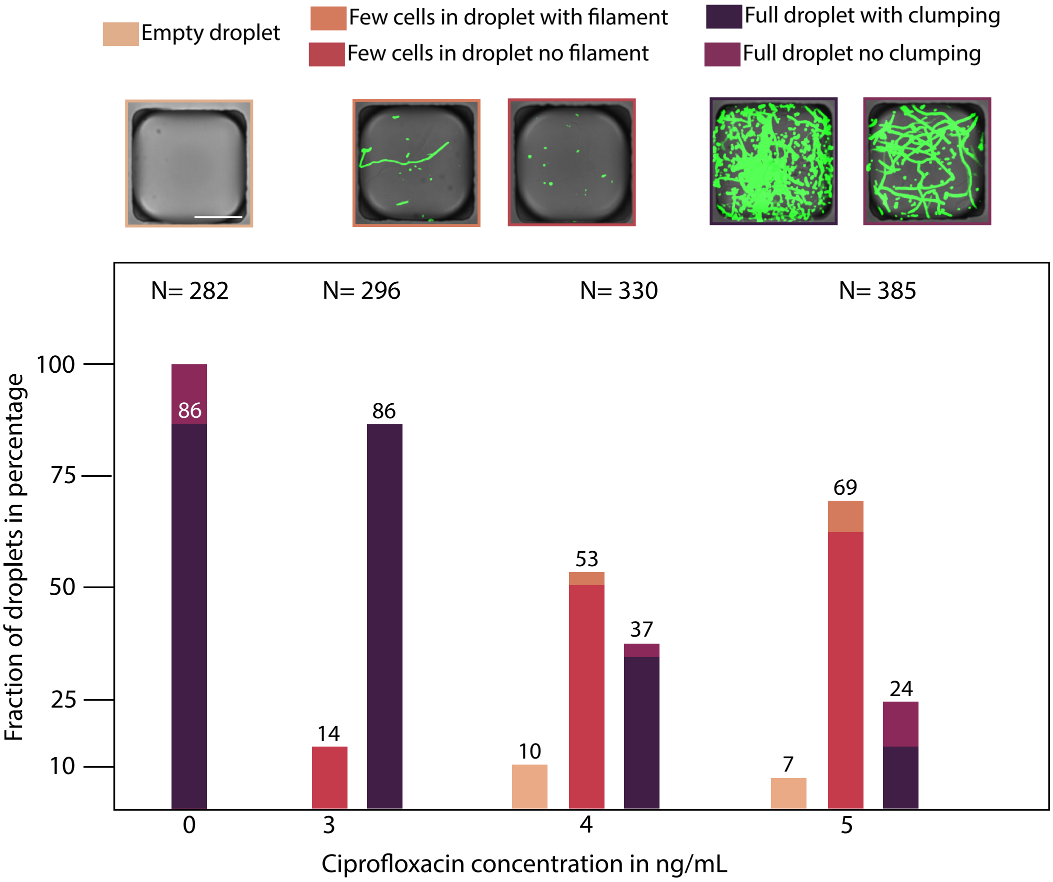

Figure 4.14: **Droplets final state with ciprofloxacin.** Distribution of different phenotype with 3 ng/ml, 4 ng/ml and 5 ng/ml of ciprofloxacin. Images at the top were taken at 4 ng/ml and illustrates the different phenotype that can be found (from left to right): when the droplet is empty, when there are few cells with and without filamentation, when the droplet is full with and without the cells clumping (scale bar 50 μm). Data from the 31.01.2023-1 experiment.

with cells, leading to clumping, and droplets densely filled with cells without any clumping.

Timelapse

In order to conduct a more in-depth investigation, we performed timelapse experiments where we tracked the progress of each droplet over time. We employed a similar acquisition methodology as the time point experiments presented in Chapter 2, capturing a bright field image at the beginning and acquiring fluorescence images every 20 minutes thereafter.

Regardless of the final outcome of the droplet, whether it is positive (exhibiting growth) or negative (showing no growth), filamentation predominantly occurs between 40 to 60 minutes after loading the cells in contact with ciprofloxacin (Figure 4.15). Prior to the onset of filamentation, there are only a few instances of cell division observed.

Following filamentation, two possible outcomes can emerge. Firstly, the cells may resume dividing, resulting in a positive droplet (Figure 4.16). Alternatively,

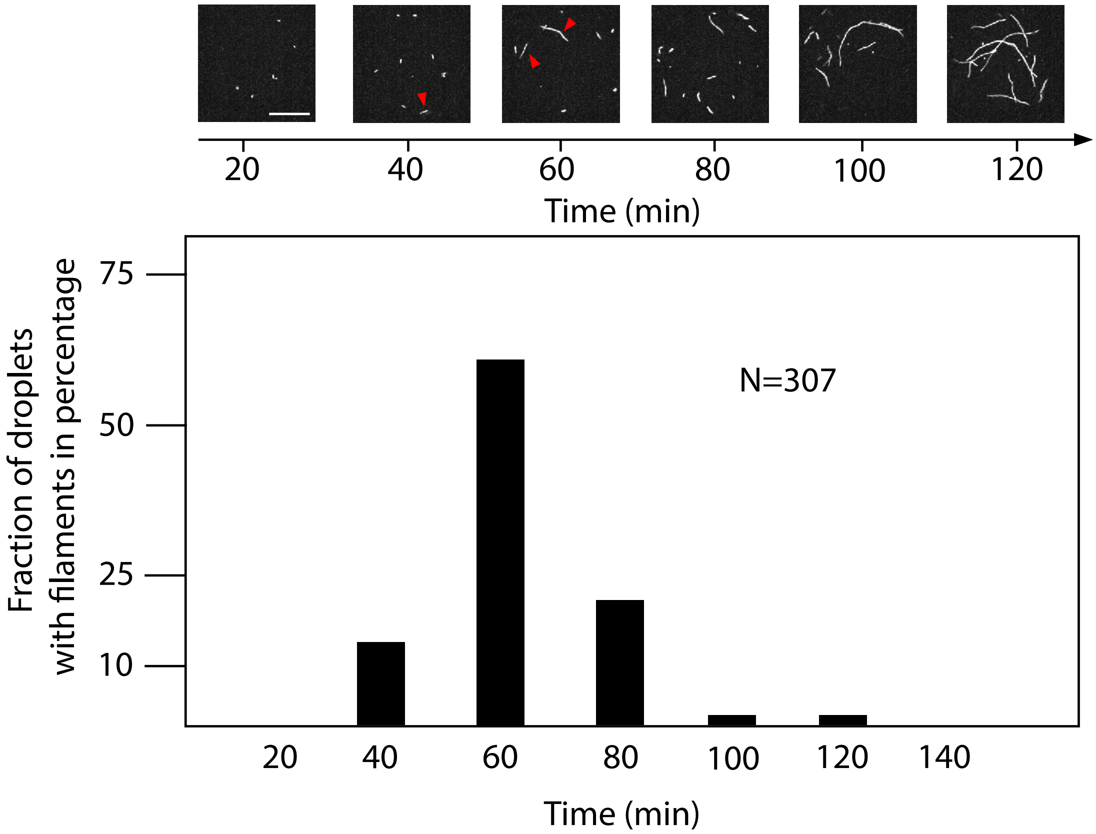

Figure 4.15: **Beginning of filamentation.** Distribution of the beginning of filamentation in the droplets with 5 ng/ml of ciprofloxacin. In the images at the top, beginning of filamentation is shown with the red arrows (scale bar 50 μm).

the cells may fail to divide, leading to a fading fluorescence signal in the filament, indicating cell death (Figure 4.17).

When the cells undergo recovery, the first division can be observed approximately 60 to 100 minutes after the initial elongation commenced (see Figure 4.16). Conversely, if the cells fail to divide again, they remain in a filamentous state for a significantly longer period, lasting about 200 to 220 minutes before the filament begins to fade, leading to cell death (Figure 4.17).

This timeline effectively illustrates the various stages of the SOS response (Figure 4.18). Firstly, the activation of genes involved in ”Repair and Mutagenesis” occurs. These genes code for proteins such as UvrABC excinuclease, which is crucial for nucleotide excision repair, and RecA, required for homologous recombination [112].

Secondly, the activation of ”Cell Division Inhibition” genes, like the *sulA* gene, takes place. The SulA protein is a component of the SOS response and serves as a DNA damage-inducible inhibitor of cell division [112, 113]. Cell division inhibition occurs approximately 60 minutes after exposure to ciprofloxacin, as depicted in Figure 4.15.

Once DNA repair has been completed, certain ”Recovery” genes induced by the SOS response contribute to the recovery phase. These genes facilitate the resumption of synthesis in preexisting replication forks, while establishing new forks at the replication origin. Additionally, recovery genes may play a role in regulating the

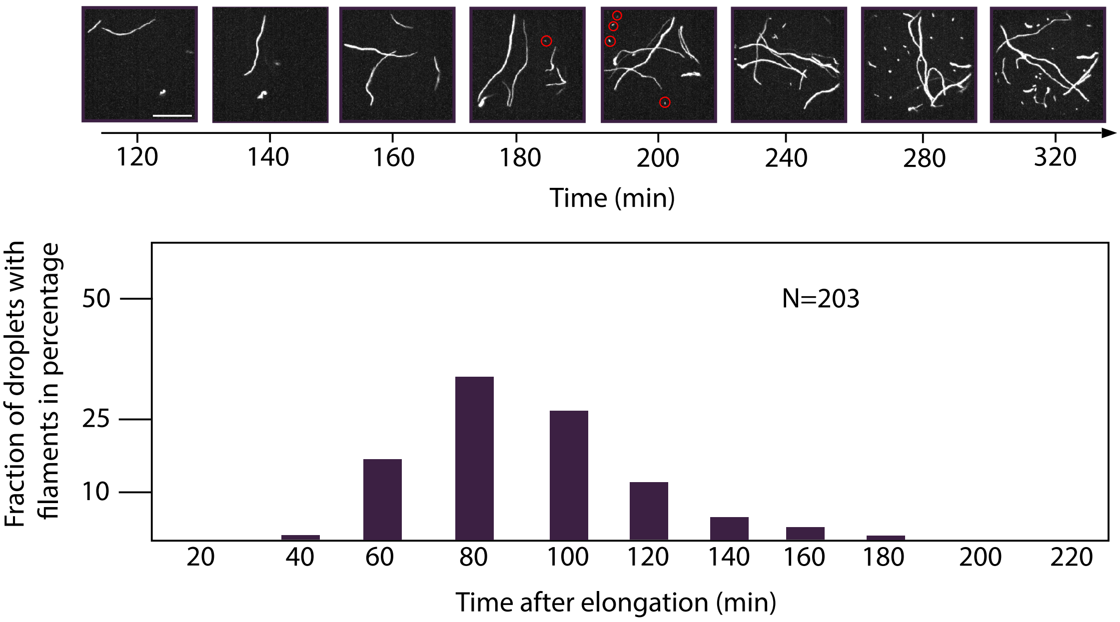

Figure 4.16: **Beginning of division after elongation in positive droplets.** Distribution of the beginning of division after elongation in droplets with 5 ng/ml of ciprofloxacin. In the images at the top the first divisions are shown with the red circles (scale bar 50 μm).

”Repair and Mutagenesis” genes that are no longer necessary [114]. This recovery process occurs approximately 80 minutes after cell division was halted (Figure 4.16).

If the DNA cannot be repaired within a certain time frame, various outcomes may arise. The cell may perish due to an inability to replicate, or certain ”Lethal” genes might trigger cell death to prevent nutrient consumption by dying cells [114]. In Figure 4.17, some cells vanish around 200 minutes after elongation initiation, while others neither disappear nor divide.

4.2.2 Gentamicin

In contrast to ciprofloxacin, the presence of gentamicin does not result in cell elongation. Figure 4.1 illustrates an increase in density: as the concentration of gentamicin rises, the intensity of positive droplets also increases. This can be attributed to the mechanism of action of gentamicin, which is an aminoglycoside antibiotic. Gentamicin binds to the ribosomal A site and interferes with translation, leading to the production of non-viable proteins that accumulate and eventually cause cell death [115]. As depicted in Figure 4.12 and 4.19, the accumulation of these non-viable proteins results in an elevated cell density. The cells become larger and wider.

We identified various phenotypes: a minimal number of droplets were empty (between 7% and 9% in different concentrations), while most negative droplets contained a few cells in a planktonic state: 8% at 0.5 µg/ml 51 and 42 % at 0.6 and 0.7 µg/ml and 88% at 0.8 µg/ml. Among the positive droplets, the majority exhibited clumping, although a few did not exhibit clumping at all (see Figure 4.1).

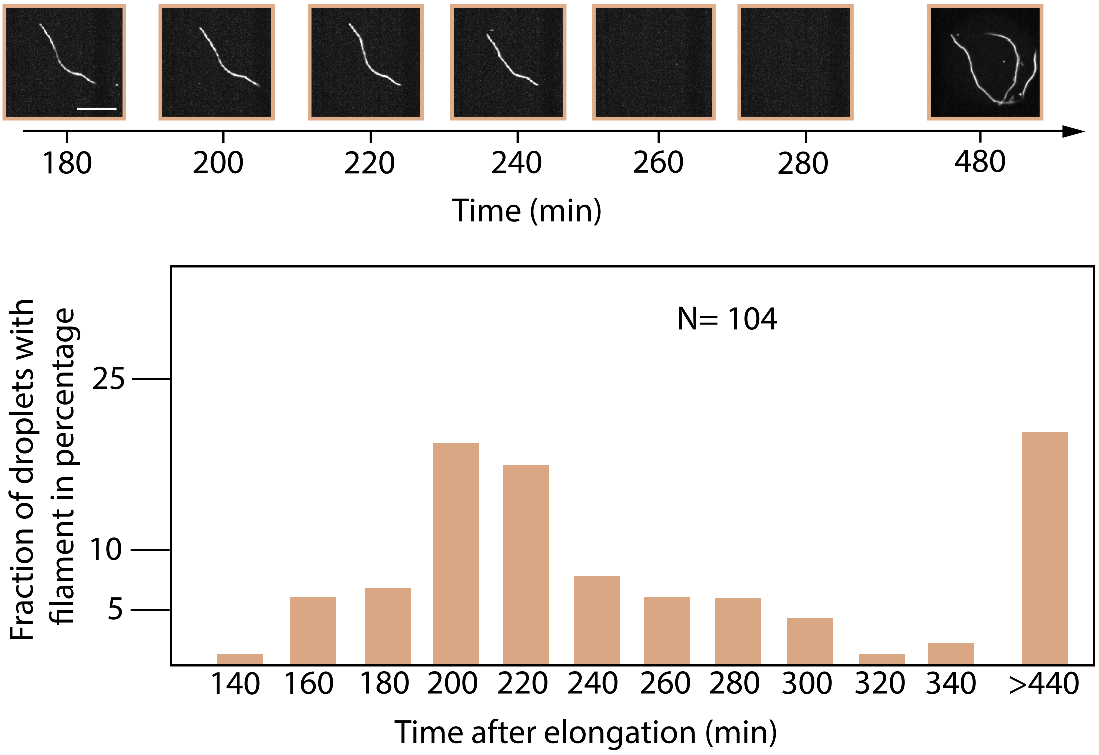

Figure 4.17: **Beginning of filament fading in negative droplets.** Distribution of the beginning of filament fading in droplets with 5 ng/ml of ciprofloxacin after elongation. In the images at the top, no division is occurring and the fluorescent disappear between 240 and 260 minutes after inoculation with ciprofloxacin. After 480 min (end of the timelapse), some cell are still fluorescent but never formed a colony after elongation (scale bar 50 μm).

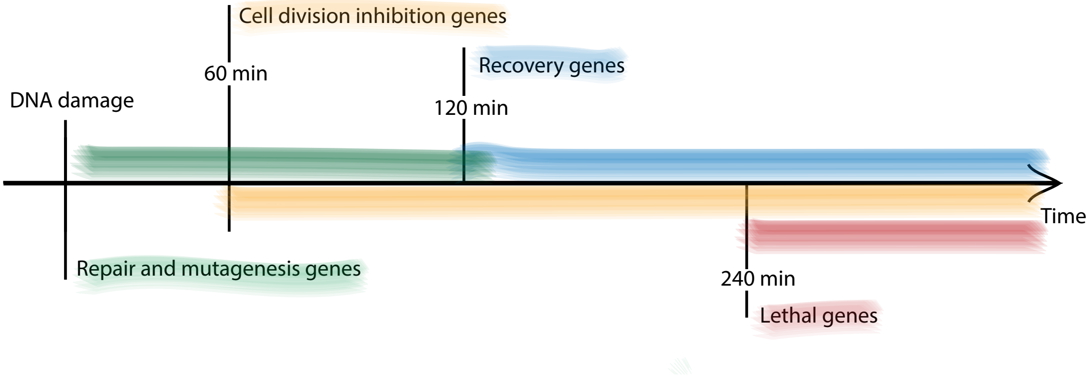

Figure 4.18: **SOS response timeline.** After DNA damage, the *repair and mutagenesis* genes are activated, followed by the *cell division inhibition* genes, the *recovery* genes and in some cases the *lethal* genes.

4.2.3 Tetracyclin

Tetracycline targets the same ribosomal subunit as gentamicin [115]. However, the difference lies in their effects: tetracycline is bacteriostatic, meaning it inhibits bacterial growth without killing the cells. It achieves this by targeting protein synthesis, thereby halting metabolism. In contrast to gentamicin, tetracycline does

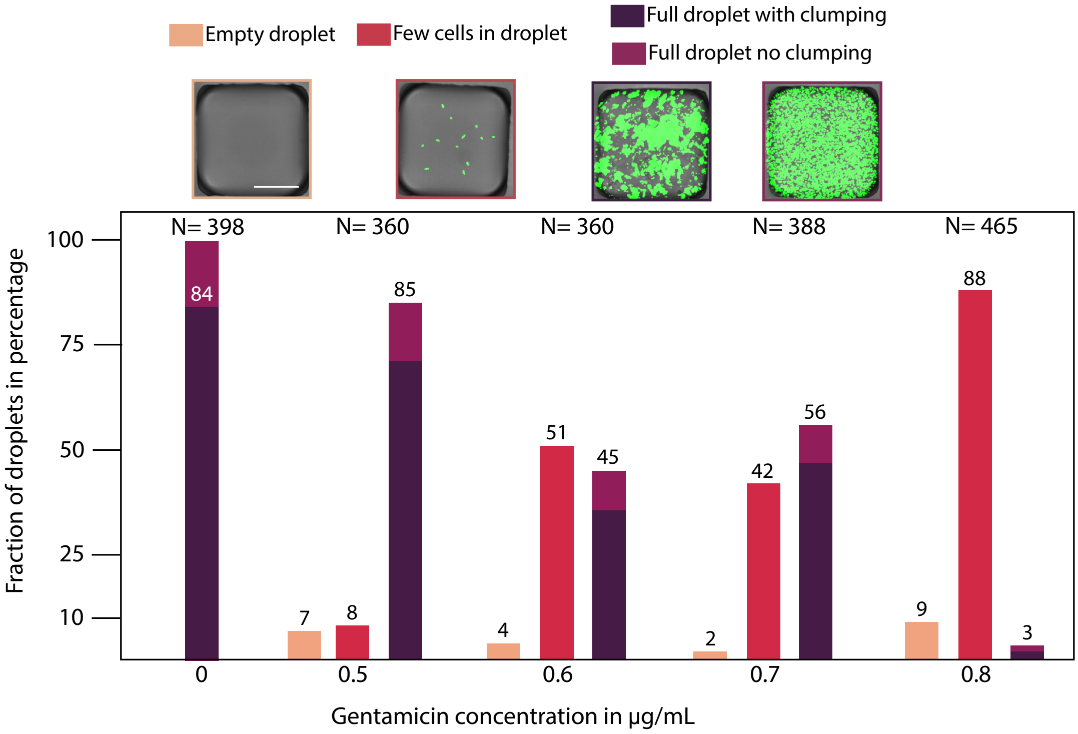

Figure 4.19: **Droplets final state with gentamicin.** Distribution of different phenotype with 0.5 µg/ml, 0.6 µg/ml, 0.7 µg/ml and 0.8 µg/ml of gentamicin. Images at the top were taken at 0.6 µg/ml and illustrates the different phenotype that can be found (from left to right): when the droplet is empty, when there are few cells, when the droplet is full with and without the cells clumping (scale bar 50 μm). Data from the 10.01.2023-1 and 10.01.2023-2 experiment.

not induce cell death [116]. Figure 4.5 demonstrates that as the concentration of tetracycline increases, the intensity of positive droplets decreases.

We observed similar phenotypes to those seen with gentamicin. These include empty droplets and negative droplets with a few cells in a planktonic state. Within the positive droplets, we observe clumping similar to what is observed with gentamicin (see Figure 4.20).

At a tetracycline concentration of 20 µg/ml, 21% of the positive droplets are in a planktonic state. This percentage remains relatively consistent at 17% when the tetracycline concentration is increased to 40 µg/ml. Similarly, for gentamicin, the proportions of droplets in a planktonic state are 17% at 0.5 µg/ml and 19% at 0.6 µg/ml. Interestingly, the proportion of clumping versus the planktonic state does not appear to be influenced by the concentration of either tetracycline or gentamicin.

4.2.4 Chloramphenicol

Similar to tetracycline, chloramphenicol is a bacteriostatic antibiotic that does not kill cells. Instead, it hinders protein synthesis, thereby halting metabolism and preventing cell growth and division [117]. Unlike tetracycline, chloramphenicol targets the 50S subunit of the ribosome, a distinct subunit involved in translation.

In contrast to other antibiotics that target translation, we do not observe bacteria clumping with chloramphenicol. However, similar to tetracycline, another bacteriostatic antibiotic, an increase in chloramphenicol concentration leads to a reduction in cell density within the droplet (see Figure 4.21). Except for a few filaments ob-

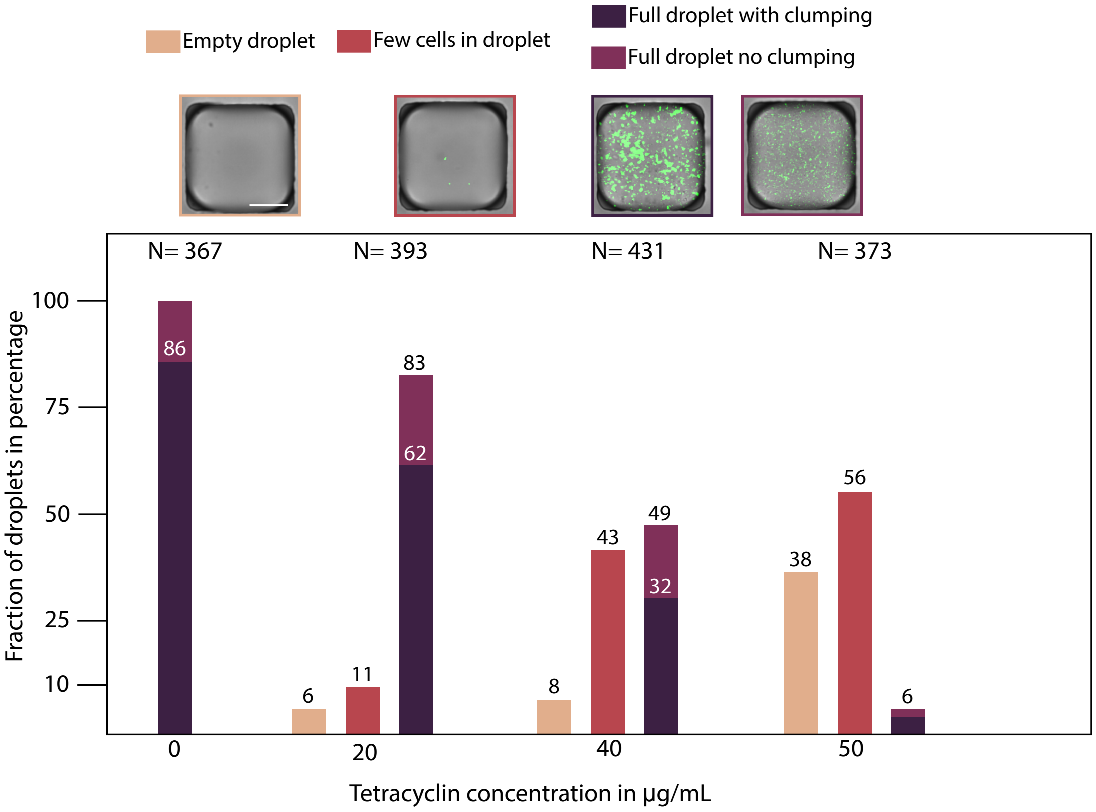

Figure 4.20: **Droplets final state with tetracyclin.** Distribution of different phenotype with 20 µg/ml, 40 µg/ml, and 50 µg/ml of tetracyclin. Images at the top were taken at 40 µg/ml and illustrates the different phenotype that can be found (from left to right): when the droplet is empty, when there are few cells, when the droplet is full with and without the cells clumping (scale bar 50 μm). Data from the 04.04.2023-1 experiment.

served at high concentrations, chloramphenicol does not seem to have a pronounced effect on the phenotype.

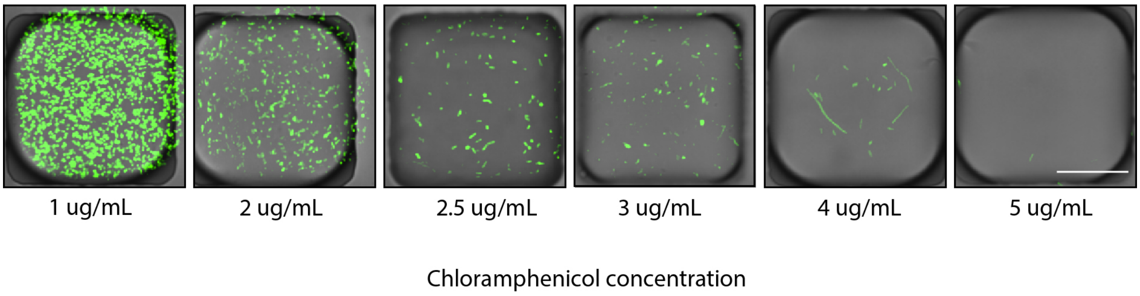

Figure 4.21: **Droplets final state with chloramphenicol.** Example of droplet final state with different concentration of chloramphenicol (scale bar 50 μm). Data from 21.02.2023-1 and 21.02.2023-2 experiment.

4.2.5 Ampicillin

Ampicillin is classified as a bactericidal antibiotic that exerts its action by irreversibly inhibiting the enzyme transpeptidase. This enzyme is vital for bacterial cell wall synthesis. Ampicillin specifically targets the third and final stage of this process, resulting in the disruption of cell wall formation and ultimately leading to cell lysis [118]. It belongs to the class of beta-lactam antibiotics.

It is worth noting that beta-lactam antibiotics, including ampicillin, can exhibit what is known as the inoculum effect. This effect implies that the effectiveness of the drug depends on the initial density of the bacterial population [16]. Consequently, we cannot assume that bacteria within the droplet behave independently. Therefore, we encountered difficulty in calculating the susceptibility of individual cells due to this inoculum effect.

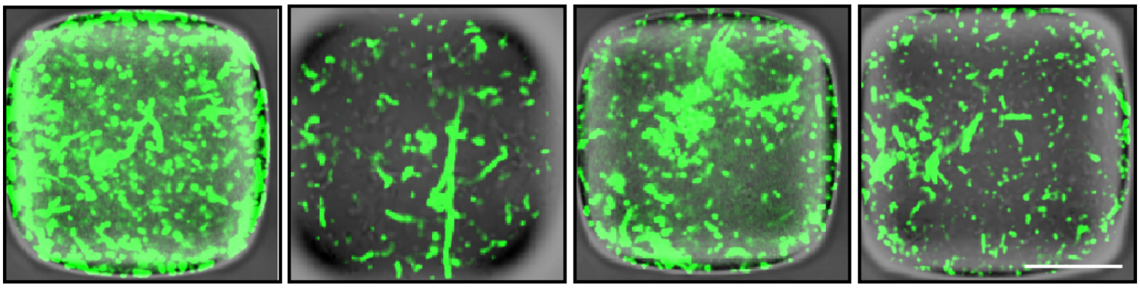

Figure 4.22: **Droplets final state with ampicillin.** Example of droplet final state with 4 µg/ml of ampicillin (scale bar 50 μm). Data from 21.02.2023-1 and 02.06.2022 experiment.

In Figure 4.22, we can observe different phenotypes resulting from exposure to 4 µg/ml of ampicillin. The effects include clumping and elongation, similar to those caused by other antibiotics. However, we also notice that certain droplets exhibit increased fluorescence in the background, which is unique to ampicillin. This observation directly correlates with the mechanism of action of ampicillin. Specifically, the cell death mechanism involves cell lysis, releasing fluorescent proteins into the surrounding media. This release leads to a significant increase in background fluorescence.

4.3 Conclusion: Bacteriostatic or Bacteriocidal ?

Bacteriostatic antibiotics exert their inhibitory effect on ribosome function by targeting both the 30S subunit (tetracycline) and the 50S subunit (chloramphenicol). At a phenotypic level, they demonstrate similarities, such as a reduction in cell density with increasing antibiotic concentration. However, they still retain their distinct mechanism of action. For instance, tetracyclin and gentamicin both target the 30S subunit of the ribosome. Despite this similarity, one exhibits bacteriostatic activity while the other is bactericidal. Surprisingly, we observed similar phenotypes in these cases like more clumping.

Bactericidal antibiotics induce cell death through different mechanisms, such as DNA damage (ciprofloxacin) or protein damage (gentamicin, ampicillin) [116]. Regardless of their diverse mechanisms, all bactericidal antibiotics are reported to trigger the formation of reactive oxygen species, contributing to cell death [114]. Additionally, we discovered that their killing action is more consistent and severe compared to bacteriostatic antibiotics, as illustrated in Figure 3.8. Remarkably, we observed distinct responses at the phenotypic level. Our microfluidics pipeline enables us to obtain high-quality images, allowing us to identify different cell phenotypes directly associated with the mechanisms of antibiotics.

In particular, when exposed to ciprofloxacin, bacteria exhibit intriguing phenotypes, such as elongation. By monitoring the content of individual droplets over time, we were able to delve into the dynamics of these phenotypes. Consequently, combining this microfluidic device with cellular biology provides a valuable means to study the SOS response and identify the various roles of genes involved in this response.

Key takeaway

Context: By employing this microfluidic pipeline with anchored droplets, it becomes possible to acquire information regarding the population level, individual level, and phenotypic characteristics under varying antibiotic concentrations. This experimental pipeline can be used with various antibiotics. **Results:** The reproducibility of digital antibiograms and single cell susceptibility varies depending on whether the antibiotic is bactericidal or bacteriostatic. When it comes to the phenotype, it can be directly linked to the mechanism of action of the antibiotic.

Chapter 5

Conclusion, perspectives, potential applications

In this manuscript, I have introduced a microfluidic platform that utilizes microfluidic droplets to investigate antibiotic susceptibility at the individual cell level. By analyzing digital antibiograms, we can derive the microfluidic MIC (µf·MIC) as well as the single-cell susceptibility, which represents the probability of a cell failing to form a colony. This platform provides us with qualitative information as well. By imaging the contents of the droplets, we can directly observe various phenotypes that are closely linked to the mechanisms of action of the antibiotics.

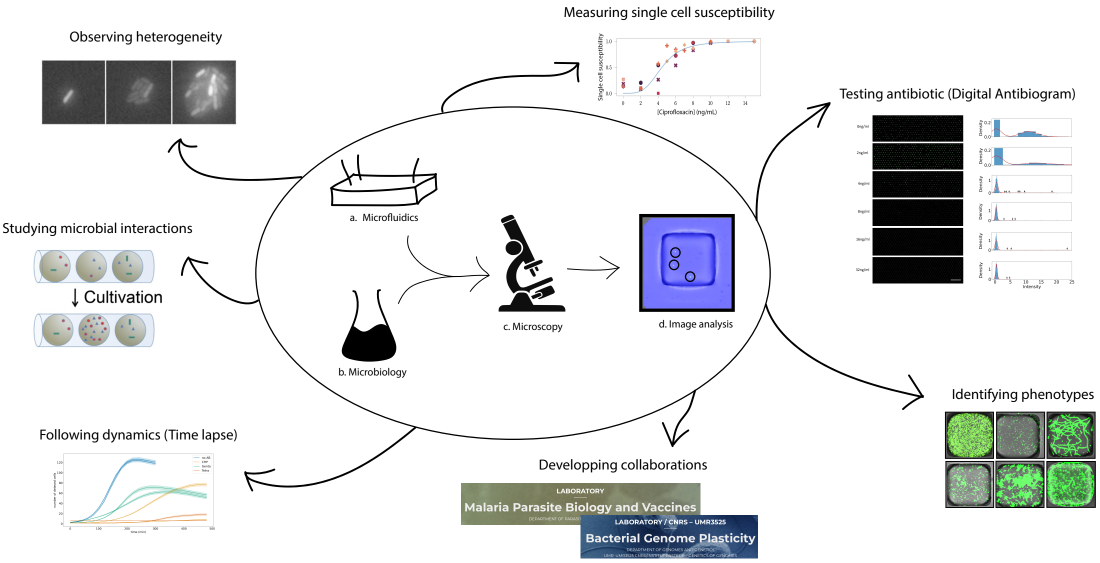

Figure 5.1: **The microfluidic pipeline and its applications.**

Compared to alternative methods, the use of anchored droplets significantly reduces cross-contamination between droplets and enables the tracking of individual droplets over time. The breaking loading technique I presented is more robust than conventional droplet generators, and the loading process can be performed without the need for syringe pumps. Furthermore, the technology has been made fully accessible for utilization. Even with complete accessibility, examining the individual cell level requires the use of fluorescent strains and a confocal microscope, which can be quite expensive. However, it is possible to modify the current process to accommodate non-fluorescent strains, as the quality of bright-field microscopy is sufficient to determine if there is growth or not. Nevertheless, this modification would result in the loss of single cell information and the ability to determine the initial number of cells.

Beyond its application as a tool for antibiotic susceptibility testing (AST), this platform holds potential for various other biological applications (Figure 5.1).

5.1 General conclusion

5.1.1 Consideration of the technical choices

Bacterial strain

Additionally, the microfluidic device can support the growth of other strains such as *K. pneumoniae* and *V. cholerae*. One advantage of using *K. pneumoniae* is its non-motile nature, which allows it to sedoment within the droplets [119]. This characteristic potentially eliminates the need to scan the entire droplet to determine the cell count. On the other hand, *V. cholerae* is an interesting model organism for antimicrobial resistance studies due to its high infectious dose [120]. However, it's important to note that both *K. pneumoniae* and *V. cholerae* are pathogens categorized as biosafety level 2, necessitating appropriate laboratory facilities for the culture and the loading steps.

Format of the chip

The microfluidic chip was specifically designed to accommodate 500 droplets, each containing 2 nl of volume. By accurately counting the number of cells in each droplet, we can achieve an average cell count per droplet, denoted as λ, of 1. Unlike other studies where most of the droplets often contain no cells ($\lambda << 1$) [16], the majority of our droplets contain a single cell ($\lambda = 1$). This approach enables us to increase the average number of cells per droplet, thereby reducing the total number of droplets required from several thousand to just 500.

Maintaining a single cell per droplet results in a concentration of 1 cell in 2nl. This concentration is equivalent to having 10^5 cells in $200\mu l$ (a well of a 96-well plate) or a concentration of 5.10^5 CFU/ml. Notably, 5.10^5 CFU/ml is the cell concentration typically used in the classical broth dilution method [121]. Therefore, by targeting an average of one cell per droplet, we achieve a bacterial inoculum that aligns with the requirements for conducting MIC experiments using the broth dilution method.

Efficiency of the pipeline

The presented microfluidic pipeline offers several advantages in terms of its applications, time efficiency, and material consumption.

During a single experiment consisting of six different conditions, we have the ability to obtain information at both the population level (across the entire chip with 500 droplets) and the single-cell level (within each individual droplet). The entire chip can be compared to a 96-well plate, but with the advantage of having 500 droplets instead of just 96 wells. Each droplet can be compared to experiments conducted on agar pads, where we can track the content within each droplet similar to observing bacteria on agar pads.

Furthermore, loading the six chips only takes approximately 30 minutes, which represents a significant time-saving compared to loading a 96-well plate and preparing agar pads. This streamlined loading process contributes to the overall efficiency of the microfluidic pipeline, allowing for more rapid experimentation while reducing material usage.

By working with smaller volumes (2 nl), we are able to observe the results of each individual droplet within a shorter timeframe. Specifically, within just 10 hours, we can determine whether a droplet has resulted in colony growth or not. In comparison, when using 96 well plates, it typically takes 24 hours to obtain the same outcome for each well [121].

5.1.2 Limitations of the pipeline

Fluorescence and confocal microscope

The use of the confocal microscope is a major constraint in the pipeline for the following reasons:

Firstly, the confocal microscope is a costly equipment that poses difficulties in its operation. In fact, initial setups may require optimization before achieving optimal performance. Moreover, in the event of any issues, such as problems with the laser, only an expert can resolve them.

Secondly, the observation of bacteria necessitates fluorescence. One approach to achieve this is by genetically modifying the bacterial strains. However, this method has limitations as it restricts the pipeline's usability to laboratory strains, excluding clinical strains.

Data storage

The data storage aspect posed a significant limitation. Acquiring 3D images requires a substantial amount of space. Specifically, scanning the six chips in the fluorescence channel in 3D occupies 40 GB, while scanning the same number of chips in bright field takes up 2 GB. To put it in perspective, a 3D scan of one chip is equivalent to 6000 photos taken with a regular mobile phone.

Handling data storage becomes even more challenging during timelapse experiments, where scans are conducted every 20 minutes. For instance, a timelapse spanning 10 hours results in 200 GB of data per chip.

These storage requirements have implications for computer disk space, image analysis time, and long-term data availability.

To address the issue of data volume, we employ a direct conversion of the acquired nd2 files into zarr files. The zarr file contains both the bright field acquisition and the fluorescence acquisition after applying the max projection (as referenced in Chapter 2). This conversion significantly reduces the size to 3 GB.

5.2 Further work

5.2.1 Training an artificial intelligence to recognize the different phenotypes

Working with droplet microfluidics entails managing a significant amount of data, and manually analyzing phenotypes can be exceedingly time-consuming. To address this challenge, we opted to train an Artificial Intelligence (AI) system to autonomously characterize the various phenotypes of bacteria within the droplets.

To train the AI, all droplets are combined regardless of the antibiotic used or its concentration.

Initially, we established a category called *junk* for droplets that should be disregarded (Figure 5.2). This category includes shrunken droplets resulting from evaporation, coalesced droplets when multiple droplets merge together, and empty anchors when no droplet is formed. The latter two cases can occur due to occasional loading malfunctions in a few anchors.

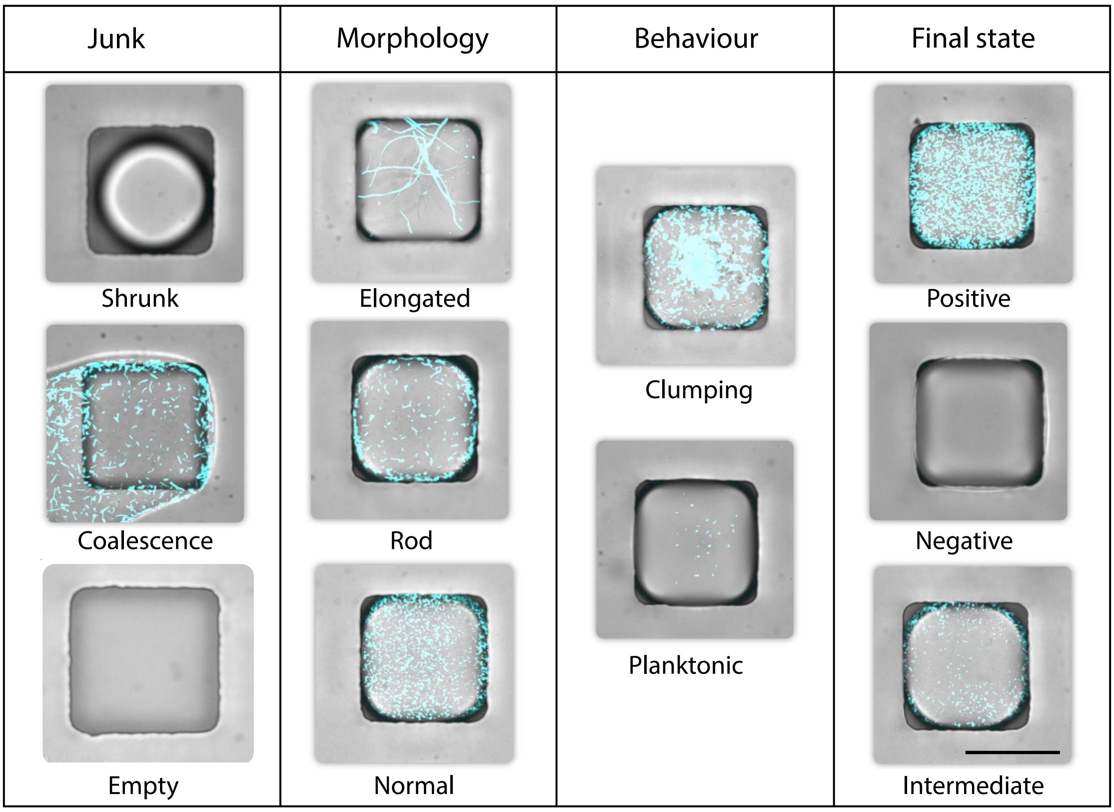

Figure 5.2: **Examples of phenotypes categories for AI training.** Droplets can be categorized in three different features: Morphology, Behaviour and final state. The junk category served to clean the data by removing not wanted droplets. Images were picked up randomly from the AI training platform (scale bar 100 µm)

Next, we defined categories for different phenotypes, which can relate to the morphology and behavior of cells within the droplets (Figure 5.2. A cell can appear *normal*, resembling a dot, or it can be *elongated* or in a *rod* shape, indicating thick oval-shaped bacteria. Phenotypes can also describe how cells behave within the droplets, such as being in a *planktonic* state or in a *clumping*. Furthermore, phenotypes can reflect the final state of the droplet, whether it shows no growth (*negative*) or growth (*positive*). For some antibiotics, the distinction between positive and negative growth may not be straightforward, resulting in an *intermediate* state where it is unclear if the growth should be considered positive.

Integrating this AI-based tool into the pipeline will provide us with additional information about phenotypes and their frequencies. By incorporating features related to morphology and cellular behavior, we can enhance the overall output and gain a better understanding of how these phenotypes interact.

5.2.2 Timelapse microscopy

As discussed in Chapter 2, employing anchored droplets enables tracking over time. We conducted timelapse microscopy experiments with various concentrations of chloramphenicol (2 and 4 µg/ml), gentamicin (0.5 and 0.6 µg/ml), and tetracycline (50 and 80 µg/ml), along with a control group without antibiotics. Each microfluidic chip was imaged at 37°C at 20-minute intervals. From the acquired images, we quantified the number of cells in each droplet and measured the corresponding fluorescence signal (Figure 5.3). Both of these parameters serve as proxies for assessing the growth within each droplet.

In Figure 5.3a, the plot illustrates the number of detected cells over time. Analyzing the number of detected cells provides valuable insights during the initial stages since individual cells can be identified from the beginning.

In Figure 5.3b, the plot demonstrates the fluorescence signal over time. Examining the fluorescence signal yields meaningful information at later time points when distinguishing individual cells within a droplet becomes challenging.

It is worth noting that for chloramphenicol, analyzing these two parameters yields contrasting information (indicated by the red arrows in Figure 5.3). This suggests that the choice between counting cells or analyzing fluorescence signal depends on the specific aspect of interest and the antibiotic being used.

The ability to observe and analyze the growth and dynamics within droplets represents a powerful tool that requires further development.

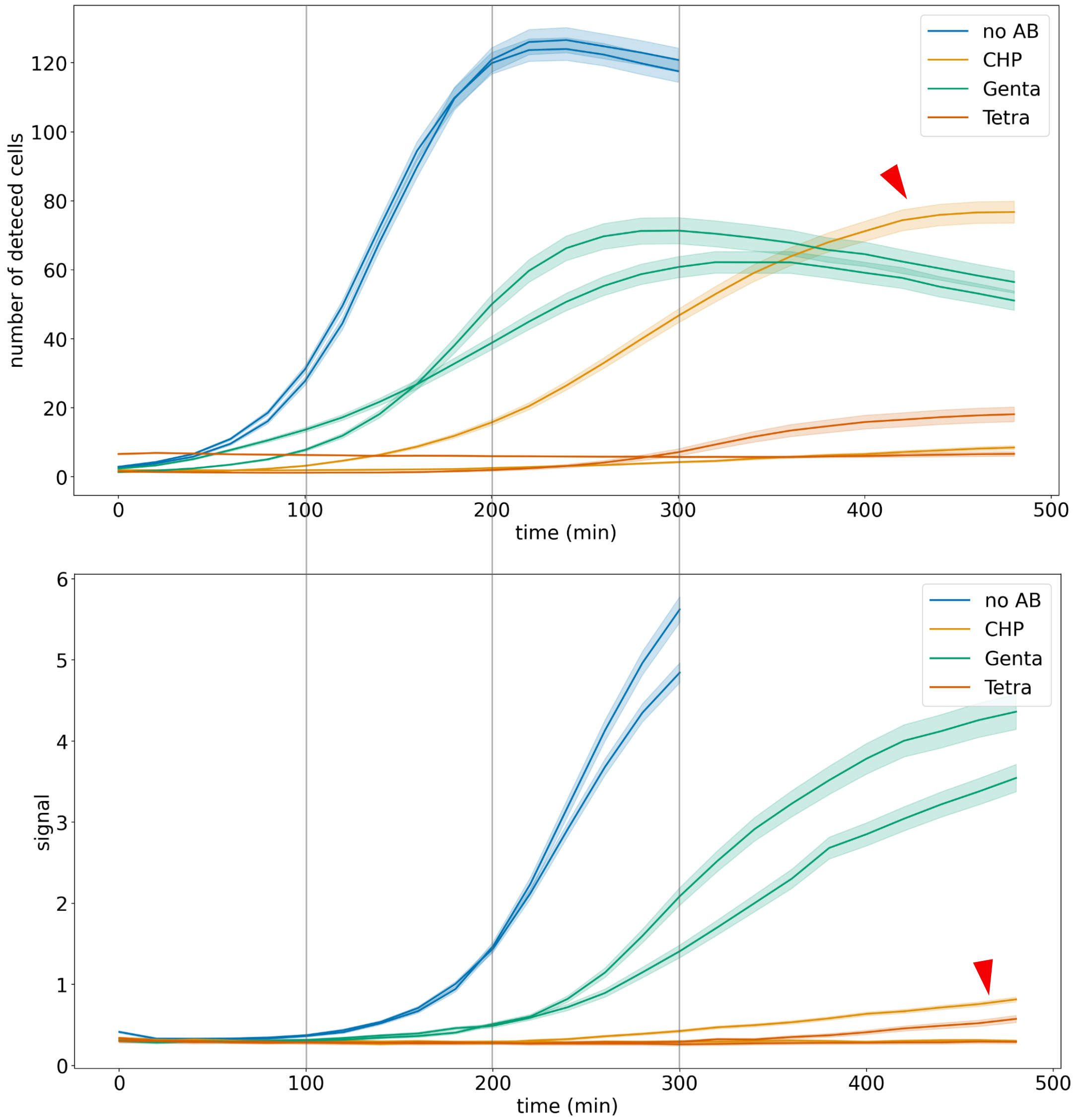

Figure 5.3: **Mean growth curves.** Mean growth curves from the 500 droplets regarding **(a)** the number of cells and **(b)** the fluorescence signal with no antibiotic (two replicates), 2 and 4 µg/ml of chloramphenicol (CHP), 0.5 and 0.6 µg/ml of gentamicin (Genta), 50 and 80 µg/ml of tetracyclin (Tetra). The red arrows point at the 2 µg/ml choramphenicol growth curve.

5.3 Other applications

5.3.1 Observing the heterogeneity

Phenotypic heterogeneity refers to the variability found among individual cells or other biological entities within populations that are genetically identical. In the field of biology, there are two types of heterogeneity: genetic heterogeneity, which arises from allelic variations within a population derived from a single cell, and phenotypic heterogeneity, which pertains to differences in the characteristics exhibited by individual organisms.

Phenotypic heterogeneity can arise from stochastic fluctuations even before any stress occurs, similar to a bet hedging strategy. It can also be driven by the environment, where individual cells sense and respond to stressors.

There are various methods to measure heterogeneity. One possibility is to examine protein or RNA levels using proteomics and transcriptomics techniques. However, these approaches often face challenges in terms of stability and have a low throughput, typically operating at large scales. Another technique, flow cytometry, allows for the identification of subpopulations and offers high throughput but has relatively low resolution [122]. On the other hand, single-cell experiments conducted using agar pads and microscopy provide high resolution but suffer from low throughput [123].

Our microfluidic chip enables us to combine high throughput and high resolution, allowing for the observation of heterogeneity within monoclonal populations. For instance, we could investigate the phenomenon of sporulation, which occurs in certain bacteria as a response to starvation. Even before any starvation occurs, some bacteria are already in the process of forming endospores [123].

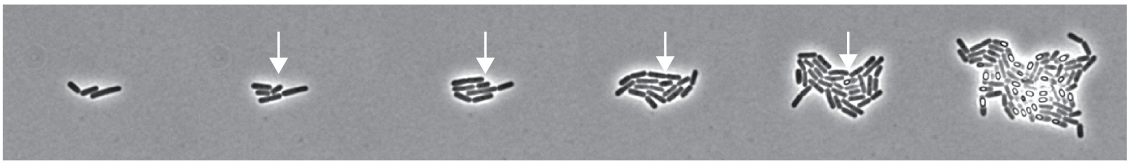

Figure 5.4: **Frame of a time lapse microscopy recording *B. subtilis*** One cell stops dividing (2nd panel from the left) and produces a spore of which the center turns bright in phase contrast microscopy. Continuing cell division of the surrounding siblings demonstrates that nutrients were not limited at the time the decision to initiate sporulation was made by the indicated cell. This first spore is thus the product of stochastic switching (from [123], copyright 2015 Elsevier).

The presence of this phenomenon is easily noticeable on agar pads (Figure 5.4), but its quantification is challenging due to the limited capacity for high-volume analysis provided by agar pads.

Another example of heterogeneity that can be observed using our microfluidic chip involves the presence of different respiratory systems. Surprisingly, certain bacteria continue to utilize anaerobic respiratory systems, as indicated by the expression of *torCAD* genes, even in the presence of oxygen. This cell-to-cell variability can be seen as an adaptive strategy to prepare for potential changes in the environment [124, 125]. In Figure 5.5, the distribution of CFP fluorescence from the constitutive *ompA* promoter appears uniform throughout the cells. In contrast, the fluorescence of YFP, which serves as a fluorescent reporter for the *torCAD* genes, exhibits variations among individual cells.

Our microfluidic chip could enable the observation of numerous other phenomena, such as biofilm formation, wherein subsets of bacteria undergo differentiation into distinct morphological cell types throughout the process. This phenomenon suggests that individual bacteria within the population perform specific functions to contribute to the formation of these structures [126].

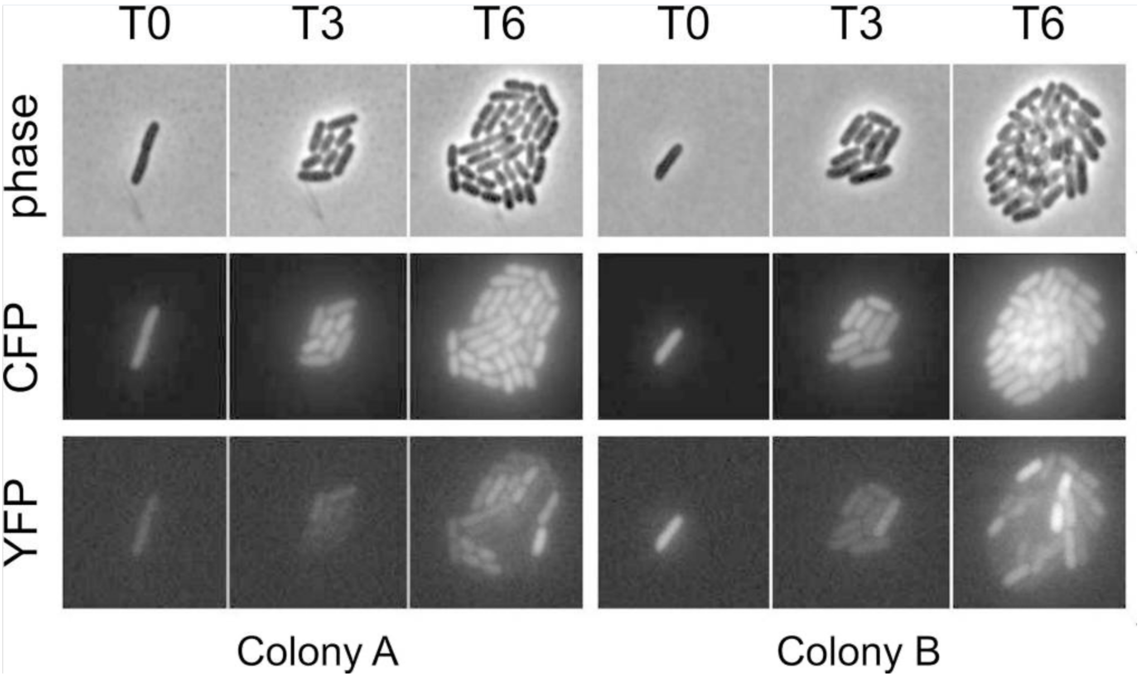

Figure 5.5: **Time-lapse microscopy of two representative microcolonies** The images shown are of two representative colonies, each derived from a single cell, shortly after immobilization on agarose pads (T0) and then 3 h (T3) and 6 h (T6) after the starting time point (approximately four and eight divisions, respectively). The rows consist of phase-contrast images (top), CFP fluorescence images (middle), and YFP fluorescence images (bottom) (from [125]), copyright 2015.

5.3.2 Microbial cohabitation

Our microfluidic platform offers potential applications in the study of microbial cohabitation. One such application involves investigating the interactions between different strains of bacteria within a single droplet. This enables us to explore scenarios such as competition between a resistant and a sensitive strain, focusing specifically on antimicrobial resistance. Additionally, we can examine bacterial conjugation, which is a primary mechanism for horizontal gene transfer. Carranza *et al.* conducted a study where they visualized the results of the conjugation process. The conjugation was performed on enriched M9 minimal media plates, and then the cells were transferred to a microscope for image recording. Images were captured at different wavelengths using fluorescent reporters to differentiate between donor, recipient, and transconjugant cells [127]. In Figure 5.6, the donor cells are depicted in red, the recipient cells in green, and the transconjugant cells (recipient cells that received plasmids from donor cells) in orange. By observing bacterial conjugation within droplets, we could potentially track the dynamic nature of this phenomenon over time in a high-throughput manner.

In a separate study by Letten *et al.*, an ecological theory is proposed to illustrate how changes in resource niche overlap can be as significant as changes in competitive ability when studying the cost of resistance (Figure 5.7). The cost of resistance refers to a reduction in the fitness of a mutant strain possessing a resistant allele compared to its antibiotic-susceptible ancestor. From an ecological standpoint, a cost of resistance is akin to a decrease in competitive ability [128]. By utilizing droplets, it should become feasible to observe the competition between resistant and sensitive strains, both with and without antibiotics, and to test their partitioning

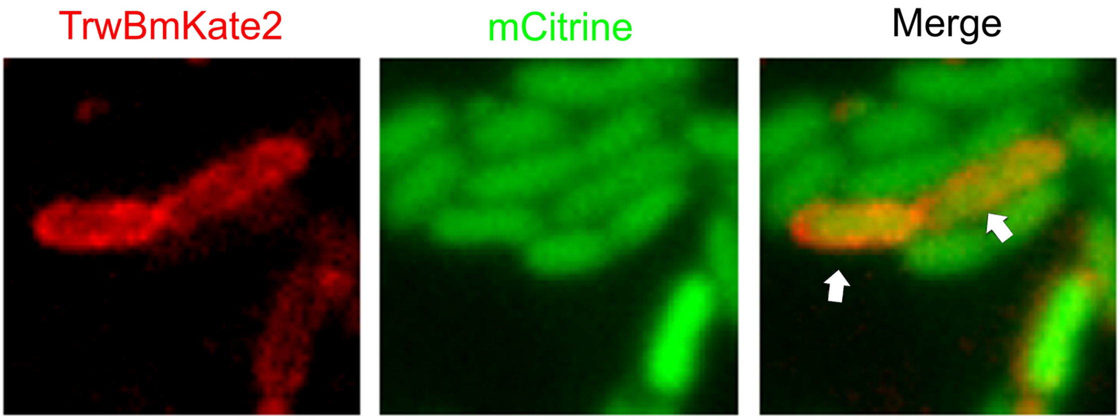

Figure 5.6: **Visualization of transconjugant cells.** MG1655 donor cells hosting R388:*trwBmKate2* were mixed with UB1637 recipient cells expressing mCitrine. Merged images show the transconjugants cells in orange (right panel). These transconjugants are UB1637 cells expressing mCitrine that, after receiving the R388 plasmid, have started to express TrwBmKate2 encoded by the plasmid. (adapted from [128], copyright 2021 Carranza *et al.*).

cost theory through experimental observations.

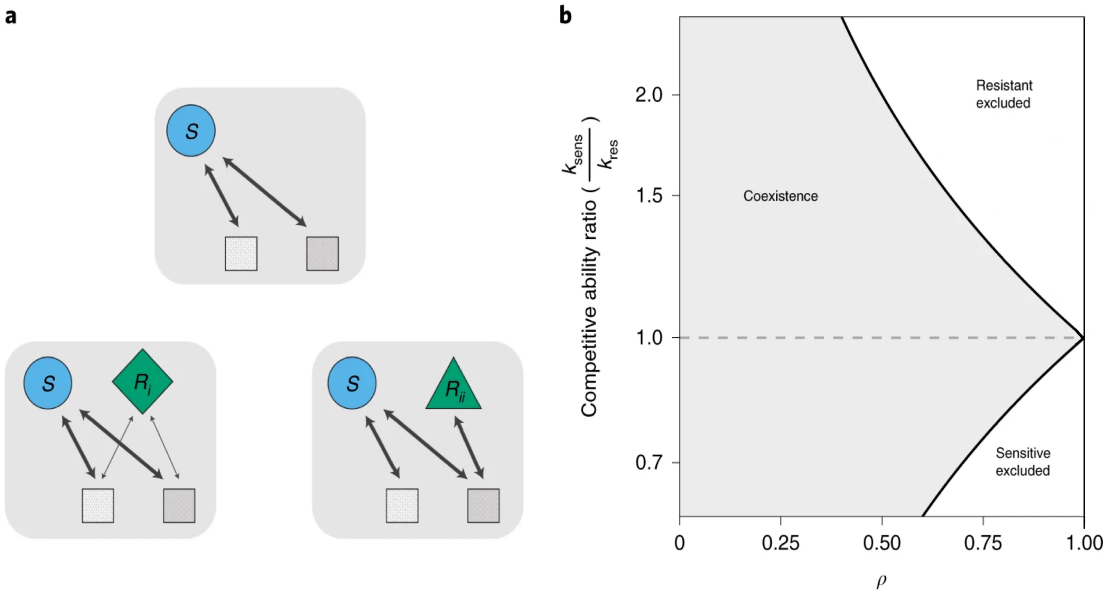

Figure 5.7: **Partitioning costs of resistance into competitive ability differences and niche overlap. (a)** Basic food webs for an antibiotic-susceptible pathogen (S) consuming two substitutable resources in the absence (top) and presence (bottom) of two different antibiotic-resistant mutants, exhibiting either an equal magnitude loss in performance on both resources (R_i, bottom left) or a loss in the ability to metabolize one of two resources with no change in performance on the other resource (R_{ii}, bottom right). **(b)** Change in niche overlap (ρ) and competitive ability differences between the susceptible and resistant strain. Grey shaded region indicates parameter space corresponding to coexistence; unshaded region indicates parameter space corresponding to exclusion. (adapted from [128], copyright 2021 Letten *et al.*).

Key takeaway

The microfluidic pipeline with anchored droplets proves to be effective for both antibiotic susceptibility testing and phenotyping at the single cell level. However, the data obtained can be further analyzed and leveraged through the use of AI or by examining the dynamics of each individual droplet in greater detail. This serves as a promising proof of concept that can be applied to a wide range of biological inquiries involving heterogeneity.

Chapter 6

Appendix

6.1 Protocols

6.1.1 Photoresist lithography

- Adjust the hot plates on 65°C, 95°C, and 180°C.
- Turn the Hg light on.
- Put the glass wafer on the 180°C hot plate for 15 minutes.
- Remove the glass wafer from the hot plate and let it cool down.
- Put the glass wafer in the Labspin and check that the vacuum is functional.
- Pour the resin Su-8 2025 for the first layer, without making air bubble. The resin has to cover 1/3 of the wafer.
- Spincoat at 3000 rpm.
- Soft bake at 65°for 1 minute and 30 seconds and at 95°for 5 minutes and 30 seconds.
- Position the quartz plate with the mask and check the alignement in the microscope (command ”microcsope down”).
- At the end of the soft bake, place the wafer with the quartz plate.
- Set up the MJB4 with an exposure time of 15 seconds and proceed to exposure.
- Immediately after, execute the post exposure baking : one minute at 65°C and 5 minutes 30 seconds at 95°C.
- Place the wafer in a beaker with Propylene glycol methyl ether acetate with shaking (120 rpm) during 4 minutes and 30 seconds.
- After, neutralize the solvent with isopropanol.
- Proceed similarly for the second layer using SU-8 2100: 5 minutes at 65°C + 20 minutes at 95°for the soft bake; 24 seconds exposure time, 5 minutes at 65°C + a0 minutes at 95°C for post exposure baking; and 10 minutes for development time.
- Finish by placing the wafer on the hot plate at 150°C for 30 min.
- Proceed to silanization by leaving the wafer under a vacuum bell overnight with 20µl of Trichloro Perfluoro Octyl silane.

6.1.2 Chip production

Day 0

- Prepare the PDMS mix, PDMS SYLGARD 184, Dow Corning at a 1:10 ratio of curing agent (20g + 2g). Mix thoroughly with a Thinky mixer.
- Pour the mix over the mold.

- Put the mold in the vacuum chamber until 1000 and then wait 30min to remove the air from the mix.
- Cured for 2h at 70°C.
- Cut everything out from the mold
- Cut the chips and punch the holes with the pink puncher (0.75mm)
- Prepare the coverslip by cleaning it with isopropanol.
- Plasma bond (CUTE Plasma, Femto Science) the chip to the coverslip.
- Proceed to surface treatment by filling (output) the chips two times with NOVEC Surface Modifier (3M) and curing for 10 minutes at 110°C.

6.1.3 Strains and Media

Day 0

- From lab stock at -80°C, restreact on LB plate.
- Incubate for an overnight at 37°C or for two days at room temperature.

Day 1

- In a 50mL Falcon tube, re-suspend one colony from the plate in 5mL of supplemented minimal Media (5mL MOPS 1X + 100uL glucose from 20% stock, final concentration 0.4%) or in 5mL LB broth.
- Add 100uL IPTG from 10mM stock.
- Incubate ON at 37°C + shaking.

Day 2

- Proceed to a 1/1000 dilution and incubate at 37°C until exponential phase is reached.
- In 1.5mL eppendorf tube prepare the MOPS or LB solution with IPTG and with drug if wanted.
- Re-inoculate at OD wanted (depending on the λ we want for the experiments) in the tube with the prepared solution.

6.1.4 Loading

Day 2

- Prepare a stock of continuous oil phase (3M Fluorinert FC40 + non-ionic surfactant RAN fluoroSurf final concentration 1%), Vortex and filter (0.2um).
- Before loading the phase, proceed to one more surface treatment with NOVEC.
- Load the 2.5ml and 100ul syringe with the continuous oil phase. No air bubbles in the tubes or syringe.

- Load the 100ul syringe with our bacterial suspension (from 90uL to 116 uL).
- Plug in the the syringe with tubes in the two input, and the waste tube to the output.
- Fill the chip through the first input with the continuous oil phase at 50ul/min and tap on the top of the chip to remove the air.
- Inject through the second input the bacterial suspension (with or without antibiotic) at 5ul/min. If there is still air, proceed to the previous step again.
- Immediately after, inject through the first input the continuous oil phase at 5ul/minute and increase until 30ul/min max until the droplets are formed.
- Cut the tubes.

6.1.5 Microscopy

Bright field acquisition

- In λ set up optical configuration: Bright field.
- In Large Image set up scan area: 3x3 fields.
- In Large Image set up stitching: 2%, overlap by blending.
- In XY, save the positions, center of each chip.
- Use PFS on.
- Check order of experiment: Large Image (Lambda).

Fluorescence acquisition, TRITC

- In λ set up optical configuration: CSU 561.
- In Large Image set up scan area: 3x3 fields.
- In Large Image set up stitching: 2%, overlap by blending.
- In XY, save the positions, center of each chip.
- Use PFS on.
- In Z series set up the step to 5ţm, 25 steps, with 120ţm range.
- In Z series set up the relative position: below to -50ţm and above to $+70$ţm.
- In Z series choose Triggered NIDAQ Piezo Z for Z device.
- Check order of experiment: Large Image (Lambda(Z series)).

6.2 Algorithms

6.2.1 Anchor

```
pip install anchor-droplet-chip

from adc import align, count, fit
from functools import partial
from importlib.metadata import version
import urllib3
import shutil
import os
import pathlib
import matplotlib.pyplot as plt
import yaml
import tifffile as tf
import seaborn as sn

__version__ = version('anchor-droplet-chip')
__version__

def load_data(url, filename, dir=None):
    if dir is not None:
        cwd = pathlib.Path.cwd()
        subfolder = cwd.joinpath(dir)
        subfolder.mkdir(exist_ok=True)
        filename = subfolder.joinpath(filename)
    else:
        filename = pathlib.Path(filename)

    if not filename.exists():
        print(f'loading {filename}')
        c = urllib3.PoolManager()

        with c.request('GET',url, preload_content=False) as resp, filename.open(mode='wb') as out_file:
            shutil.copyfileobj(resp, out_file)

        resp.release_conn()
    else:
        print(f'{filename} already exists')
    print(f'reading from disk {filename}')
    return tf.imread(filename)


def process_urls(key, config):
    if 'url' in config[key]:
        return load_data(**config[key])
    else:
        return config[key]

def load_dataset(path):
    with open(path,'r') as f:
        config  = yaml.load(f, Loader=yaml.SafeLoader)
        print (config)

    return {key: process_urls(key, config) for key in config}

data_0h = load_dataset('test_data_0h.yaml')
```

```python
data_24h = load_dataset('test_data_24h.yaml')

aligned_stack_0h, tvec_0h = align.align_stack(**data_0h)
aligned_stack_24h, tvec_0h = align.align_stack(**data_24h)

tf.imwrite('day1/00ng_BF_TRITC_bin2-aligned.tif', aligned_stack_0h, imagej=True, metadata=align.META_ALIGNED)
tf.imwrite('day2/00ng_BF_TRITC_bin2-24h-aligned.tif', aligned_stack_24h, imagej=True, metadata=align.META_ALIGNED)

counts_0h = count.stack(aligned_stack_0h)
counts_0h

poisson_lambda = fit.poisson(counts_0h.n_cells)
table = counts_0h.copy()
table.loc[:, "n_cells_final"] = counts_24h.n_cells
sns.swarmplot(data=table, x='n_cells', y='n_cells_final')


```

6.2.2 Conversion from nd2 file to zarr file for napari visualisation

```python
import nd2
import zarr_tools

data = nd2.ND2File("input.nd2").to_dask()
zarr_tools.convert.to_zarr(
    data,
    channel_axis=1,
    path="output.zarr",
    steps=4,
    name=['BF','TRITC'],
    colormap=['gray','green'],
    lut=((1000,30000),(440, 600)),
)
```

6.3 Preprint

Measuring single-cell susceptibility to antibiotics within monoclonal bacterial populations

Lena Le Quellec[1,2†], **Andrey Aristov**[1†], **Salomé Gutiérrez Ramos**[1,2], **Gabriel Amselem**[1,2], **Julia Bos**[3], **Zeynep Baharoglu**[3], **Didier Mazel**[3], **Charles N. Baroud**[1,2*]

***For correspondence:** charles.baroud@pasteur.fr (CNB)

[†]These authors contributed equally to this work

[1]Physical Institut Pasteur, Université Paris Cité, Microfluidics and Bioengineering Unit,75015 Paris, France; [2]LadHyX, CNRS, Ecole polytechnique, Institut polytechnique de Paris, 91120, Palaiseau, France; [3]Institut Pasteur, Université Paris Cité, CNRS UMR3525, Bacterial Genome Plasticity Unit,F-75015 Paris, France

---

Abstract Given the emergence of antimicrobial drug resistance, it is critical to understand the heterogeneity of response to an antibiotic within a population of cells. Since the drug can exert a selection pressure that leads to the emergence of resistant phenotypes. To date, neither bulk nor single-cell methods are able to link the heterogeneity of single-cell susceptibility to the population-scale response to antibiotics. Here we present a platform that measures the ability of individual *E. coli* cells to form small colonies at different ciprofloxacin concentrations, by using anchored microfluidic drops and an image and data analysis pipelines. The microfluidic results are benchmarked against classical microbiology measurements of antibiotic susceptibility, showing an agreement between the pooled microfluidic chip and replated bulk measurements. Further, the experimental likelihood of a single cell to form a colony is used to provide a probabilistic antibiotic susceptibility curve. In addition to the probabilistic viewpoint, the microfluidic format enables the characterization of morphological features over time for a large number of individual cells. This pipeline can be used to compare the response of different bacterial strains to antibiotics with different action mechanisms.

Introduction

Antimicrobial resistance is considered by the World Health Organization as one of the biggest threats to public health [25]. Developing new tools and methods to better understand bacterial resistance is becoming necessary. When addressing the question of bacterial response to antibiotics, most microbiology studies report the Minimum Inhibitory Concentration (MIC) at which the cells stop growing, for a given initial inoculum size (usually 10^5 cells) and after a growth time of over 24 hours. However, interpreting these MIC measurements is far from trivial and could indicate many different phenomena taking place in the cultures (high variability, inoculum effect, mechanism of action of the antibiotic) [16]. Indeed, the response of individual cells, which may then lead to colonies, can display large heterogeneity [11, 12]. For this reason the MIC is sometimes complemented with a more precise measurement, the Minimum Bactericidal Concentration (MBC). The process of determining the MBC is heavy and time-consuming and, like the MIC, only gives information about the antibiotic susceptibility on the population level. This has motivated significant effort to measure the bacterial response at a more microscopic level.

For instance, a single-cell MIC was estimated by measuring the MIC for different inoculum sizes and extrapolating the value to a single cell [5]. Classical laboratory methods, however, are difficult to scale to single-cell manipulation, both in terms of the volumes of interest and also the number of experiments that are required to obtain a significant number of replicates. In contrast, the development of microfabrication methods and microfluidics has allowed measurements to be made on individual cells in controlled environments [6]. In this area, two platforms which address questions of antibiotic response have emerged. First the so-called mother machine and its variations, where individual cells are trapped in thin channels and observed over a large number of generations [28]. These devices rely on the tracking of the initial *mother* cells by time-lapse microscopy, while removing its daughter cells as they push out of the microchannels. By fine analysis of the images under different antibiotic treatments it is possible to learn about relations between mother and daughter cells [9], or to detect the effect of rare mutations on the fitness at the single-cell level [26].

In parallel, the field of droplet microfluidics has allowed studies of a different kind. By encapsulating one or a few bacterial cells within water-in-oil droplets, the development of small colonies from individual cells [15], or the signature of their metabolism [10], can be detected with optical readouts. The addition of antibiotics in solution within the droplets can then be used to determine the bacteria's susceptibility. This basic principle has, in recent years, been developed in two main directions. Either to improve the simplicity of use [13, 19] or to improve the precision of the measurements [22, 23, 27]. These droplets approaches have the potential to be transferred to clinical studies, as reviewed in recent papers [18, 30, 14].

Although these droplet methods constitute important milestones, they suffer from several drawbacks: First, they require specific and sophisticated equipment including precise flow control systems to ensure droplet size homogeneity, as well as high-speed electronics, lasers, and data acquisition, to perform the measurements on flowing droplets. Second, the latest methods do not allow the droplets to be followed in time or to relate the final state to the initial state of the droplets. Finally, the link between the single-cell measurements and the classical biological measurements has never been explicitly tested. As such, it is difficult to relate the droplet-based measurements with the vast quantity of data obtained in traditional experiments.

Here, we present an open-access microfluidic platform that addresses some of these issues. The platform is based on *rails and anchors* that were introduced a few years ago [1]. Those droplets are formed within microfabricated wells and remain stationary for the duration of the experiment, including for the observation of biological processes within them [2, 3]. As such, the platform only requires simple microfabrication, low-precision flow control and allows to complete time-lapse measurements. The microfluidic setup is augmented with an original and dedicated image acquisition and analysis pipeline that extracts the relevant information from the chips in an automated manner. By providing the image and data analysis as open-source code, the platform will be easy to integrate in most academic laboratories. Moreover, the current study addresses the interpretation of the biological measurements for the first time. By doing so it links the droplet-level approach, used in most droplet-based experiments, with a single-cell analysis. This analysis is used to obtain unique measurements of the single-cell susceptibility to antibiotics.

Results

Microfluidic platform and initial observations

The microfluidic device used in this study is based on a geometry described previously [3, 4]. It consists of a triangular array of 501 individual wells, or anchors, that can each hold a single aqueous droplet (Fig. 1a). The chip format is well suited for imaging on an inverted microscope, either using wide-field illumination or confocal mode, as discussed below.

Loading the chip and distributing the bacterial solution into droplets is straightforward and takes about 5 min (see Method for the detailed steps, and Fig. 1 b, c, d). Briefly, the device is first entirely filled with oil (FC40, 3M) containing 0.5% surfactant (FluoSurf, Emulseo, France). Then, the aqueous suspension of bacteria is flowed through the device. In a last step, the oil is flowed again through the device, which leads to the formation and immobilization of droplets containing bacteria, directly on the anchors. The volume of each droplet is 2 nl and is primarily determined by the volume of the anchor [2]. This loading procedure is simple to set up and can be mastered in only a couple of trials. Indeed, the droplet formation step is robust to fluctuations in flow rate. It can be performed using syringe pumps or using hand-held syringes. Also note that the whole loading procedure is performed while the output is connected to a waste tube, and the bacterial suspension is constantly encapsulated in an inert oil layer. This makes the protocol suitable in principle to handling pathogens, since the bacterial solution remains in a closed circuit.

E. coli W3110 with a fluorescent reporter (RFP) in the ptac site (ptac::RFP) allows us to detect bacterial cells and the growth of the colonies using the red fluorescent protein (RFP) . A sample fluorescence image of the trapping area of the chip, acquired after 24 hours of incubation, is shown in Fig. 1e. The bacteria at this stage form bright fluorescent colonies that can readily be imaged using epifluorescence or confocal microscopy. Empty droplets are also present on the device, since the cells are randomly distributed. The number of empty droplets is related to the average number of bacteria per drop, which is in turn related to the initial concentration of the bacterial suspension. Starting from different initial dilutions, therefore, allows us to tune the average number of cells per droplet and the number of positive droplets within the chip in the absence of antibiotics.

Before moving on to testing the effects of antibiotics in the microfluidic device, we to benchmark the bacterial fitness in the microfluidic device compared with standard multi-well plate experiment. This is done by following the growth of the fluorescent intensity in the droplets, using time-lapse epifluorescence microscopy, while performing in parallel a standard growth-curve measurement on a fluorescence plate reader from the same batch culture. The growth curves for the two cases are shown in Fig. 1f. The curves from the microfluidic device show a large variability between individual droplets, as a result

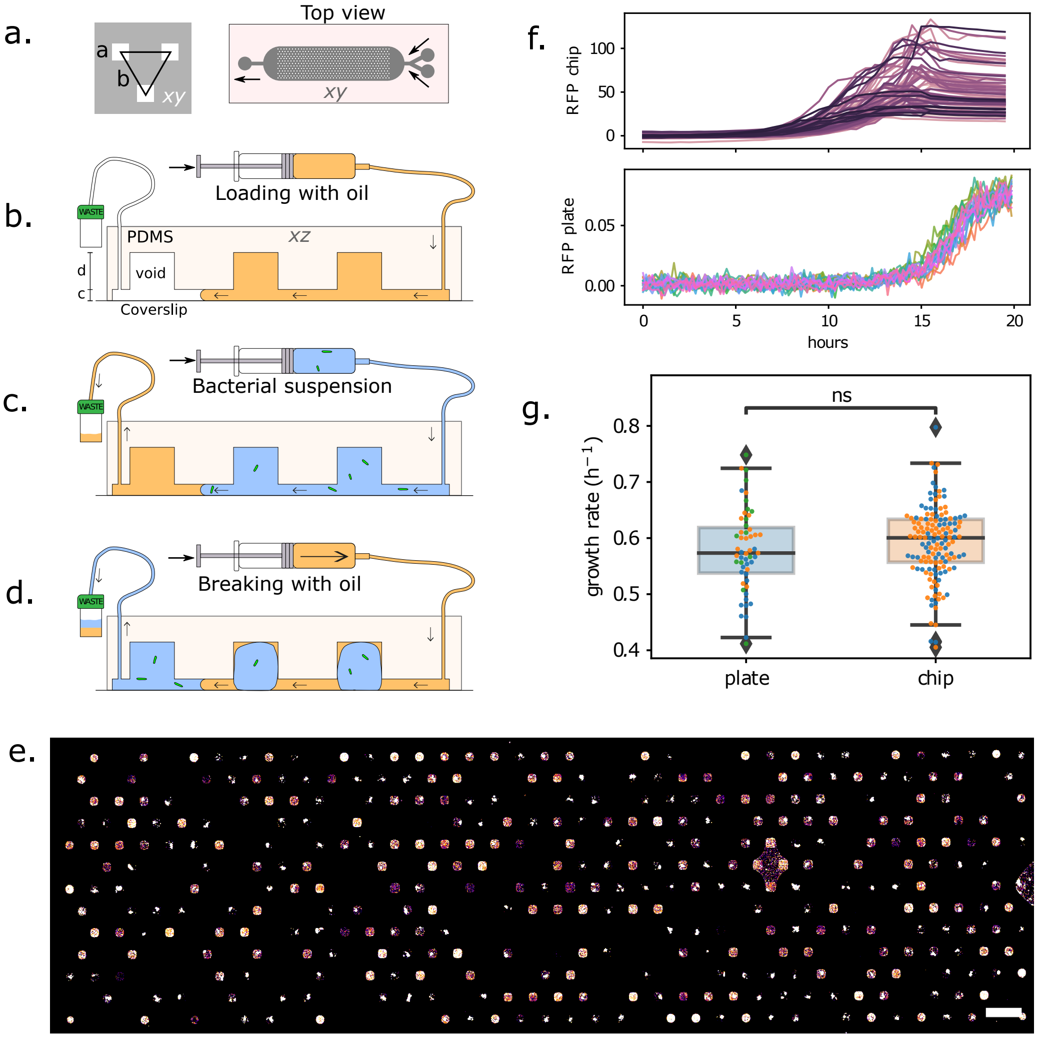

Figure 1. (a) Microfluidic chip design. Left: a unit cell consists of a triangular arrangement of square anchors, each of size $a = 120$ µm and distance $b = 360$ µm. Right: design of the full chip, which includes a main chamber with 501 anchors, 2 input channels on the right and 1 outlet channel on the left. **(b)** Side-view (not to scale), showing the channel height $c = 30$ µm and anchor depth $d = 100$ µm. The loading protocol begins by filling the chamber with oil, then **(c)** replacing the oil with bacterial suspension, and **(d)** breaking the bacterial suspension into individual droplets, anchored in their respective wells. **(e)** Z-projection of a confocal stack of the chip after 24 h incubation (scalebar: $500\ \mu$m). **(f)** Growth curves in 501 individual droplets on the chip (top), and in each well of a 96-well plate (bottom). **(g)** Measured growth rates for bacteria in the microfluidics chip (2 replicates), and in the 96-well plate (3 replicates). Growth rates were obtained by fitting an exponential function to the growth curves during the first 10 hours of growth. P-value=0.24 obtained with Welch's t-test for indetependent samples.

of distribution of the number of initial cells and of the cell-to-cell variability [7]. In contrast, the multiwell plate experiments are insensitive to these stochastic elements and grow in a reproducible and regular manner. Fitting the individual growth curves with an exponential function for the first 10 hours of growth shows that the difference in growth rates in the microfluidic device and in the multiwell plates is statistically not significant, see Fig. 1g. Hence, the microfluidic results can be compared to standard microbiology techniques.

Imaging and analysis pipelines

Once the microfluidic device is loaded, the aim of the experiments is to identify which droplets within the array produce a population of cells after 24h and to link the final state with the initial number of cells in each droplet. These measurements are performed by first imaging the chip shortly after the loading and then after overnight incubation. Image analysis of the initial and final time points then yields a table that identifies each droplet in the array. Each droplet is then associated with measured quantities such as the initial number of cells, its final state, as well as the antibiotic concentration for a given experiment (see schematic in Fig. 2).

As such, the ability to acquire and analyze large amounts of imaging data is fundamental to obtain the antibiotic response curves. While the array format lends itself naturally to measuring droplet contents at different time points, the requirement to detect single cells at early times imposes high-resolution imaging. This runs into data handling limitations associated with the large file sizes and large number of experiments. These different constraints led us to develop automated imaging and analysis pipelines whose implementation was instrumental for obtaining the results below. The imaging steps are described below and the image and data analysis pipelines are provided as open-source packages at the following GitHub repository: https://github.com/BaroudLab/anchor-droplet-chip.

The aim of the pipeline is to generate a table with one line for each droplet, which includes a unique label, the antibiotic concentration, as well as the initial number of cells and final state for the droplet, as described in Fig. 2.

Initial state.

The initial number of cells per droplet is obtained by imaging the freshly loaded chip first in bright-field, and second by acquiring a confocal z-stack of the device in the RFP channel. The bright-field image is used to detect the positions of the droplets, by adjusting for arbitrary shift and tilt of each acquisition (see Methods). In turn, the confocal stack is reduced to a single image by using a maximum projection of the fluorescent intensity. The resulting fluorescent image allows us to count the number of individual bacteria within each droplet (Fig. 2c). The algorithm proved sufficiently robust to perform unsupervised automated analysis of the data from the chips.

Since the cells are expected to follow a Poisson distribution in the droplets [3], a quick quality control is performed at the end of the first scan, by verifying the distribution of number of cells per droplet, and checking that it indeed follows the expected shape, see Fig. 2i. This calculation also allows us to obtain a value of the Poisson parameter λ and to adjust the cell dilution if necessary in order to work in the desired range of λ.

Note that the loading and scanning each take about 10 minutes and the initial image

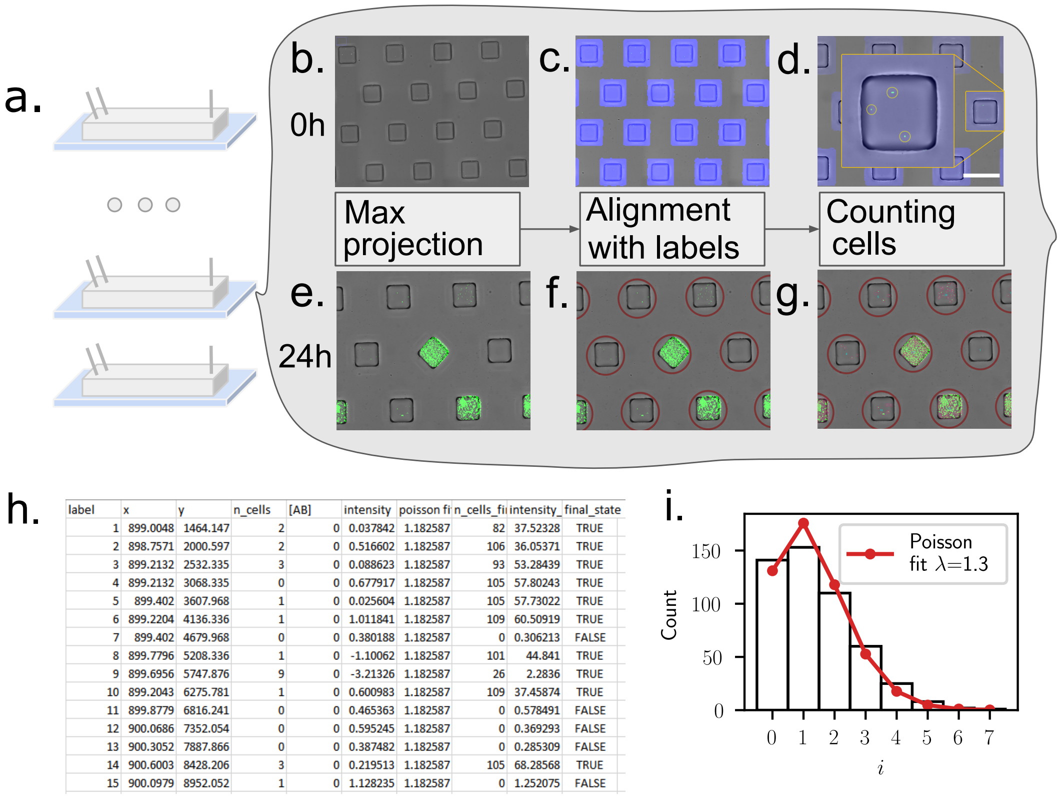

label	x	y	n_cells	[AB]	intensity	poisson fi	n_cells_fi	intensity_	final_state
1	899.0048	1464.147	2	0	0.037842	1.182587	82	37.52328	TRUE
2	898.7571	2000.597	2	0	0.516602	1.182587	106	36.05371	TRUE
3	899.2132	2532.335	3	0	0.088623	1.182587	93	53.28439	TRUE
4	899.2132	3068.335	0	0	0.677917	1.182587	105	57.80243	TRUE
5	899.402	3607.968	1	0	0.025604	1.182587	105	57.73022	TRUE
6	899.2204	4136.336	1	0	1.011841	1.182587	109	60.50919	TRUE
7	899.402	4679.968	0	0	0.380188	1.182587	0	0.306213	FALSE
8	899.7796	5208.336	1	0	-1.10062	1.182587	101	44.841	TRUE
9	899.6956	5747.876	9	0	-3.21326	1.182587	26	2.2836	TRUE
10	899.2043	6275.781	1	0	0.600983	1.182587	109	37.45874	TRUE
11	899.8779	6816.241	0	0	0.465363	1.182587	0	0.578491	FALSE
12	900.0686	7352.054	0	0	0.595245	1.182587	0	0.369293	FALSE
13	900.3052	7887.866	0	0	0.387482	1.182587	0	0.285309	FALSE
14	900.6003	8428.206	3	0	0.219513	1.182587	105	68.28568	TRUE
15	900.0979	8952.052	1	0	1.128235	1.182587	0	1.252075	FALSE

Figure 2. Imaging and image analysis pipeline. **(a)** The experiment begins by loading several chips with bacterial suspensions at different antibiotic concentrations. **(b)** Overlay of the bright-field image of the chip, and of the maximum projection of a fluorescent confocal z-stack. Images are acquired minutes after loading (0 h). **(c)** The bright-field image is used to identify the alignment with respect to the microscope stage and to create a unique mask around the positions of the individual anchors. **(d)** Detecting the fluorescent peaks in the maximum projection enables to count the initial number of cells per droplet. **(e)-(g)** Similar imaging and analysis operations are performed 24 h after the loading, to identify positive and negative droplets. **(h)** The data from the initial and final images are collected in a table that provides a unique label for each droplet, as well as the number of cells at 0 h and at 24 h. Each droplet is assigned a final status of positive or negative, depending on whether the final number of cells is larger than a predefined threshold of 15 cells. **(i)** A quality control step is performed using the single-cell detection at $t = 0$ by comparing the cell number distribution with a Poisson distribution. This leads to an estimate of the Poisson parameter λ for each chip.

validation occurs within a few minutes as well. This yields a first measurement of the loading in under 30 minutes for each microfluidic chip.

Final state.

The contents of each droplet are later measured at the experimental endpoint, typically after an overnight incubation ($t = 18 - 24$ h): each chip is scanned, this time using simple epi-fluorescence to optimize time and disk storage. The final image of each chip is re-aligned with the template acquired at initial times to identify each droplet, a registration step made straightforward by the fact that droplets are anchored at predefined positions. Then, cells are detected within each droplet, as shown in Fig. 2e-g. In the current experiments, we focus on the bottom of the microfluidic device where cells are more likely to be detected if the droplet is positive. Different quantities can be obtained from the final image as proxies for the ability of cells to grow within the drop. We count the number of cells in the final image, although mean or total fluorescence intensity can also be used. The main requirement for the measurements is to be sufficiently robust to yield a cutoff between positive and negative droplets, a classification which is also included in the data table. The final result is a csv table that contains the relevant information on the initial and final states of each droplet within each microfluidic device.

Note that the protocols described above can be modified for particular situations. For instance time-lapse microscopy can be performed on the chips to obtain time-resolved measurements. Similarly, confocal imaging can be used at later times to obtain a more precise cell count or fluorescent intensity, or to identify the morphology of the cells. Although these cases would require small modification in the pipeline, the main bricks of the analysis discussed above can still be used in a modular fashion.

Microfluidic *vs.* microplate antibiogram

The microfluidics and imaging protocols described above can be combined to obtain an antibiotic susceptibility curve, by loading several chips in parallel, using known concentrations of antibiotics and bacteria in each chip. Performing these measurements is simplified by the standardized microfluidic format and analysis codes, making it possible to run six to twelve chips in parallel, each with a different concentration. Confronting the microfluidic measurements against standard microbiological techniques proves crucial to understand how to interpret the microfluidics data.

In each experimental run, one chip is loaded with the same bacterial concentration as the others but without any antibiotic. This control chip allows us to estimate the value of the average number of cells per droplet at initial times, λ, for the given run:

$$\lambda \simeq -\ln(\hat{p}_{-}), \qquad (1)$$

where $\hat{p}_{-}$ is the fraction of empty to total droplets on the test chip. This estimate comes from the assumption that the initial number of cells per droplet follows a Poisson distribution [7]. A higher value of λ means that drops contain a larger average number of cells initially.

A typical set of images from the experimental endpoint is shown in Fig. 3a. In these images the bright spots correspond to droplets where bacteria grew, while dark spots within the regular matrix correspond to droplets that do not contain a sufficient population of cells. These dark positions correspond either to droplets that did not contain any

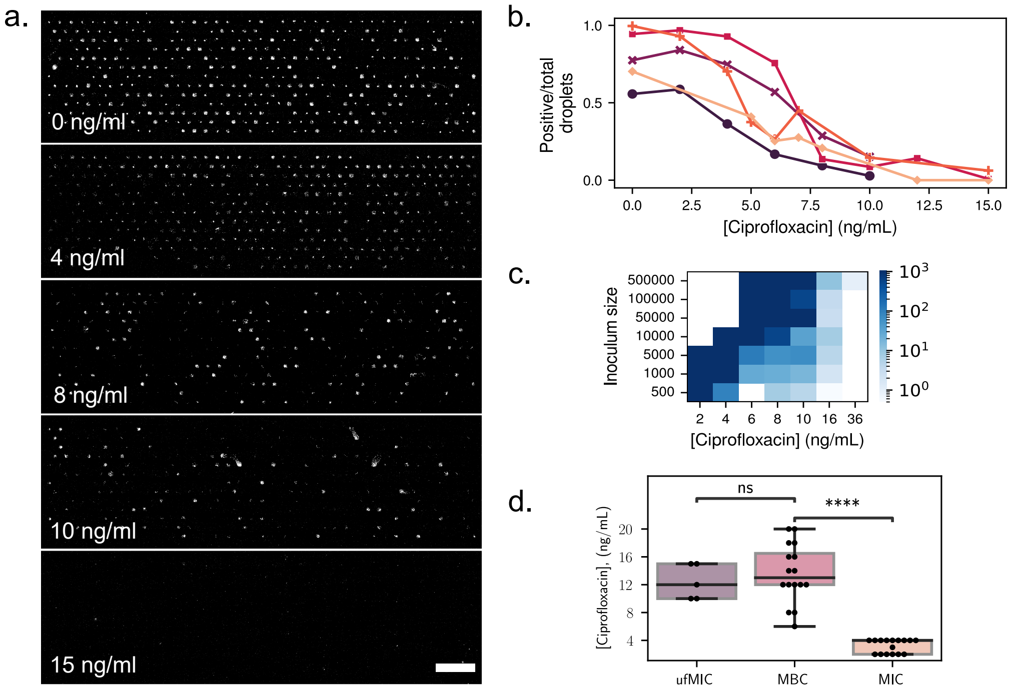

Figure 3. (a) Antibiogram chips with different concentrations of ciprofloxacin, and an initial average number of cells per droplet $\lambda = 1.3$. Bright spots correspond to droplets where bacterial growth occured. Scale bar: 1 mm. Fraction of positive droplets at the end of the experiment, normalized by the total number of droplets containing at least one bacterium at the beginning of the experiment, for different concentrations of ciprofloxacin. Each color corresponds to a different run, at a different date and with a different value of λ. **(c)** Result of MBC experiments. Bacteria were grown in 96-well plates under different antibiotic concentrations, and starting with different inoculum sizes. The wells were scanned after 24 hours, and the contents of negative wells were replated on antibiotic-free petri dishes for 24 addidtional hours. The number of colonies on the petri dishes after incubation directly represents the number of surviving bacteria in each well. The color corresponds to the number of colonies on the petri dishes. **(d)** Values of the MBC (petri dishes), MIC (96-well plates) and μf·MIC on the chip, where the total number of cells per chip is used as inoculum size. P-values 6e-8 for MBC vs. MIC and 0.9 for ufMIC vs MBC obtained with Welch's t-test for independent samples.

cells initially or to droplets where the cells did not form colonies e.g. due to the antibiotic stress. This antibiogram, allows to determine a measure of the antibiotic susceptibility of the bacteria, which we denote µf·MIC. The µf·MICcorresponds to the lowest antibiotic concentration that will inhibits the growth in 95% of the droplets.

As expected, the fraction of positive droplets decreases as the concentration of antibiotics is increased. This decrease is quantified in Fig. 3b, where the number of positive droplets is shown to decrease towards zero as the concentration of the antibiotic ciprofloxacin increases, independently of the value of λ.

The interpretation of this "digital" measurement and its relation with classical microbiology measurements is not obvious. To understand its significance, measurements from the microfluidic format were confronted with measurements in a standard multiwell plate, using the same samples. Two classical microbiology measurements were performed on the samples. First, the minimum inhibitory concentration (MIC) was determined with a standard microtitre broth dilution method (see Methods). The MIC corresponds to the lowest antibiotic concentration that will inhibits visible growth. Then, the minimum bactericidal concentration (MBC) was obtained by replating the contents of the negative wells on antibiotic-free petri dishes. The number of colonies on the petri dishes after 24 hours of incubation directly represents the number of surviving bacteria in each well. The MBC thus provides a more precise measure of the antibiotic concentration that is lethal to the bacteria, compared to the MIC. We find that the number of colonies growing from negative wells is very large below a critical value of the ciprofloxacin concentration of 10 ng/mL, after which it drops dramatically to below ≈ 100 colonies, and eventually asymptotes to zero with increasing antibiotic concentration, see Fig. 3c.

A comparison of the measurements obtained from the three techniques (µf·MIC, MIC, and MBC) is shown in Fig. 3d, as a function of inoculum size. The inoculum size used for the µf·MIC corresponds to the total number of cells per chip. The classical MIC measurement (at $t = 24$ h) is shown to be the least sensitive of the three measurements, since it finds a critical value of the concentration that is well below the value that is necessary to kill all of the cells. In contrast, the values of the MBC and of the µf·MIC are in the same range. They both show similar trends with the inoculum size, namely a slow but detectable increase with the initial number of bacterial cells.

This close correspondence between the MBC and the µf·MIC, obtained by pooling together the total number of cells in the chip, indicates that the results in the microfluidic chip can be treated as a population-level measurement: all the bacteria from a single chip form a small population, whose ability to survive to a given concentration of antibiotics depends on its initial size. This result indicates that cells are behaving in an independent manner.

Computing single-cell antibiotic susceptibility

Beyond population level measurements, the objective is to provide insights about the antibiotic susceptibility of individual cells within a monoclonal population. This is achieved by taking a probabilistic viewpoint on the ability for a single cell to produce a colony at a given antibiotic concentration. Experimentally, we count the number of bacteria in each droplet at the beginning and at the end of an experiment for six antibiotic concentrations, see Fig. 4a. At the end of an experiment, the image analysis algorithm counts the number of bacteria at the bottom of the droplets. While this number does not reflect the exact total number of cells in the droplet at late times, it is an acceptable proxy to differentiate positive from negative droplets .

A threshold value to distinguish positive from negative droplets is chosen at $n_{\text{final}} = 15$ cells to separate best the two populations (colony or no colony). The number of positive and negative droplets for each condition and each initial number of cells is then determined. As a result, the probability of a droplet to contain a colony at the end-point can be plotted as a function of its initial number of bacteria i, and of the antibiotic concentration C_{AB}. We call this probability $p(i, C_{\text{AB}})$: it represents the probability to produce a colony starting from i cells, under a concentration of antibiotics C_{AB}. The evolution of p is shown as a heat-map in Fig. 4b. We observe that $p(i, C_{\text{AB}})$ decreases as the antibiotic concentration increases, but that it increases with the initial number of cells in a droplet; when more cells are in a droplet initially, more antibiotics are needed to prevent the growth of a colony after an overnight incubation.

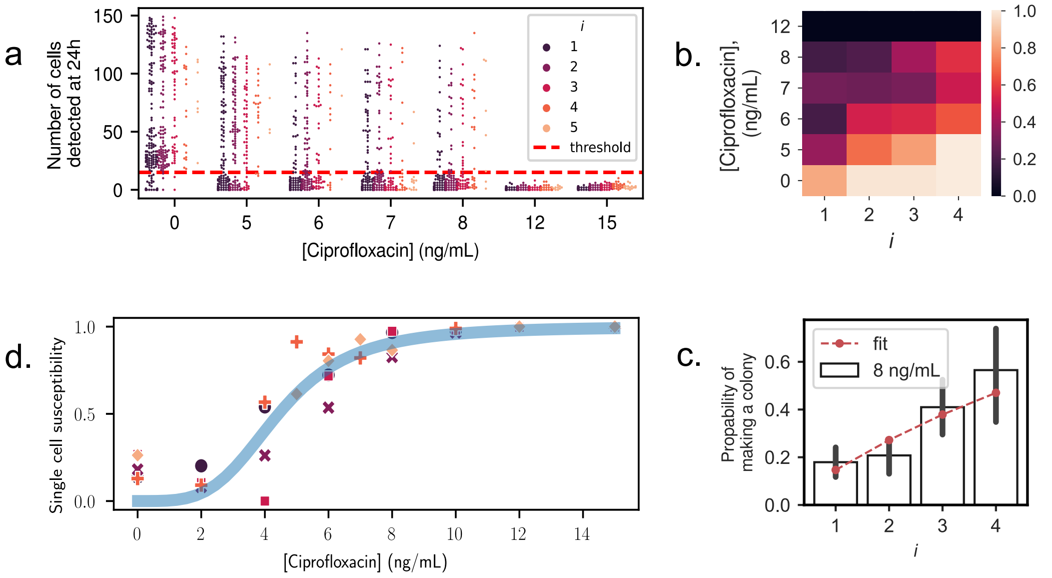

Figure 4. Single-cell antibiotic susceptibility. **(a)** Final number of cells, counted at the bottom of each droplet at $t = 24\ h$, as a function of antibiotic concentration. Colors indicate the initial number of cells i in the droplet at $t = 0$. The horizontal dashed line is the threshold, fixed at 15 cells, chosen to define the final droplet state as positive or negative. **(b)** Survival probability, computed using Eq. (3), as a function of the initial cell number i and antibiotic concentration. **(c)** The probability to produce a colony as a function of initial number of cells, for $C_{\text{AB}} = 8$ ng/mL. Bars indicate experimental measurements from counting positive cells. Dashed line shows fit according to Eq. (2), assuming independent outcomes for each cell and fitting for q. For additional fits, see Supp. Fig. S1 **(d)** The single-cell antibiotic susceptibility is plotted for all antibiotic concentrations and all experimental replicates (points). The data is well-fitted with a two-parameter Hill function (line): $h(C_{\text{AB}}) = C^n_{\text{AB}}/(K + C^n_{\text{AB}})$, with best fit values $n = 3.9$ and $K = 4.4$.

Counting the number of bacteria at initial times, and the fraction of positive droplets at the end of the experiment, enables to infer the susceptibility of a single cell to a concentration of antibiotic $C_{\rm AB}$. This single-cell susceptibility, which we denote $q(C_{\rm AB}) = 1 - p(1, C_{\rm AB})$, is defined as the probability for a single cell to die (equivalently not form a colony) at concentration $C_{\rm AB}$. If additionally all bacteria are assumed to behave independently, the probability for i cells to die is $q(C_{\rm AB})^i$. The probability for i cells to form a colony is therefore the probability for at least one of them to form a colony, and we then have:

$$p(i, C_{\rm AB}) = 1 - q(C_{\rm AB})^i. \tag{2}$$

For each concentration of antibiotics, the probability $p(i, C_{\rm AB})$ was estimated by counting the number $\mathcal{N}_i$ of droplets containing exactly i cells at the beginning of the experiment. Among these $\mathcal{N}_i$ droplets, a number $N^+(i, C_{\rm AB})$ droplets were positive at the end of the experiment. We then have:

$$p(i, C_{\rm AB}) = \frac{N^+(i, C_{\rm AB})}{\mathcal{N}_i}. \tag{3}$$

The probability $p(i, C_{\rm AB})$ was fitted to the functional form of Eq. (2) with $q(C_{\rm AB})$ as a single fit parameter, as shown in Fig. 4c (see SI Fig. S1 for all data). The good agreement between the data and the theory confirms that the bacteria may indeed be considered as independent of each other (see in Fig. 4c), at least for the low number of cells present initially at the beginning of the experiments. Then if we write $q^\star(C_{\rm AB})$ the best fit value of $q(C_{\rm AB})$, this value provides the best estimate of the single-cell susceptibility to drug concentration $C_{\rm AB}$, using all experimental data at hand and assuming that all cells are independent.

The single-cell susceptibility $q^\star(C_{\rm AB})$ is expected to take a sigmoidal shape, with a value near 0 in the absence of drugs (all bacteria form colonies), and increases non-linearly with the drug concentration until reaching a plateau at $q^\star(C_{\rm AB}) = 1$. This is confirmed by the experimental measurements, as shown in Fig. 4d. These data are arbitrarily fitted to a Hill function: $h(C_{\rm AB}) = C_{\rm AB}^n/(K + C_{\rm AB}^n)$, with K and n being two fit parameters, providing a good match between experiments and the fitted function.

Identifying morphology changes under antibiotic stress

This microfluidic device and image analysis pipeline is a very powerful tool to obtain quantitative information at the single-cell level as seen in Fig. 4. But more than quantitative information, the anchored droplet format provides a unique ability to access qualitative data and to follow the evolution of the bacterial colonies within each droplet over time. The tracking of the droplet contents can be performed by time-lapse microscopy on the chips. Since the droplet position is invariant throughout the experiment, identifying the progeny of an individual cell can be achieved. Examples of a sample droplet contents can be seen in Fig. 5 and the accompanying movies, first in the absence of antibiotics (Fig. 5a) or under a sub-MIC concentration of ciprofloxacin (Fig.5b).

In the absence of antibiotics, almost all droplets display bacteria in their planktonic state, swimming in the droplets and showing the typical size and shape for *E. coli* in culture. A few hours into the experiments and as the populations begin to grow, cells in some droplets start to adhere to each other, eventually forming clumps. The presence of these clumps could be attributed to the presence of adhesion proteins like fimbrial adhesins that may then contribute to biofilm formation of *E. coli* [8, 21].

The morphological change of bacteria in the presence of antibiotics often begins with the elongation of the cells into long filaments: this corresponds to 83% of cases in the

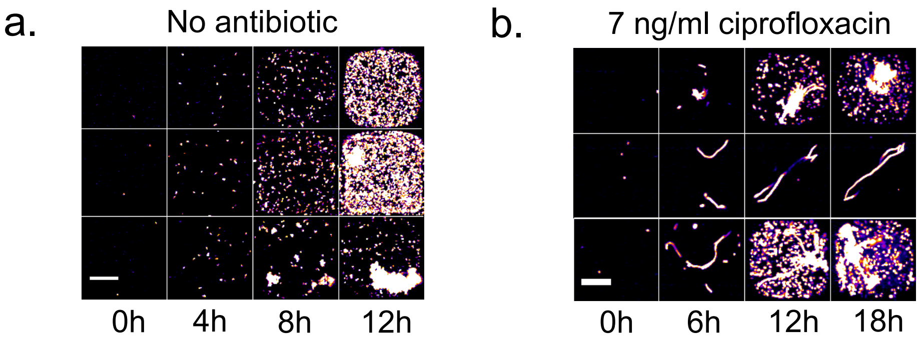

Figure 5. Example of bacterial growth in three independent droplets growth **(a)** without antibiotic, and **(b)** with sub-MIC concentrations of ciprofloxacin (7 ng/mL). Scale bar: $50\ \mu\mathrm{m}$. Even at sub-MIC concentrations, the presence of ciprofloxacin leads to a filamentous bacterial morphology.

experiments at sub-MIC antibiotic concentration (7 ng/mL). The filamentation is due to the SOS response triggered by the presence of ciprofloxacin; cell-division stops but the cell metabolism continues, leading to cell volume growth. The elongated cells can then begin to produce offspring after several hours (50% of all cases) or can arrest their growth and stay in the filamentous form (33% of all cases). This is in agreement with observations on agar plates [11].

In some cases, no elongation is found. These droplets correspond either to cells that were in a dormant state (10% of all cases is expected) [17] or to cells that suffered too much damage and died due to the antibiotics (7% of all cases) as no fluorescence can be detected. As a result of these dynamics, nearly all of the droplets that form colonies contain cells having the filamentous form as well. Nevertheless, the ability to image the contents of the droplets provides a very precise indication of the state of the cells within them. This in turn is informative about the ability of the cells to overcome the antibiotic stress.

Discussion

As the emergence of antibiotic resistance is accelerating, it is crucial to understand the variability of antibiotic response on the single-cell level. This has motivated work using dilution methods to determine the MIC on petri dishes [12] or in liquid media [5], or using precision microscopy on agar [11]. In parallel, microfluidic methods have been used to provide better controlled conditions and statistics over a large number of individual cells [6, 28]. In recent years a flurry of droplet-based approaches has provided information showing the heteroresistance of a bacterial population [23], digital antibiotic susceptibility [27, 29], or even providing pathogen identification [14]. These droplet-based methods have shown that the encapsulation within droplets can be used to explore the progeny of individual cells as they respond to antibiotic stress. By relying on snapshots of moving droplets, these methods cannot relate the initial and final states of each droplet, nor can they identify the biological mechanisms that allow cells to overcome the antibiotic stress at sub-MIC concentrations.

In this context the device and analysis pipeline presented here combine the advantages of microscopy with those of droplet-based methods. Indeed the ability to identify the initial state of each droplet allows us to work at much higher cell numbers per droplet, which translates to similar statistics as previous papers [27] while using a much lower number of droplets in total. Moreover the ability to provide time-resolved measurements on each droplet provides unique qualitative information about the adaptation of the cells, similarly to other microscpy-based methods [11]. Finally, the streamlined experimental and analysis pipeline allows us to load and image the chip in under 30 minutes, followed by an overnight incubation and a second scan requiring only a few minutes. As a result the complete campaign for obtaining an antibiogram can be performed robustly in a few hours. In contrast, the classical (petri-dish) method requires an initial overnight incubation in a 96 well plate, followed by a second overnight incubation on 50 to 80 petri dishes and manual counting of the colonies thereafter.

Beyond the performance aspects, it is important to benchmark the microfluidic measurements against standard microbiology protocols. The comparison of MIC, MBC, and µf·MIC shows that the results in the microfluidic chip can be treated as a population-level measurement, since the µf·MIC matches the MBC when accounting for the starting inoculum size. In addition to this, the detection of individual cells and the ability to perform a large number of single-cell assays in parallel allow us to develop a probabilistic treatment of the outcome within each droplet forming a colony after 24 hours. The probability for an individual cell to produce a colony at a given antibiotic concentration thus describes the heterogeneity of responses in the population.

This platform can now be used to address the single-cell response to antibiotics while screening different bacteria and molecules having different mechanisms of action. The expectation is that this screening will translate into both quantitative (shape of the single cell susceptibility curve) and qualitative (shape of the cells) differences among the conditions. The ability to encapsulate tens or hundreds of cells within the droplets, in a controlled manner, will then allow the exploration of collective behaviors and non-monotonic time-evolution of the response to antibiotics [24]. More complex experiments can also be envisaged, e.g. by recovering the contents of individual drops and performing -omics measurements on them or by varying the antibiotic concentration in time, as described previously [4]. Taken together, the different operations that can be combined into this platform constitute a major step forward in the study of antibiotic response both for scientific questions and for medical applications.

Methods

Microfluidics and microfabrication

Microfabrication and chip design

To produce microfluidic chips for the experiments, a custom mold was made using 2-layer-SU-8 photoresist lithography. The bottom layer contains the channels with 2 inputs and 1 output. The upper layer contains inverted microwells of squares shapes 120x120 um and space 240 um apart. As shown in Fig. 1 (a), the wells are organized in 13 rows of 39 and 38 wells respectively for odds and even rows. The channel height is 30 um and the well height is 130 um.

Next, PDMS and its curing agent (PDMS SYLGARD 184, Dow Corning) are mixed at a 1:10 ratio and poured into the mold. The mold is placed in a vacuum chamber for 30 minutes to eliminate air bubbles and then cured for 3 hours at 70 °C. Once the PDMS is cured, the chip is cut off from the mold and plasma bonded (CUTE Plasma, Femto

Science) to the coverslip.

Hydrophobic treatment

Prior to loading, the chips are surface treated with hydrophobic solution (NOVEC 1720 surface modifier/electronic grade coating 3M). To do so, two surface treatments were done after the plasma bonding by filling the chip with the hydrophobic solution and curing it for 10 minutes at 110°C. A third surface treatment is done prior to loading.

Chip loading

As described in Fig. 1, using a syringe pump (NEMESYS), the chip is first filled through the first input with a continuous oil phase (3M Fluorinert FC40 with non-ionic surfactant RAN fluoSurf final concentration 1 %) while purging the air bubbles. Then, through the second input, the continuous oil phase is replaced by the bacterial suspension. Finally, the continuous oil phase is injected again at a very low flow rate, breaking the droplets apart and leaving them locked in the wells.

Cell culture and preparation

Strain

The experiments were performed using the *E. coli* W3110 strain JEK1037 [20] labeled with red fluorescent protein (lacYZ:RFP).

Antibiotic Solution

Ciprofloxacin (Sigma-Aldrich) was solubilized in 0.1 N HCl (Sigma-Aldrich) at 25 mg/mL. The stock was then diluted with MiliQ water to 1 μg/mL. The final concentration of ciprofloxacin used was between 0 and 32 ng/mL.

Cell culture

From the -80°C stock, the cells were streaked on LB agar plate and incubated overnight at 37°C. The next day one isolated colony is inoculated in supplemented minimal media (MOPS with glucose final concentration 0.4%) and IPTG is added at 0.05 mM to induce the expression of the RFP. The bacterial suspension is incubated overnight at 37°C with shaking.

Cell dilution

In order to get one to five cells per droplet, the optical density of the solution, measured at 600nm, was calibrated. This was achieved as follows: the calibration was known by using digital counting : the chip was loaded with the diluted bacterial suspension without antibiotics, incubated at 37°C overnight, and then imaged. The empty wells were counted, and assuming a well can only be empty if no cells is loaded, the initial loading parameter λ was computed. λ is the Poisson parameter which corresponds to the mean number of cells per droplet and can be directly obtained by $-\ln(N_{(-)}/N_{total})$. Where $N_{(-)}$ is the number of negative droplets and N_{total} is the total number of droplets. λ is monitored by the concentration of the bacterial suspension and directly linked to the optical density.

Growth characterization and antibiotic susceptibility

Growth curves

For growth characterization cells were loaded at different dilutions (500 to 500,000 cells per well) in a 96-well plate. The plate was then placed in the plate reader (Thermo Scientific Varioskan LUX) for 24 hours at 37°C with shaking. The optical density at 600 nm (OD) and the RFP fluorescence signal (excitation 488 nm and emission 520 nm) were measured every 10 minutes.

In parallel, cells were loaded to the chip with an average of one cell per droplet. This corresponds to one cell per droplet on average. The chip was then placed under the microscope and the RFP signal was measured every 30 minutes.

MIC and MBC

The minimum inhibitory concentration (MIC) and minimum bactericidal concentration (MBC) were obtained to characterize the antibiotic susceptibility at the population level.

Cells are loaded in a 96 well plate at different dilutions (500 to 500,000 cells per well) and with different ciprofloxacin concentration ranging from 2 to 36 ng/mL. The plate is then incubated for 24 hours at 37°C with shaking.

The MIC is determined as the antibiotic concentration of the first negative well, i.e. the well at which the OD is the same as the OD of an empty well.

Then, the contents of the negative wells are plated on LB agar plates and incubated for 24 hours at 37°C. The number of colonies from each of these plates is counted. The MBC is determined as the concentration where the number of colonies decrease sharply from more than a hundred cells to less than a dozen cells.

Single-cell susceptibility

To characterize the single-cell susceptibility to antibiotic, at least 10 microfluidic chips are fabricated and loaded per experiment : a control chip without antibiotic, and nine more with serial concentrations of ciprofloxacin (from 2 to 36 ng/mL). The bacterial suspension is prepared with the antibiotic and immediately loaded into the chip. The chip is imaged, using fluorescence microscopy, right after in order to determine the exact number of cells in each well.

Then, the chip is immersed in a container filled with Milli Q water to prevent evaporation and incubated overnight at 37°C. After incubation, a scan of each chip, measuring the RFP signal is performed, using fluorescence microscopy.

Microscopy and image acquisition

Microscopy images are acquired using spinning disk confocal microscope (Nikon Ti2 + Yokogawa) with a 20x 0.7 NA air objective lens (Nikon Inc.) and with 2x2 pixels binning (set directly in camera properties (Hammamatsu Orca 4)). Images of the complete chip are obtained by stitching individual images with a 5% overlap. The imaging rate is optimized by acquiring first a bright-field image of the complete chip. The RFP signal is then obtained either in confocal mode, using 3D stack.

For the 3D stack, using triggered NIDAQ Piezo Z, planes are acquired with a step of 1 μm, for a total penetration of 120 μm.

The total area of the device is about 1.4 by 0.4 mm, which translates to 40 kpix long dataset using 350 nm pixel size. However, some chips could be tilted due to manual bonding, which effectively increases the necessary scanning area, resulting in much bigger images.

Image analysis

Image registration

First the 3D fluorescence stack is converted to 2D using maximum projection (see Fig. S2 b,e). Both channels, 2D bright-field and 2D fluorescence images, are merged together and saved as a tif stack. Then a well-labelled template image and a well-labelled mask are made and aligned to the experimental images (see Fig. S2 c,f).

Note that the protocols described above can be modified for particular situations. For instance time-lapse microscopy can be performed on the chips, in order to obtain time-resolved measurements. Similarly, confocal imaging can be used at later times in order to obtain a more precise cell count or fluorescent intensity, or to identify the morphology of the cells in particular cases. Although these cases would require small modification in the pipeline, the main bricks of the analysis discussed above can still be used in a modular fashion, without major changes in the general approach.

Cell counting

After image registration, every droplet is associated with the labeled area defined by the mask. Inside this mask, peak detection is performed to detect single fluorescent cells. To avoid false detection, due to noise, a preprocessing is performed as follows: First, a Gaussian filter, and subsequent peak detection using Scipy function peak_local_max with an absolute threshold of two. The number of peak per label is then recorded into a table for further processing.

Acknowledgements

This project was partially funded by ANR grant UniBAC (ANR-17-CE13-0010). The authors would like to thank the support of the Microfluidics and Biomaterials platform at Institut Pasteur. We also thank Erik Maikranz for useful discussions.

Supplementary information

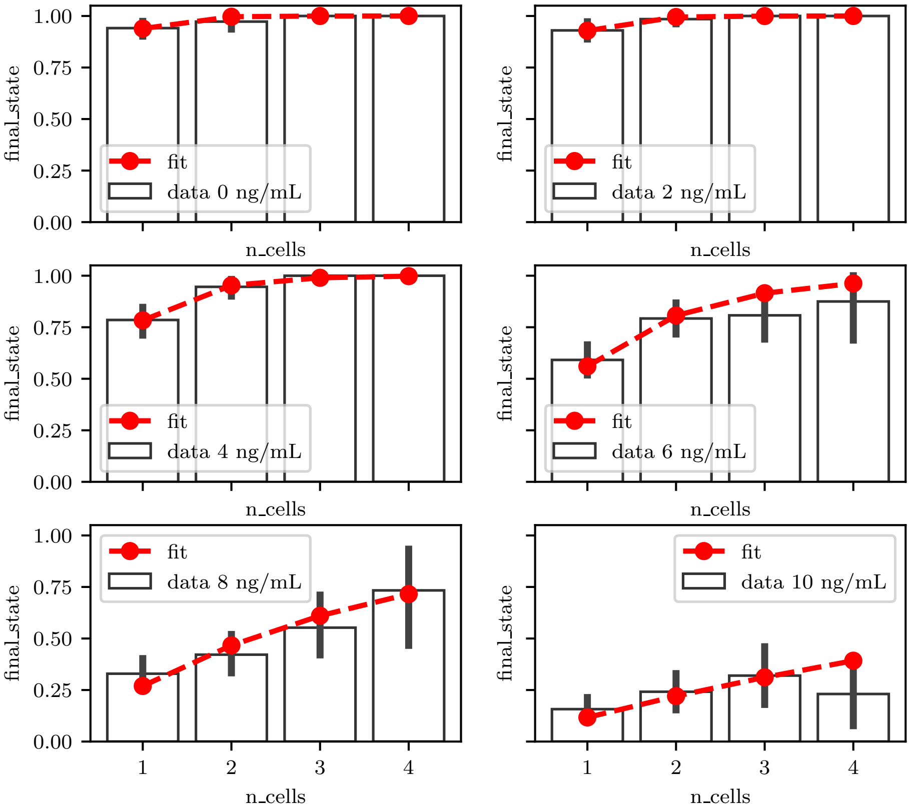

Figure S1. Fitting susceptibility to susceptibility for different concentrations of ciprofloxacin.

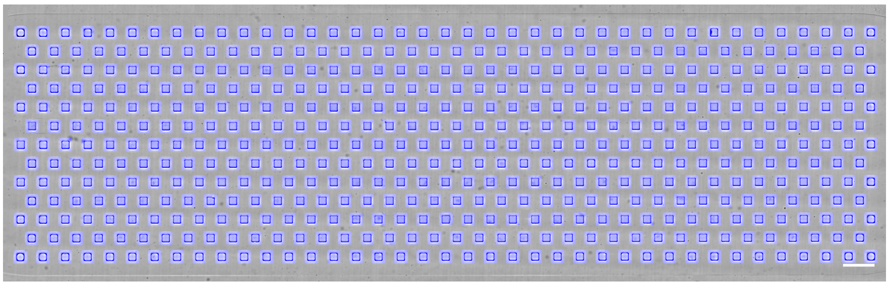

Figure S2. Template (grayscale) + mask (blue) used for alignment and segmenting the droplets. Scalebar 500 um

References

[1] **Abbyad P**, Dangla R, Alexandrou A, Baroud CN. Rails and anchors: guiding and trapping droplet microreactors in two dimensions. Lab on a Chip. 2011; 11(5):813–821.

[2] **Amselem G**, Brun P, Gallaire F, Baroud CN. Breaking anchored droplets in a microfluidic Hele-Shaw cell. Physical Review Applied. 2015; 3(5):054006.

[3] **Amselem G**, Guermonprez C, Drogue B, Michelin S, Baroud CN. Universal microfluidic platform for bioassays in anchored droplets. Lab Chip. 2016; 16(21):4200–4211. http://xlink.rsc.org/?DOI=C6LC00968A, doi: 10.1039/C6LC00968A, publisher: Royal Society of Chemistry.

[4] **Amselem G**, Sart S, Baroud CN. Universal anchored-droplet device for cellular bioassays. In: *Methods in Cell Biology*, vol. 148 Elsevier; 2018.p. 177–199.

[5] **Artemova T**, Gerardin Y, Dudley C, Vega NM, Gore J. Isolated cell behavior drives the evolution of antibiotic resistance. Molecular Systems Biology. 2015 Jul; 11(7):822. https://www.embopress.org/doi/full/10.15252/msb.20145888, doi: 10.15252/msb.20145888, publisher: John Wiley & Sons, Ltd.

[6] **Balaban NQ**, Merrin J, Chait R, Kowalik L, Leibler S. Bacterial Persistence as a Phenotypic Switch. Science. 2004 Sep; 305(5690):1622–1625. doi: 10.1126/science.1099390.

[7] **Barizien A**, Suryateja Jammalamadaka M, Amselem G, Baroud CN. Growing from a few cells: combined effects of initial stochasticity and cell-to-cell variability. Journal of the Royal Society Interface. 2019; 16(153):20180935.

[8] **Beloin C**, Michaelis K, Lindner K, Landini P, Hacker J, Ghigo JM, Dobrindt U. The transcriptional antiterminator RfaH represses biofilm formation in Escherichia coli. Journal of bacteriology. 2006; 188(4):1316–1331.

[9] **Bergmiller T**, Andersson AMC, Tomasek K, Balleza E, Kiviet DJ, Hauschild R, Tkačik G, Guet CC. Biased partitioning of the multidrug efflux pump AcrAB-TolC underlies long-lived phenotypic heterogeneity. Science. 2017; 356(6335):311–315. doi: 10.1126/science.aaf4762, iSBN: 1095-9203 (Electronic) 0036-8075 (Linking).

[10] **Boedicker JQ**, Li L, Kline TR, Ismagilov RF. Detecting bacteria and determining their susceptibility to antibiotics by stochastic confinement in nanoliter droplets using plug-based microfluidics. Lab on a Chip. 2008; 8(8):1265–1272.

[11] **Bos J**, Zhang Q, Vyawahare S, Rogers E, Rosenberg SM, Austin RH. Emergence of antibiotic resistance from multinucleated bacterial filaments. Proceedings of the National Academy of Sciences. 2015; 112(1):178–183. http://www.pnas.org/lookup/doi/10.1073/pnas.1420702111, doi: 10.1073/pnas.1420702111, iSBN: 0027-8424 (Print).

[12] **Coates J**, Park BR, Le D, Şimşek E, Chaudhry W, Kim M. Antibiotic-induced population fluctuations and stochastic clearance of bacteria. Elife. 2018; 7:e32976.

[13] **Derzsi L**, Kaminski TS, Garstecki P. Antibiograms in five pipetting steps: precise dilution assays in sub-microliter volumes with a conventional pipette. Lab Chip. 2016; 16(5):893–901. http://xlink.rsc.org/?DOI=C5LC01151E, doi: 10.1039/C5LC01151E, publisher: Royal Society of Chemistry ISBN: 1473-0197.

[14] **Hsieh K**, Mach KE, Zhang P, Liao JC, Wang TH. Combating Antimicrobial Resistance via Single-Cell Diagnostic Technologies Powered by Droplet Microfluidics. Acc Chem Res. 2022 Jan; 55(2):123–133. https://pubs.acs.org/doi/10.1021/acs.accounts.1c00462, doi: 10.1021/acs.accounts.1c00462.

[15] **Huebner A**, Srisa-Art M, Holt D, Abell C, Hollfelder F, Demello A, Edel J. Quantitative detection of protein expression in single cells using droplet microfluidics. Chemical communications. 2007; (12):1218–1220.

[16] **Jepson AK**, Schwarz-Linek J, Ryan L, Ryadnov MG, Poon WC. What is the 'minimum inhibitory concentration'(mic) of pexiganan acting on escherichia coli?—a cautionary case study. In: *Biophysics of infection* Springer; 2016.p. 33–48.

[17] **Jõers A**, Kaldalu N, Tenson T. The Frequency of Persisters in <i>Escherichia coli</i> Reflects the Kinetics of Awakening from Dormancy. Journal of Bacteriology. 2010; 192(13):3379–3384. https://journals.asm.org/doi/abs/10.1128/JB.00056-10, doi: 10.1128/JB.00056-10.

[18] **Kaminski TS**, Scheler O, Garstecki P. Droplet microfluidics for microbiology: techniques, applications and challenges. Lab Chip. 2016; 16:2168–2187. http://pubs.rsc.org/en/Content/ArticleLanding/2016/LC/C6LC00367B, doi: 10.1039/C6LC00367B, publisher: Royal Society of Chemistry ISBN: 1473-0197.

[19] **Kao YT**, S Kaminski T, Postek W, Guzowski J, Makuch K, Ruszczak A, Stetten Fv, Zengerle R, Garstecki P. Gravity-driven microfluidic assay for digital enumeration of bacteria and for antibiotic susceptibility testing. Lab on a Chip. 2020; 20(1):54–63. https://pubs.rsc.org/en/content/articlelanding/2020/lc/c9lc00684b, doi: 10.1039/C9LC00684B, publisher: Royal Society of Chemistry.

[20] **Keymer JE LGLDAR Galajda P**. . ; .

[21] **Klemm P**. Fimbrial Adhesins of Escherichia coli. Reviews of Infectious Diseases. 1985 05; 7(3):321–340. https://doi.org/10.1093/clinids/7.3.321, doi: 10.1093/clinids/7.3.321.

[22] **Liu X**, Painter RE, Enesa K, Holmes D, Whyte G, Garlisi CG, Monsma FJ, Rehak M, Craig FF, Smith CA. High-throughput screening of antibiotic-resistant bacteria in picodroplets. Lab Chip. 2016; 16:1636–1643. http://dx.doi.org/10.1039/C6LC00180G, doi: 10.1039/C6LC00180G, publisher: Royal Society of Chemistry ISBN: 8620871129.

[23] **Lyu F**, Pan M, Patil S, Wang JH, Matin AC, Andrews JR, Tang SKY. Phenotyping antibiotic resistance with single-cell resolution for the detection of heteroresistance. Sensors and Actuators B: Chemical. 2018 Oct; 270:396–404. https://linkinghub.elsevier.com/retrieve/pii/S0925400518309493, doi: 10.1016/j.snb.2018.05.047.

[24] **Meredith HR**, Andreani V, Ma HR, Lopatkin AJ, Lee AJ, Anderson DJ, Batt G, You L. Applying ecological resistance and resilience to dissect bacterial antibiotic responses. Science Advances. 2018; 4(12):eaau1873. https://www.science.org/doi/abs/10.1126/sciadv.aau1873, doi: 10.1126/sciadv.aau1873.

[25] **O'neill J**. Antimicrobial resistance. Tackling a crisis for the health and wealth of nations. 2014; .

[26] **Robert L**, Ollion J, Robert J, Song X, Matic I, Elez M. Mutation dynamics and fitness effects followed in single cells. Science. 2018; 359(6381):1283–1286.

[27] **Scheler O**, Makuch K, Debski PR, Horka M, Ruszczak A, Pacocha N, Sozański K, Smolander OP, Postek W, Garstecki P. Droplet-based digital antibiotic susceptibility screen reveals single-cell clonal heteroresistance in an isogenic bacterial population. Sci Rep. 2020 Feb; 10(1):3282. https://www.nature.com/articles/s41598-020-60381-z, doi: 10.1038/s41598-020-60381-z, number: 1 Publisher: Nature Publishing Group.

[28] **Wang P**, Robert L, Pelletier J, Dang WL, Taddei F, Wright A, Jun S. Robust growth of Escherichia coli. Current biology. 2010; 20(12):1099–1103.

[29] **Zhang P**, Kaushik AM, Hsieh K, Li S, Lewis S, Mach KE, Liao JC, Carroll KC, Wang TH. A Cascaded Droplet Microfluidic Platform Enables High-Throughput Single Cell Antibiotic Susceptibility Testing at Scale. Small Methods. 2022; 6(1):2101254. https://onlinelibrary.wiley.com/doi/abs/10.1002/smtd.202101254, doi: 10.1002/smtd.202101254, _eprint: https://onlinelibrary.wiley.com/doi/pdf/10.1002/smtd.202101254.

[30] **Zhou W**, Le J, Chen Y, Cai Y, Hong Z, Chai Y. Recent advances in microfluidic devices for bacteria and fungus research. TrAC Trends in Analytical Chemistry. 2019; 112:175–195. https://www.sciencedirect.com/science/article/pii/S0165993618305193, doi: https://doi.org/10.1016/j.trac.2018.12.024.

Bibliography

[1] J O'neill. Antimicrobial resistance: Tackling a crisis for the health and wealth of nations. *Tackling a crisis for the health and wealth of nations*, 2014.

[2] Alys K Jepson, Jana Schwarz-Linek, Lloyd Ryan, Maxim G Ryadnov, and Wilson CK Poon. What is the 'minimum inhibitory concentration'(mic) of pexiganan acting on escherichia coli?—a cautionary case study. In *Biophysics of infection*, pages 33–48. Springer, 2016.

[3] Julia Bos, Qiucen Zhang, Saurabh Vyawahare, Elizabeth Rogers, Susan M. Rosenberg, and Robert H. Austin. Emergence of antibiotic resistance from multinucleated bacterial filaments. *Proceedings of the National Academy of Sciences*, 112(1):178–183, 2015. ISBN: 0027-8424 (Print).

[4] Jessica Coates, Bo Ryoung Park, Dai Le, Emrah Şimşek, Waqas Chaudhry, and Minsu Kim. Antibiotic-induced population fluctuations and stochastic clearance of bacteria. *Elife*, 7:e32976, 2018.

[5] Tatiana Artemova, Ylaine Gerardin, Carmel Dudley, Nicole M Vega, and Jeff Gore. Isolated cell behavior drives the evolution of antibiotic resistance. *Molecular Systems Biology*, 11(7):822, July 2015. Publisher: John Wiley & Sons, Ltd.

[6] Nathalie Q. Balaban, Jack Merrin, Remy Chait, Lukasz Kowalik, and Stanislas Leibler. Bacterial persistence as a phenotypic switch. *Science*, 305(5690):1622–1625, Sep 2004.

[7] Ping Wang, Lydia Robert, James Pelletier, Wei Lien Dang, Francois Taddei, Andrew Wright, and Suckjoon Jun. Robust growth of escherichia coli. *Current biology*, 20(12):1099–1103, 2010.

[8] Tobias Bergmiller, Anna M.C. Andersson, Kathrin Tomasek, Enrique Balleza, Daniel J. Kiviet, Robert Hauschild, Gašper Tkačik, and Călin C. Guet. Biased partitioning of the multidrug efflux pump AcrAB-TolC underlies long-lived phenotypic heterogeneity. *Science*, 356(6335):311–315, 2017. ISBN: 1095-9203 (Electronic) 0036-8075 (Linking).

[9] Lydia Robert, Jean Ollion, Jerome Robert, Xiaohu Song, Ivan Matic, and Marina Elez. Mutation dynamics and fitness effects followed in single cells. *Science*, 359(6381):1283–1286, 2018.

[10] A Huebner, M Srisa-Art, D Holt, C Abell, F Hollfelder, AJ Demello, and JB Edel. Quantitative detection of protein expression in single cells using droplet microfluidics. *Chemical communications*, (12):1218–1220, 2007.

[11] James Q Boedicker, Liang Li, Timothy R Kline, and Rustem F Ismagilov. Detecting bacteria and determining their susceptibility to antibiotics by stochastic confinement in nanoliter droplets using plug-based microfluidics. *Lab on a Chip*, 8(8):1265–1272, 2008.

[12] Ladislav Derzsi, Tomasz S. Kaminski, and Piotr Garstecki. Antibiograms in five pipetting steps: precise dilution assays in sub-microliter volumes with a conventional pipette. *Lab Chip*, 16(5):893–901, 2016. Publisher: Royal Society of Chemistry ISBN: 1473-0197.

[13] Yu-Ting Kao, Tomasz S. Kaminski, Witold Postek, Jan Guzowski, Karol Makuch, Artur Ruszczak, Felix von Stetten, Roland Zengerle, and Piotr Garstecki. Gravity-driven microfluidic assay for digital enumeration of bacteria and for antibiotic susceptibility testing. *Lab on a Chip*, 20(1):54–63, 2020. Publisher: Royal Society of Chemistry.

[14] X Liu, R E Painter, K Enesa, D Holmes, G Whyte, C G Garlisi, F. J. Monsma, M Rehak, F F Craig, and C A Smith. High-throughput screening of antibiotic-resistant bacteria in picodroplets. *Lab Chip*, 16:1636–1643, 2016. Publisher: Royal Society of Chemistry ISBN: 8620871129.

[15] Fengjiao Lyu, Ming Pan, Sunita Patil, Jing-Hung Wang, A.C. Matin, Jason R. Andrews, and Sindy K.Y. Tang. Phenotyping antibiotic resistance with single-cell resolution for the detection of heteroresistance. *Sensors and Actuators B: Chemical*, 270:396–404, October 2018.

[16] Ott Scheler, Karol Makuch, Pawel R. Debski, Michal Horka, Artur Ruszczak, Natalia Pacocha, Krzysztof Sozański, Olli-Pekka Smolander, Witold Postek, and Piotr Garstecki. Droplet-based digital antibiotic susceptibility screen reveals single-cell clonal heteroresistance in an isogenic bacterial population. *Sci Rep*, 10(1):3282, February 2020. Number: 1 Publisher: Nature Publishing Group.

[17] Tomasz S Kaminski, Ott Scheler, and Piotr Garstecki. Droplet microfluidics for microbiology: techniques, applications and challenges. *Lab Chip*, 16:2168–2187, 2016. Publisher: Royal Society of Chemistry ISBN: 1473-0197.

[18] Wenting Zhou, Jian Le, Yang Chen, Ying Cai, Zhanying Hong, and Yifeng Chai. Recent advances in microfluidic devices for bacteria and fungus research. *TrAC Trends in Analytical Chemistry*, 112:175–195, 2019.

[19] Kuangwen Hsieh, Kathleen E. Mach, Pengfei Zhang, Joseph C. Liao, and Tza-Huei Wang. Combating Antimicrobial Resistance via Single-Cell Diagnostic Technologies Powered by Droplet Microfluidics. *Acc. Chem. Res.*, 55(2):123–133, January 2022.

[20] Paul Abbyad, Rémi Dangla, Antigoni Alexandrou, and Charles N Baroud. Rails and anchors: guiding and trapping droplet microreactors in two dimensions. *Lab on a Chip*, 11(5):813–821, 2011.

[21] Gabriel Amselem, PT Brun, François Gallaire, and Charles N Baroud. Breaking anchored droplets in a microfluidic hele-shaw cell. *Physical Review Applied*, 3(5):054006, 2015.

[22] Gabriel Amselem, Cyprien Guermonprez, Benoît Drogue, Sébastien Michelin, and Charles N. Baroud. Universal microfluidic platform for bioassays in anchored droplets. *Lab Chip*, 16(21):4200–4211, 2016. Publisher: Royal Society of Chemistry.

[23] Neil Convery and Nikolaj Gadegaard. 30 years of microfluidics. *Micro and Nano Engineering*, 2:76–91, 2019.

[24] Saleema Saleh-Lakha and Jack T. Trevors. Perspective: Microfluidic applications in microbiology. *Journal of Microbiological Methods*, 82(1):108–111, 2010.

[25] Gustave Ronteix, Shreyansh Jain, Christelle Angely, Marine Cazaux, Roxana Khazen, Philippe Bousso, and Charles Baroud. A multiscale immuno-oncology on-chip system (miocs) establishes that collective t cell behaviors govern tumor regression. 03 2021.

[26] Sébastien Sart, Gustave Ronteix, Shreyansh Jain, Gabriel Amselem, and Charles N. Baroud. Cell culture in microfluidic droplets. *Chemical Reviews*, 122(7):7061–7096, 2022. PMID: 35179881.

[27] Louise Fournier, Thibault de La Taille, and Cédric Chauvierre. Microbubbles for human diagnosis and therapy. *Biomaterials*, 294:122025, 03 2023.

[28] Witold Postek and Piotr Garstecki. Droplet microfluidics for high-throughput analysis of antibiotic susceptibility in bacterial cells and populations. *Accounts of Chemical Research*, 55(5):605–615, 2022. PMID: 35119826.

[29] Iulia Oita, Hadewych Halewyck, Bert Thys, Bart Rombaut, Yvan Heyden, and Debby Mangelings. Microfluidics in macro-biomolecules analysis: Macro inside in a nano world. *Analytical and bioanalytical chemistry*, 398:239–64, 09 2010.

[30] J. K. Nunes and H. A. Stone. Introduction: Microfluidics. *Chemical Reviews*, 122(7):6919–6920, 2022. PMID: 35414183.

[31] Sundar Hengoju, Miguel Tovar, DeDe Kwun Wai Man, Stefanie Buchheim, and Miriam A. Rosenbaum. *Droplet Microfluidics for Microbial Biotechnology*, pages 129–157. Springer International Publishing, Cham, 2022.

[32] John Paul Urbanski, William Thies, Christopher Rhodes, Saman Amarasinghe, and Todd Thorsen. Digital microfluidics using soft lithography. *Lab Chip*, 6:96–104, 2006.

[33] George M. Whitesides, Emanuele Ostuni, Shuichi Takayama, Xingyu Jiang, and Donald E. Ingber. Soft lithography in biology and biochemistry. *Annual Review of Biomedical Engineering*, 3(1):335–373, 2001. PMID: 11447067.

[34] Adriana San-Miguel and Hang Lu. Microfluidics as a tool for c. elegans research. *WormBook: The Online Review of C. elegans Biology [Internet]*, 2018.

[35] Babak Ziaie, Antonio Baldi, Ming Lei, Yuandong Gu, and Ronald A Siegel. Hard and soft micromachining for biomems: review of techniques and examples of applications in microfluidics and drug delivery. *Advanced Drug Delivery Reviews*, 56(2):145–172, 2004. Biosensing and Drug Delivery at the Microscale.

[36] Anna V. Nielsen, Michael J. Beauchamp, Gregory P. Nordin, and Adam T. Woolley. 3d printed microfluidics. *Annual Review of Analytical Chemistry*, 13(1):45–65, 2020. PMID: 31821017.

[37] Nirveek Bhattacharjee, Arturo Urrios, Shawn Kang, and Albert Folch. The upcoming 3d-printing revolution in microfluidics. *Lab Chip*, 16:1720–1742, 2016.

[38] Alloysius Chibuike Ogodo, Dawn Ify Agwaranze, Morumda Daji, and Rufus Emamoge Aso. Chapter 13 - microbial techniques and methods: basic techniques and microscopy. In Chukwuebuka Egbuna, Kingsley C. Patrick-Iwuanyanwu, Muhammad Ajmal Shah, Jonathan C. Ifemeje, and Azhar Rasul, editors, *Analytical Techniques in Biosciences*, pages 201–220. Academic Press, 2022.

[39] Vera Ortseifen, Martina Viefhues, Lutz Wobbe, and Alexander Grünberger. Microfluidics for biotechnology: Bridging gaps to foster microfluidic applications. *Frontiers in Bioengineering and Biotechnology*, 8, 2020.

[40] Ziyi He, Hao Wu, Xianghua Yan, and Wu Liu. Recent advances in droplet microfluidics for microbiology. *Chinese Chemical Letters*, 33(4):1729–1742, 2022.

[41] Yue Yu, Hui Wen, Sihong Li, Haojie Cao, Xuefei Li, Zhixin Ma, Xiaoyi She, Lei Zhou, and Shuqiang Huang. Emerging microfluidic technologies for microbiome research. *Frontiers in Microbiology*, 13, 2022.

[42] Lucie Poggi Ariel Amir Guy-Franck Richard Charles N. Baroud Nadia Vertti-Quintero, Ethan Levien. Time-resolved microfluidics unravels individual cellular fates during double-strand break repair. *BMC Biology*, 2022.

[43] Roberto Rusconi, Melissa Garren, and Roman Stocker. Microfluidics expanding the frontiers of microbial ecology. *Annual Review of Biophysics*, 43(1):65–91, 2014. PMID: 24773019.

[44] Vinodh Kandavalli, Praneeth Karempudi, Jimmy Larsson, and Johan Elf. Rapid antibiotic susceptibility testing and species identification for mixed samples. *Nature Communications*, 13(1):6215, 2022.

[45] Sebastián Jaramillo-Riveri, James Broughton, Alexander McVey, Teuta Pilizota, Matthew Scott, and Meriem El Karoui. Growth-dependent heterogeneity in the dna damage response in escherichia coli. *Molecular Systems Biology*, 18(5):e10441, 2022.

[46] Moran Bercovici Govind V. Kaigala Frederico Paratore, Vesna Bacheva. Reconfigurable microfluidics. *Nature Reviews Chemistry*, 6, 2022.

[47] Piotr Garstecki, Michael J. Fuerstman, Howard A. Stone, and George M. Whitesides. Formation of droplets and bubbles in a microfluidic t-junction—scaling and mechanism of break-up. *Lab Chip*, 6:437–446, 2006.

[48] Xavier Casadevall i Solvas and Andrew deMello. Droplet microfluidics: recent developments and future applications. *Chem. Commun.*, 47:1936–1942, 2011.

[49] Pingan Zhu and Liqiu Wang. Passive and active droplet generation with microfluidics: a review. *Lab Chip*, 17:34–75, 2017.

[50] Meng Sun, Swastika S. Bithi, and Siva A. Vanapalli. Microfluidic static droplet arrays with tuneable gradients in material composition. *Lab Chip*, 11:3949–3952, 2011.

[51] Dawn E. Cohen, Thomas Schneider, Michelle Wang, and Daniel T. Chiu. Self-digitization of sample volumes. *Analytical Chemistry*, 82(13):5707–5717, 2010.

[52] Raphaël F-X Tomasi, Sébastien Sart, Tiphaine Champetier, and Charles N Baroud. Individual control and quantification of 3d spheroids in a high-density microfluidic droplet array. *Cell reports*, 31(8):107670, 2020.

[53] Shaojiang Zeng, Xiaoyan Pan, Qingquan Zhang, Bingcheng Lin, and Jianhua Qin. Electrical control of individual droplet breaking and droplet contents extraction. *Analytical chemistry*, 83(6):2083–2089, 2011.

[54] Katherine S. Elvira, Fabrice Gielen, Scott S. H. Tsai, and Adrian M. Nightingale. Materials and methods for droplet microfluidic device fabrication. *Lab Chip*, 22:859–875, 2022.

[55] Jigang Wu, Guoan Zheng, and Lap Man Lee. Optical imaging techniques in microfluidics and their applications. *Lab Chip*, 12:3566–3575, 2012.

[56] Michiel Muller. *Introduction to confocal fluorescence microscopy*, volume 69. SPIE press, 2006.

[57] Gufeng Wang and Ning Fang. Detecting and tracking nonfluorescent nanoparticle probes in live cells. *Methods in enzymology*, 504:83–108, 2012.

[58] Walter Lang et al. *Nomarski differential interference-contrast microscopy.* Carl Zeiss Oberkochen, 1982.

[59] Matthew R Arnison, Kieran G Larkin, Colin JR Sheppard, Nicholas I Smith, and Carol J Cogswell. Linear phase imaging using differential interference contrast microscopy. *Journal of microscopy*, 214(1):7–12, 2004.

[60] Andreas Stemmer, Markus Beck, and Reto Fiolka. Widefield fluorescence microscopy with extended resolution. *Histochemistry and cell biology*, 130:807–817, 2008.

[61] Andor. An overview of spinning disk confocal microscopy. *Oxford Instruments.*

[62] Daniel Taylor, Nia Verdon, Peter Lomax, Rosalind J Allen, and Simon Titmuss. Tracking the stochastic growth of bacterial populations in microfluidic droplets. *Physical Biology*, 19(2):026003, feb 2022.

[63] Shay Mailloux, Lisa Ramirez, and Jun Wang. Microfluidic single-cell functional proteomics. *Microfluidic Methods for Molecular Biology*, pages 141–159, 2016.

[64] Shaun W. Lim, Tuan M. Tran, and Adam R. Abate. Pcr-activated cell sorting for cultivation-free enrichment and sequencing of rare microbes. *PLOS ONE*, 10(1):1–16, 01 2015.

[65] Noorsher Ahmed Adam R. Abate Freeman Lan, Benjamin Demaree. Single-cell genome sequencing at ultra-high-throughput with microfluidic droplet barcoding. *Nature Biotechnology*, 35, 2017.

[66] Robert J. Meagher and Meiye Wu. *Microfluidic Approaches to Fluorescence In Situ Hybridization (FISH) for Detecting RNA Targets in Single Cells*, pages 95–112. Springer International Publishing, Cham, 2016.

[67] Janina Bahnemann and Alexander Grünberger. *Microfluidics in Biotechnology: Overview and Status Quo*, pages 1–16. Springer International Publishing, Cham, 2022.

[68] Nae Yoon Lee. Recent progress in lab-on-a-chip technology and its potential application to clinical diagnoses. *International neurourology journal*, 17(1):2, 2013.

[69] Roman Netzer, Deni Ribičić, Marianne Aas, Laura Cavé, and Trisha Dhawan. Absolute quantification of priority bacteria in aquaculture using digital pcr. *Journal of Microbiological Methods*, 183:106171, 2021.

[70] Simon F. Berlanda, Maximilian Breitfeld, Claudius L. Dietsche, and Petra S. Dittrich. Recent advances in microfluidic technology for bioanalysis and diagnostics. *Analytical Chemistry*, 93(1):311–331, 2021. PMID: 33170661.

[71] Janette V. Pham, Mariamawit A. Yilma, Adriana Feliz, Murtadha T. Majid, Nicholas Maffetone, Jorge R. Walker, Eunji Kim, Hyo Je Cho, Jared M. Reynolds, Myoung Chong Song, Sung Ryeol Park, and Yeo Joon Yoon. A review of the microbial production of bioactive natural products and biologics. *Frontiers in Microbiology*, 10(JUN), 2019. Cited by: 245; All Open Access, Gold Open Access, Green Open Access.

[72] Suresh Neethirajan, Isao Kobayashi, Mitsutoshi Nakajima, Dan Wu, Saravanan Nandagopal, and Francis Lin. Microfluidics for food, agriculture and biosystems industries. *Lab Chip*, 11:1574–1586, 2011.

[73] Shahrzad Yazdi and Arezoo M Ardekani. Bacterial aggregation and biofilm formation in a vortical flow. *Biomicrofluidics*, 6(4):044114, 2012.

[74] Kim Lewis. Persister cells, dormancy and infectious disease. *Nature Reviews Microbiology*, 5(1):48–56, 2007.

[75] A. Karimi, D. Karig, A. Kumar, and A. M. Ardekani. Interplay of physical mechanisms and biofilm processes: review of microfluidic methods. *Lab Chip*, 15:23–42, 2015.

[76] Junghyun Kim, Hee-Deung Park, and Seok Chung. Microfluidic approaches to bacterial biofilm formation. *Molecules*, 17(8):9818–9834, 2012.

[77] Yutaka Yawata, Jen Nguyen, Roman Stocker, and Roberto Rusconi. Microfluidic studies of biofilm formation in dynamic environments. *Journal of Bacteriology*, 198(19):2589–2595, 2016.

[78] Jeroen Raes Karolin Faust. Microbial interactions: from networks to models. *Nature Reviews Microbiology*, 10, 2012.

[79] Marcella M. Gomez Job L. Grant Philip A. Romero Ophelia S. Venturelli Sonali Gupta, Tyler D. Ross. Investigating the dynamics of microbial consortia in spatially structured environments. *Nature communications*, 11, 2020.

[80] Jihyang Park, Alissa Kerner, Mark A Burns, and Xiaoxia Nina Lin. Microdroplet-enabled highly parallel co-cultivation of microbial communities. *PloS one*, 6(2):e17019, 2011.

[81] Alina Burmeister and Alexander Grünberger. Microfluidic cultivation and analysis tools for interaction studies of microbial co-cultures. *Current Opinion in Biotechnology*, 62:106–115, 2020. Energy Biotechnologyy Environmental Biotechnology.

[82] Zeeshan A. Khan, Mohd F. Siddiqui, and Seungkyung Park. Current and emerging methods of antibiotic susceptibility testing. *Diagnostics*, 9(2), 2019.

[83] Bhagaban Behera, G.K. Anil Vishnu, Suman Chatterjee, V.S.N. Sitaramgupta V, Niranjana Sreekumar, Apoorva Nagabhushan, Nirmala Rajendran, B.H. Prathik, and Hardik J. Pandya. Emerging technologies for antibiotic susceptibility testing. *Biosensors and Bioelectronics*, 142:111552, 2019.

[84] Helen K. Alexander and R. Craig MacLean. Stochastic bacterial population dynamics restrict the establishment of antibiotic resistance from single cells. *Proceedings of the National Academy of Sciences*, 117(32):19455–19464, 2020.

[85] James J Biemer. Antimicrobial susceptibility testing by the kirby-bauer disc diffusion method. *Annals of Clinical & Laboratory Science*, 3(2):135–140, 1973.

[86] Taradon Luangtongkum, Teresa Y Morishita, Amna B El-Tayeb, Aaron J Ison, and Qijing Zhang. Comparison of antimicrobial susceptibility testing of campylobacter spp. by the agar dilution and the agar disk diffusion methods. *Journal of Clinical Microbiology*, 45(2):590–594, 2007.

[87] Irith Wiegand, Kai Hilpert, and Robert EW Hancock. Agar and broth dilution methods to determine the minimal inhibitory concentration (mic) of antimicrobial substances. *Nature protocols*, 3(2):163–175, 2008.

[88] Zining Hou, Yu An, Karin Hjort, Klas Hjort, Linus Sandegren, and Zhigang Wu. Time lapse investigation of antibiotic susceptibility using a microfluidic linear gradient 3d culture device. *Lab on a Chip*, 14(17):3409–3418, 2014.

[89] Pengfei Zhang, Aniruddha M. Kaushik, Kuangwen Hsieh, Sixuan Li, Shawna Lewis, Kathleen E. Mach, Joseph C. Liao, Karen C. Carroll, and Tza-Huei Wang. A Cascaded Droplet Microfluidic Platform Enables High-Throughput Single Cell Antibiotic Susceptibility Testing at Scale. *Small Methods*, 6(1):2101254, 2022. _eprint: https://onlinelibrary.wiley.com/doi/pdf/10.1002/smtd.202101254.

[90] Inês Miranda, Andrews Souza, Paulo Sousa, João Ribeiro, Elisabete M. S. Castanheira, Rui Lima, and Graça Minas. Properties and applications of pdms for biomedical engineering: A review. *Journal of Functional Biomaterials*, 13(1), 2022.

[91] Feng Hua, Yugang Sun, Anshu Gaur, Matthew A. Meitl, Lise Bilhaut, Lolita Rotkina, Jingfeng Wang, Phil Geil, Moonsub Shim, John A. Rogers, and Anne Shim. Polymer imprint lithography with molecular-scale resolution. *Nano Letters*, 4(12):2467–2471, 2004.

[92] Marie–Claire Bélanger and Yves Marois. Hemocompatibility, biocompatibility, inflammatory and in vivo studies of primary reference materials low-density polyethylene and polydimethylsiloxane: A review. *Journal of Biomedical Materials Research*, 58(5):467–477, 2001.

[93] Phu Tuan Anh Nguyen, Matthieu Vandamme, and Artem Kovalenko. Collapse and cavitation during the drying of water-saturated pdms sponges with closed porosity. *Soft Matter*, 16:9693–9704, 2020.

[94] Jean-Christophe Baret. Surfactants in droplet-based microfluidics. *Lab Chip*, 12:422–433, 2012.

[95] Olaf Wagner, Julian Thiele, Marie Weinhart, Linas Mazutis, David A. Weitz, Wilhelm T. S. Huck, and Rainer Haag. Biocompatible fluorinated polyglycerols for droplet microfluidics as an alternative to peg-based copolymer surfactants. *Lab Chip*, 16:65–69, 2016.

[96] Regulation of the european parliament and of the council on fluorinated greenhouse gases, amending directive (eu) 2019/1937 and repealing regulation (eu) no 517/2014. *European comission.*

[97] Frederick C Neidhardt, Philip L Bloch, and David F Smith. Culture medium for enterobacteria. *Journal of bacteriology*, 119(3):736–747, 1974.

[98] Maria P MacWilliams and Min K Liao. Luria broth (lb) and luria agar (la) media and their uses protocol. *ASM MicrobeLibrary. American Society for Microbiology*, 2006, 2006.

[99] A Barizien, MS Suryateja Jammalamadaka, G Amselem, and Charles N Baroud. Growing from a few cells: combined effects of initial stochasticity and cell-to-cell variability. *Journal of the Royal Society Interface*, 16(153):20180935, 2019.

[100] M. H. Zwietering, I. Jongenburger, F. M. Rombouts, and K. van ’t Riet. Modeling of the bacterial growth curve. *Applied and Environmental Microbiology*, 56(6):1875–1881, 1990.

[101] J O’neill. Tackling drug-resistant infections globally: Final report and recommendations. *Tackling a crisis for the health and wealth of nations*, 2016.

[102] B. Waclaw. *Evolution of Drug Resistance in Bacteria*, pages 49–67. Springer International Publishing, Cham, 2016.

[103] LA Magdanova and NV Golyasnaya. Heterogeneity as an adaptive trait of microbial populations. *Microbiology*, 82:1–10, 2013.

[104] Arvi Jõers, Niilo Kaldalu, and Tanel Tenson. The frequency of persisters in ¡i¿escherichia coli¡/i¿ reflects the kinetics of awakening from dormancy. *Journal of Bacteriology*, 192(13):3379–3384, 2010.

[105] Roy Haggerty, Eugènia Martí, Alba Argerich, Daniel von Schiller, and Nancy B. Grimm. Resazurin as a “smart” tracer for quantifying metabolically active transient storage in stream ecosystems. *Journal of Geophysical Research: Biogeosciences*, 114(G3), 2009.

[106] Christophe Beloin, Kai Michaelis, Karin Lindner, Paolo Landini, Jörg Hacker, Jean-Marc Ghigo, and Ulrich Dobrindt. The transcriptional antiterminator rfah represses biofilm formation in escherichia coli. *Journal of bacteriology*, 188(4):1316–1331, 2006.

[107] Hannah R. Meredith, Virgile Andreani, Helena R. Ma, Allison J. Lopatkin, Anna J. Lee, Deverick J. Anderson, Gregory Batt, and Lingchong You. Applying ecological resistance and resilience to dissect bacterial antibiotic responses. *Science Advances*, 4(12):eaau1873, 2018.

[108] George A Pankey and LD Sabath. Clinical relevance of bacteriostatic versus bactericidal mechanisms of action in the treatment of gram-positive bacterial infections. *Clinical infectious diseases*, 38(6):864–870, 2004.

[109] Silvie Bernatová, Ota Samek, Zdeněk Pilát, Mojmír Šerỳ, Jan Ježek, Petr Jákl, Martin Šiler, Vladislav Krzyžánek, Pavel Zemánek, Veronika Holá, et al. Following the mechanisms of bacteriostatic versus bactericidal action using raman spectroscopy. *Molecules*, 18(11):13188–13199, 2013.

[110] Christine C. Sanders. Ciprofloxacin: In Vitro Activity, Mechanism of Action, and Resistance. *Reviews of Infectious Diseases*, 10(3):516–527, 05 1988.

[111] Ariel Erental, Ziva Kalderon, Ann Saada, Yoav Smith, and Hanna Engelberg-Kulka. Apoptosis-like death, an extreme sos response in escherichia coli. *MBio*, 5(4):e01426–14, 2014.

[112] Celina Janion. Inducible sos response system of dna repair and mutagenesis in escherichia coli. *International journal of biological sciences*, 4(6):338, 2008.

[113] Chris Jones and I Barry Holland. Role of the sulb (ftsz) protein in division inhibition during the sos response in escherichia coli: Ftsz stabilizes the inhibitor sula in maxicells. *Proceedings of the National Academy of Sciences*, 82(18):6045–6049, 1985.

[114] Richard D’Ari. The sos system. *Biochimie*, 67(3-4):343–347, 1985.

[115] Satoko Yoshizawa, Dominique Fourmy, and Joseph D Puglisi. Structural origins of gentamicin antibiotic action. *The EMBO journal*, 17(22):6437–6448, 1998.

[116] Michael A. Kohanski, Daniel J. Dwyer, Boris Hayete, Carolyn A. Lawrence, and James J. Collins. A common mechanism of cellular death induced by bactericidal antibiotics. *Cell*, 130(5):797–810, 2007.

[117] A S Weisberger. Inhibition of protein synthesis by chloramphenicol. *Annual Review of Medicine*, 18(1):483–494, 1967. PMID: 5337537.

[118] B Denise Raynor. Penicillin and ampicillin. *Primary Care Update for OB/GYNS*, 4(4):147–152, 1997.

[119] John V Ashurst and Adam Dawson. Klebsiella pneumonia. 2018.

[120] Soo hun Yoon and Christopher M Waters. Vibrio cholerae. *Trends in microbiology*, 27(9):806–807, 2019.

[121] Beata Kowalska-Krochmal and Ruth Dudek-Wicher. The minimum inhibitory concentration of antibiotics: Methods, interpretation, clinical relevance. *Pathogens*, 10(2):165, 2021.

[122] Arvi Joers, Niilo Kaldalu, and Tanel Tenson. The frequency of persisters in escherichia coli reflects the kinetics of awakening from dormancy. *Journal of bacteriology*, 192(13):3379–3384, 2010.

[123] Ard Jan Grimbergen, Jeroen Siebring, Ana Solopova, and Oscar P Kuipers. Microbial bet-hedging: the power of being different. *Current opinion in microbiology*, 25:67–72, 2015.

[124] Jeffrey N Carey, Erin L Mettert, Manuela Roggiani, Kevin S Myers, Patricia J Kiley, and Mark Goulian. Regulated stochasticity in a bacterial signaling network permits tolerance to a rapid environmental change. *Cell*, 173(1):196–207, 2018.

[125] Manuela Roggiani and Mark Goulian. Oxygen-dependent cell-to-cell variability in the output of the escherichia coli tor phosphorelay. *Journal of bacteriology*, 197(12):1976–1987, 2015.

[126] Vera Bettenworth, Benedikt Steinfeld, Hilke Duin, Katrin Petersen, Wolfgang R. Streit, Ilka Bischofs, and Anke Becker. Phenotypic heterogeneity in bacterial quorum sensing systems. *Journal of Molecular Biology*, 431(23):4530–4546, 2019. Underlying Mechanisms of Bacterial Phenotypic Heterogeneity and Sociobiology.

[127] Andrew D Letten, Alex R Hall, and Jonathan M Levine. Using ecological coexistence theory to understand antibiotic resistance and microbial competition. *Nature ecology & evolution*, 5(4):431–441, 2021.

[128] Gerardo Carranza, Tamara Menguiano, Fernando Valenzuela-Gómez, Yolanda García-Cazorla, Elena Cabezón, and Ignacio Arechaga. Monitoring bacterial conjugation by optical microscopy. *Frontiers in Microbiology*, 12:750200, 2021.

ECOLE DOCTORALE

Titre : Mesure de l'hétérogénéité au sein de la population bactérienne monoclonale en gouttelettes microfluidiques ancrées : le cas de la de réponse antibiotique

Mots clés : Microbiologie, Microfluidique, Antibiotique

Résumé : L'émergence de nouvelles souches bactériennes résistantes représente un défi mondial majeur. Une population bactérienne résistante peut émerger à partir d'une seule cellule qui acquiert soit une résistance, soit une persistance. Par conséquent, il est nécessaire de développer de nouvelles approches pour comprendre le mécanisme de réponse aux antibiotiques, telles que des techniques de dépistage rapide et fiable de la sensibilité aux antibiotiques, ainsi que des études sur des cellules individuelles.

Dans cette étude, nous proposons une nouvelle plateforme utilisant des micro-gouttelettes ancrées et des protocoles d'analyse d'images pour mesurer la croissance de petites communautés à partir de cellules bactériennes individuelles. En raison de l'indépendance de chaque gouttelette, ce format de culture cellulaire 3D nous permet de contrôler précisément le contenu de chaque gouttelette tout en suivant la descendance d'une cellule individuelle.

Grâce à cette approche, nous pouvons suivre la croissance d'une cellule individuelle jusqu'à la formation d'une colonie en utilisant la vidéomicroscopie. De plus, en exposant les cellules des gouttelettes microfluidiques à la ciprofloxacine, un antibiotique, nous pouvons observer les changements morphologiques au niveau de chaque cellule individuelle. Grâce à notre dispositif microfluidique, nous pouvons étudier de manière quantitative la réponse aux antibiotiques des cellules individuelles au sein d'une population bactérienne monoclonale.

Nous démontrons qu'il est possible de détecter une hétérogénéité au sein d'une population monoclonale d'E. coli, ce qui nous permet de déduire la sensibilité d'une cellule individuelle à l'antibiotique, que nous appelons la μf·MIC (Concentration minimale inhibitrice microfluidique). Cette μf·MIC nous permet non seulement d'évaluer la sensibilité aux antibiotiques de la population dans son ensemble, mais aussi la sensibilité aux antibiotiques à l'échelle individuelle.

En utilisant ce système microfluidique et cette méthodologie d'imagerie, nous fournissons des informations à la fois qualitatives et quantitatives sur la réponse des antibiotiques. Cette approche nous permet d'accroître notre compréhension du fonctionnement des divers antibiotiques en fournissant des informations sur leur mécanisme d'action.

Title : Measuring heterogeneity within monoclonal bacterial population in anchored microfluidic droplets: The case of antibiotic response.

Keywords : Microbiology, Microfluidics, Antibiotics

Abstract : The emergence of new resistant bacterial strains is a worldwide challenge. A resistant bacterial population can emerge from a single cell that acquires resistance or persistence. Hence, new ways of tackling the mechanism of antibiotic response, such as fast and reliable antibiotic susceptibility testing screening techniques and single cell studies are required. It is necessary to see what happens at the single cell level, in order to understand what happens at the population level.

Here, we present a new platform based on anchored micro-droplets and image analysis protocols to measure the growth of small communities starting from individual bacterial cells. As each droplet is independent from one to another, this 3D cell culture format allows us to finely control the content within each droplet, while following the progeny of an individual cell.

Therefore, we can follow the growth from individual cell to a colony using time lapse imaging. Plus, by adding ciprofloxacin, the cells in the microfluidic droplets can be subjected to antibiotic stress and we are able to observe the morphological changes at the single cell level. Using our microfluidic device, we can quantitatively investigate the antibiotic response of individual cells from a monoclonal bacterial population. We demonstrate that it is possible to detect heterogeneity outcomes within a monoclonal population of E. coli from which we can deduce single-cell susceptibility to antibiotic that we call the μf·MIC (microfluidic Minimum Inhibitory Concentration). This μf·MIC gives us access not only to the population antibiotics susceptibility but also to the antibiotic susceptibility within the population.

Using this microfluidic and imaging pipeline, we offer both qualitative and quantitative insights into the response of antibiotics. This approach enables us to enhance our comprehension of how different antibiotics function by providing information about their mechanism of action.

Institut Polytechnique de Paris
91120 Palaiseau, France